2002

High resolution modeling of transport in porous media

Guangli Liu
Louisiana State University and Agricultural and Mechanical College, gliu@lsu.edu

HIGH RESOLUTION MODELING OF TRANSPORT IN POROUS MEDIA

A Dissertation

Submitted to the Graduate Faculty of the
Louisiana State University and
Agriculture and Mechanical College
In partial fulfillment of the
requirements for the degree of
Doctor of Philosophy

in

The Gordon A. & Mary Cain Department of Chemical Engineering

by
Guangli Liu
B.S., Yantai University, 1989
M. S., Beijing University of Chemical Technology, 1992
May 2002

ACKNOWLEDGEMENTS

I would like to express my sincere gratitude to my adviser, Dr. Thompson, who provided me with relentless support, helpful guidance and suggestions, and endless patience, without which this dissertation would not be possible to be done.

I also want to give my appreciation to all my dissertation committee members for their time and support.

I wish to give my thanks to Kimberly-Clark Corp. and the Department of Chemical Engineering for providing me with financial support during the my dissertation study.

Also thanks to Gang Guo, Honggao Liu, and Le Yan for the all their help.

TABLE OF CONTENTS

LIST OF TABLES

LIST OF FIGURES

ABSTRACT

This dissertation presents research on the pore-level modeling of transport in porous media. The focus of this work is on high-resolution modeling, a rigorous approach that represents detailed geometry and first-principle physics at the streamline scale. Three major topics are presented in this dissertation: an efficient approach for solving Stokes flow in essentially arbitrary disordered porous media, high-resolution versus network simulations of dispersion phenomena, and a stochastic model for solving interfacial mass transfer from source spheres in porous media. First an approach was developed for solving the equations for Stokes flow in a comparatively large, very heterogeneous two-dimensional porous media with high efficiency (approximately $N*\ln(N)$) using a combination of domain decomposition and the boundary element method. The second topic discussed in this dissertation is the high-resolution versus network simulation of dispersion in porous media for the purpose of evaluating the network discretization effects on hydrodynamic simulation and the nodal mixing assumption for solute transport. It was found that molecular diffusion is not reflected properly with the nodal mixing assumption in the high Peclet number range. The third topic is the development of a stochastic model for simulating interfacial mass transfer at the surface of a single source sphere in a heterogeneous porous medium, which is valid in both low and high Peclet number range.

CHAPTER 1. INTRODUCTION

Porous media are made up of pore space and a solid matrix. The pore spaces are typically connected, which allows transport processes such as fluid flow, mass transfer, and heat transfer to take place inside. Transport in porous media is an important part of many engineering processes such as chromatography, reactor design, environmental remediation, petroleum recovery, catalysis, ion exchange etc. The structure of porous media is usually very complex so it is customary to model porous media by ignoring the micro mechanical details within the pores and instead to work with the volume-averaged laws that treat a porous medium as a macroscopically uniform continuum. At this scale, porous media are described by parameters such as permeability, and dispersion coefficients.

Both permeability and the dispersion coefficient (as well as other parameters) have a strong dependence on the pore structure and pore-level physics, which generally requires them to be estimated experimentally or through the use of existing empirical relations. However, experiments can be slow and costly, while generalized empiricism has not proved to be effective for many complex processes such as multiphase flow.

A more fundamental approach is to model transport processes in porous media from first principle physics, which are well known at the discrete pore level. However, this approach requires a detailed description of the pore-space geometry, which is rarely known, and in cases where it is known, the mathematics can become intractable. Network modeling is a common approach that simplifies the pore space into bonds and pores. Pore-level heterogeneity is built into the model by allowing the conductivity of the bonds to vary according to a random distribution or according to a one-to-one mapping from a real porous material. The simplified structure of a network model allows the flow field to be solved from a system of linear algebraic equations if mass conservation is imposed at each network junction, and the Hagen-Poiseuille equation (or a similar linear equation) is applied to each

bond. The strength of network modeling is that a significant amount of pore geometry information can be incorporated, but the flow calculations are sufficiently simple that very large networks can be handled efficiently.

While network modeling is a very powerful method for resolving pore-scale phenomena, this type of modeling has a number of important limitations. The most significant limitation is the need to subdivide the pore space into discrete pores and pore throats. Because most real porous materials contain a continuum interconnected pore space, this discretization process is inevitably somewhat arbitrary. A second significant limitation of the network approach is the inability to resolve flow at the streamline scale. While numerous authors have superimposed equations derived from streamline-scale transport within the network structure (Koplik, 1982; Hoefner and Fogler, 1988; Dillard and Blunt, 2000), the validity of these approaches requires that the detailed hydrodynamics within the simplified network are equivalent to the hydrodynamics in the true pore space. Applications for which the lack of streamline-scale information is a problem include solute dispersion and any phenomenon that involves boundary-layer transport.

High-resolution modeling, in which the momentum equations are solved directly within the discrete pore geometry, is the most rigorous approach to modeling transport in porous media. This approach is necessary for certain types of fundamental studies in which the detailed velocity profile is required. One example is interfacial mass transfer in the porous media, where spatial variations in the mass-transfer rate will occur because of the disorder and heterogeneity found in most porous media (Guo and Thompson, 2001). In cases where mass transfer occurs from discrete sites distributed within the porous medium, local variations are important because the average rate of mass transfer may be significantly different than what is predicted from empirical correlations. This discrepancy would be particularly evident if a spatial correlation existed between the location of the discrete sites for mass

transfer and other morphologic parameters that influence flow. For real processes, this type of correlation is probably more the norm than the exception because of the high degree of coupling found in most porous-media transport processes. A second example is size-exclusion chromatography during macromolecular transport (Lecourtier and Chauveteau, 1983; Brown and Sorbie, 1988). This process occurs because large molecules tend to travel along faster streamlines away from the solid surface. A third example is dispersion, for which network modeling has been applied successfully (Sahimi et al., 1983; Sahimi et al., 1986). However, high-resolution modeling can help to clarify the contribution of molecular diffusion; since network models lack detailed flow information at each pore, effects associated with molecular diffusion cannot be represented well. This problem is discussed further in Chapter 5.

While overcoming the limitations of network models, high-resolution modeling also introduces enormous challenges. These challenges include the following:

1. A significant hurdle is obtaining a detailed description of the pore space in the porous media. Finney (1976) made pioneering efforts by mapping out the detailed structure of a bead pack with 2000 spheres. Thin-sections have commonly been used to analyze porous media, and even to reconstruct three-dimensional images (Bakke and Øren, 1997). A more recent approach is the use of high-resolution microtomography, which allows non-destructive imaging of many types of materials. An attractive alternative is computer-generated porous materials. The challenge of employing computer generated media is how to represent the randomness and heterogeneity of a real medium.
2. The second challenge is to solve the fundamental flow equations in the domain of pore space. Stokes flow can oftentimes be assumed because of small void spaces and low velocities, which lead to low Reynolds number flows. Analytic solutions to the Stokes equation exist

only for simple geometries, so porous media problems generally require numerical approaches. If the structure is regular, one has more flexibility in choosing a numerical approach. However, for disordered media, the computational problems are much larger, and solution methods are more restricted. Typical limitations can include size, solid volume fraction, particle shape, and particle spacing, depending on the method. Classical numerical approach like finite element or finite difference methods rapidly becomes intractable as the domain size increases or the physics of the transport processes becomes complex. The Lattice-Boltzmann method can be used to solve the flow solutions in complex media (Koch and Ladd, 1997; Maier et al., 1998). However, the slow convergence at low porosities can be a concern for some applications.

3. The third challenge for high-resolution modeling is to reproduce more complicated transport phenomena such as interfacial mass transfer. For this example, in addition to the flow solution, a separate model needs to be developed to address the issue of dissolution near the sphere surface.

Since high-resolution modeling employs first-principle physics, it can be also used to evaluate the validity of other modeling approaches. For example, assumptions associated with network models can be evaluated, which in turn can lead to improvements in network modeling algorithms. Because of the simplicity of the network model, it is not likely to be replaced by high-resolution modeling except in cases where streamline resolution is absolutely necessary.

The objective of this work is to address a series of issues related to high-resolution modeling. The primary effort was on developing efficient technique(s) for solving the Stokes equation in large disordered porous media. Of specific interest was removing limitations associated with pore structure or porosity that are present in existing high-resolution techniques. A second objective of the work

was to use the modeling to gain insight into certain fundamental transport processes. A random-walk model was developed to study the influence of local hydrodynamics on interfacial mass transfer in porous media. Additionally, dispersion was simulated in both network models and high-resolution models for the purpose of evaluating the validity of the network-model algorithms.

In this dissertation, Chapter 2 gives a background and literature review. Chapter 3 describes the method that was developed for solving the Stokes flow in a disordered media. Chapter 4 compares network models and the high-resolution model, focusing on solute dispersion. Chapter 5 describes a numerical approach for modeling interfacial mass transfer in porous media, which makes use of the hydrodynamic solution given in Chapter 3.

CHAPTER 2. BACKGROUND AND LITERATURE REVIEW

This chapter gives a background discussion of modeling flow and solute transport in porous media. In keeping with the content of this dissertation, we focus on the pore-level modeling of flow, dispersion, and interfacial dissolution phenomena.

2.1 Modeling Flow in Porous Media

Darcy's law is the well-known equation for describing fluid flow in porous media (Equation 2.1). It assumes a linear relationship between the pressure gradient ∇p and the volume flow rate per unit area $\mathbf{q}$. The permeability $\mathbf{k}$ is a 3D tensor quantity that represents fluid conductivity in the medium; it is often reduced to a scalar if the medium is isotropic.

$$\mathbf{q} = -\frac{\mathbf{k}}{\mu} \cdot \nabla p \tag{2.1}$$

Implicit in Darcy's law is the assumption that the porous medium is a continuum medium where flow or other transport properties such as permeability or dispersion coefficients can be derived from averaging the pore-level transport over an appropriate representative elementary volume (Whitaker, 1985).

Typically these macroscopic parameters have a strong dependence on the pore structure and physics of the transport processes. The need to understand these dependences from a fundamental perspective dictates the need for the modeling at the microscopic scale.

2.1.1 Network Modeling of Pore Level Flow

The philosophy employed in network modeling is to represent a complex pore space as a simple network, thereby retaining certain important qualities (interconnectedness, pore-size distribution) while providing a domain in which simple flow calculations can be made. In general, a network is composed of bonds that represent capillary conduits, and nodes that represent pore junctions (of

several bonds). Network models were first introduced by Fatt (1956) to study capillary pressure behavior in porous media. In Fatt's work, the porous medium is represented as a two-dimensional regular lattice, where two adjacent nodes are always connected by a capillary tube of uniform diameter. It is assumed that the pressure drop only occurs within bonds, and fluid is completely mixed within each node. Therefore, each bond can be assigned a hydraulic conductivity, which is the ratio of flow rate to pressure drop. If a bond is a cylindrical capillary, the conductivity is usually calculated from the Hagen-Poiseuille equation for laminar flow in a tube. The conductivity of each bond can be assigned by selecting appropriate diameters. The continuity equation is written for each node in the network in terms of the bond conductivities and the pressures at each node. The result is a system of linear equations that can be solved for the unknown pressures and thus the flow rates.

Historically, network modeling was performed in simple structures: regular 2D and 3D lattices whose bonds were decorated with a distribution of radii. Modern network models are much more representative of true pore structures (Bryant et al., 1993; Bakke and Oren, 1997; Liang et al., 2000). Additionally, network modeling has been used to study a wide range of topics including relative permeability (Blunt and Bryant, 1992), dispersion (Sahimi et al., 1983; 1986), non-Newtonian Flows (Shah and Yortsos, 1995), reactive flows (Fredd and Fogler, 1998), non-Darcy Flows (Thauvin and Mohanty, 1998), contaminant transport (Dillard and Blunt, 2000), and fluid flow in fibrous materials (Ghassemzadeh et al., 2001; Thompson, 2002).

While network modeling is a very powerful method for resolving pore-scale phenomena, this type of modeling has a number of important limitations. The most significant limitation is the need to subdivide the pore space into discrete pores and pore throats. In real porous media, the distinction between pores and throats is not obvious, and the choice of how to perform discretization becomes somewhat arbitrary. A second significant limitation of the network approach is the inability to resolve

flow at the streamline scale. While numerous authors have superimposed equations derived from streamline-scale transport within the network structure (Koplik, 1982; Hoefner and Fogler, 1988; Dillard and Blunt, 2000), this approach implicitly requires that the detailed hydrodynamics within the simplified network are similar to the hydrodynamics in the true pore space. Applications for which streamline-scale information is required include solute dispersion and any phenomenon that involves boundary-layer transport.

2.1.2 High-Resolution Model of Flow in Porous Media

High-resolution modeling refers to solving the fundamental flow equations in the pore space of porous materials. The challenge of this approach comes from complexity of both the governing flow equations and the pore space geometry.

Stokes flow over a periodic packing of cylinders is a simplified problem that has been examined extensively. Hasimoto (1959) obtained the periodic fundamental solution to the Stokes problem by Fourier series expansion, and applied the results to a dilute array of uniform spheres. Hasimoto's solution gives the drag on each sphere in terms of an expansion in fractional powers of concentration of the packing. Hasimoto has given the first few terms of the expansion for dilute packing. By modifying Hasimoto's approach, the more general problem (with smaller porosity) was solved by Sangani and Acrivos (1982), who recast the Stokes equation in terms of the stream function and vorticity and employed a truncated series solution for these two variables that satisfied specific boundary conditions on the periodic unit cell. Coefficients in the series were found by approximately satisfying the remaining boundary conditions. Sangani and Yao successfully extended this approach to solve the thermal conduction (Sangani and Yao, 1988a) and viscous flow (Sangani and Yao, 1988b) problems in random packings of cylinders. Sangani and Mo (1994) were able to obtain

solutions in somewhat larger random domains. They accounted for lubrication forces using multipole expansions along the centerline of near-particle gaps.

Zick and Homsy (1982) used a boundary integral method to solve the Stokes flow in the periodic array of spheres. They used Hasimoto's fundamental solution to formulate a Fredholm integral equation of the first kind for the force distribution on an array of spheres for arbitrary sphere concentration. The unknown in the equation is the surface stress vector and the parameters include the mean flow, packing characteristics, and particle concentration. The integral equations were solved numerically by a Galerkin method to obtain the pressure drop through the porous media. Larson and Higdon (1986; 1987) studied microscopic flow patterns near the surface of a two-dimensional porous medium that is represented as a semi-infinite lattice of cylinders. The Stokes equation in each unit cell was transformed into a boundary integral equation. The flow field in each unit cell near the surface was calculated using an iterative approach. Instead of solving for flow in sphere or cylinder packings, Koplik obtained an analytical solution of flow in the pores of a regular, two-dimensional network (Koplik, 1981). Koplik assumed Stokes flow in each pore, and also assumed that the velocity profile at each port/pore throat junction satisfied a Poiseuille flow profile. An analytical solution is obtained by extending the Fourier series at each port.

Because of the complexity of pore-space geometry, classical numerical methods for solving flow in the porous media are typically restricted to small or periodic domains. Lemaitre and Adler (1990) use a modified finite difference method to simulate Stokes flow through simulated fractal porous materials. Lee et al. (1995) derived certain boundary value problems for a unit cell from the homogenization theory, which accounts for the effects of micro-scale mechanics on macro-scale processes. The cell problems were solved using the finite element method. Also using the finite element method, Saeger et al. (1995) solved the Stokes equation and Ohm's law for fluids in periodic

bicontinuous porous media of simple cubic (SC), body-centred cubic (BCC) and face-centred cubic (FCC) symmetry. Permeability was computed for flow in each configuration. The dependence of permeability on micro-scale properties such as curvature was analyzed.

The lattice-Boltzmann method provides a flexible method for modeling flow in porous materials. In particular, it is readily applied to arbitrary domain shapes and can be applied to flows having finite Reynolds numbers. The problem of 2D flow through random discs has been modeled by Koch and Ladd (1997) for Reynolds numbers of order 100 and lower. Maier et al. (1998) also applied the Lattice Boltzmann to relatively large 3D packings. Verberg and Ladd (1999) have recently developed a time-independent version of this technique for low-Reynolds number flow, which converges much more quickly than the traditional method. Using the time-independent technique, flow in 2D random arrays of up to 790 particles was modeled. The disadvantages of the lattice-Boltzmann method are slow convergence (using the traditional technique), especially at low porosities (Verberg and Ladd, 1992), and also the need for very fine discretization throughout a domain to accurately resolve velocity profiles in small constrictions or very near to particle surfaces.

For all of the above high-resolution methods, the one best suited for a given problem depends on details of that problem and the specific information that one requires from its solution. In this work, we sought to improve certain capabilities that were identified as part of a larger project to develop hybrid modeling techniques for very large heterogeneous porous media. First, we require that the high-resolution part of the modeling (e.g., where streamline resolution of flow is obtained) can be applied over relatively large characteristic lengths without assuming a smaller scale for periodicity. This attribute is crucial when modeling media where spatial correlation exists. Second, it was necessary that the algorithm be effective for arbitrary particle spacing, and porosity (and ideally, arbitrary pore structures). Finally, we required a method that allows for very accurate recovery of

point velocities in the immediate region of specified solid-fluid interfaces. This last requirement is associated with studies of interfacial transport, where the hydrodynamics within thin concentration (or temperature) boundary layers around particle surfaces must be known accurately.

2.2 Pore Level Modeling of the Dispersion and Interfacial Mass Transfer in the Porous Media

In this section, techniques for the pore-level modeling of dispersion and interfacial mass transfer are presented. Since the random walk method is often used for solving the convection-diffusion equation (the pore level equation governing solute transport), a brief review of this method will also be given in the end.

2.2.1 Pore Level Modeling of Dispersion in Porous Media

While Darcy's law describes the averaged flow over a representative volume, the dispersion coefficient describes the averaged transport caused by solute dispersion. It is usual to assume that dispersion is Fickian at a sufficiently large characteristic scales, and hence the governing macroscopic equation has the same form of the convection-diffusion equation. Because the prediction of dispersion coefficients is difficult, pore-level models of dispersion are used to better understand the dependence of the dispersion coefficients on the pore structure and microscale transport properties.

A great deal of fundamental research has been directed at dispersion processes in porous media. Koch and Brady (1985) give a comprehensive analysis using an asymptotic approach. By ensemble-averaging the basic conservation laws in a porous medium, a macroscopic equation of mass conservation is obtained, from which the dispersion term is obtained for the long-time limit. Dispersion mechanisms were analyzed asymptotically over a range of Peclet numbers. In another work by the same authors (Koch and Brady, 1987), nonlocal dispersion was analyzed by averaging the concentration field in the presence of an advective field. It was found that the characteristic time for a tracer to sample the diffusive boundary layer is proportional to $Pe^{1/3}$ while the time for a tracer to

sample the interior of the solid is proportional to Pe. When the media length to the microscale size ratio L/a is not large compared to $Pe^{1/3}$ and Pe for the boundary layer dispersion and holdup dispersion respectively, the residence-time distribution (RTD) is non-Gaussian so that local dispersion theory is not applicable.

Sahimi pioneered the use of network modeling for solute dispersion using a Monte Carlo method (Sahimi et al., 1983; 1986). In summary, the flow in each capillary tube of the network model can be solved using a general network-modeling approach in which zero pressure drop is assumed at each network junction, and the Hagen-Poiseuille equation is applied to each bond. Once known, bond flow rates are used in a Monte Carlo method to simulate the solute transport through the network. Specifically, a substantial number of tracer particles (which represent the solute molecules or fluid packets of some concentration) are followed through the network by expanding their movements into two terms. One is the convective term, which is determined by the local flow field. The second is a random displacement term, which is meant to capture molecular diffusion effects. The final position and travel time of the each tracer particle are recorded for the calculation of dispersion coefficients. Simulation results show that the dispersion is diffusive and the dispersion coefficients are sensitive to geometry and topological characteristics of the random system. The nodal mixing assumption of the network model is investigated and the results show that the longitudinal dispersivity, which is defined as the ratio of the dispersion coefficient over the mean velocity, is independent of the mean flow rate. In reality, it is observed to rise gently with increasing mean flow rate.

Since molecular diffusion is not included in Sahimi's work, the Peclet number is unknown. Hence, the dependence of the dispersion coefficients on the Peclet number cannot be clarified. Sobie and Clifford (1991) include the molecular diffusion coefficients in their research, and give simulation results for a full range of Pe. However, molecular diffusion is limited only to network bonds, so that

nodal mixing effects are neglected. In this dissertation, the nodal mixing issue is discussed in Chapter 4, and the results will be compared with a high-resolution dispersion simulation.

2.2.2 Pore Level Modeling of Interfacial Mass Transfer in Porous Media

The problem of mass transfer from a single particle in uniform unbounded flow can be approached using first principles. In the limit $Pe \to \infty$ (and for low-Reynolds number flow), the Sherwood number takes the form $Sh = A \cdot Pe^{1/3}$ for solid particles of most any shape (Leal, 1992). The coefficient A can be determined using the concentration (or thermal) boundary-layer equations. For the specific case of a spherical particle in Stokes flow, Acrivos and Goddard (1965) obtained the two-term expansion

$$Nu = Pe^{1/3}[0.6245 + 0.46Pe^{-1/3} + O(Pe^{-1/3})], \tag{2.2}$$

For packed beds and porous media, equations for mass transfer are built upon similar scaling arguments as long as $Pe >> 1$. For instance, Karabelas et al. (1971) found experimentally that $Sh = 4.58Pe^{1/3}$ for a single sphere in a cubic packing under conditions $Re < 10$ and $Pe \to \infty$.

Jia et al. (1999) studied how variations in this functionality affect macroscopic transport in porous media. They examined the dissolution of trapped organic ganglia using both visual micromodels and pore network simulations. Of particular interest is their sensitivity analysis of the parameters A and m in the general relationship $Sh = A \cdot Pe^m$. They showed that macroscopic mass transfer behavior is moderately sensitive to A and highly sensitive to m. This observation, when contrasted against the wide range of empirical functions in use, shows the need to improve fundamental knowledge about mass-transfer in heterogeneous porous media.

Theoretical analyses of heat or mass transfer in packed beds is more difficult than for unbounded spheres because of the influence of neighboring particles. In many studies, porous media are simplified using periodic media, which reduces the difficulty of solving the flow problem. Pfeffer and

Happel (1964) expanded the steady-state convection-diffusion equation in a power series of the spherical angle, with coefficients being functions of radial position. Velocities were found using a sphere-in-cell approach, and diffusion in the angular direction was neglected, thus allowing for numerical solution of the coefficients. This approach allowed for direct solution of the Nusselt number for various porosities and Peclet numbers. The $Pe^{1/3}$ functionality was recovered in the high-*Pe* limit. Sørensen and Stewart (1974a) obtained the velocity field in a cubic array using a numerical solution to the streamfunction equations. Using this solution, they developed a numerical solution to the boundary layer equations over the surface of a sphere in the packing (Sørensen and Stewart, 1974b). Their results agreed fairly well with those of Karabelas et al. (1971), despite the differences between regular and disordered packings. Baier et al. (1999) examined local mass transfer in regular arrays of dilute cylinders (which ensured that no recirculation occurred). Velocities were calculated numerically, and local Nusselt numbers for mass transfer were calculated along particle surfaces from the boundary-layer equations. As one would expect, local Nusselt numbers are highest along surfaces where the gap to neighboring particles is smallest because the velocity gradient is higher. Local Nusselt numbers are lowest at downstream stagnation points. The collective effect of these local differences is seen in the Peclet number coefficient (*A* in our notation), which is a function of packing geometry. The Peclet-number exponents from their calculations equaled 1/3 for all geometries since boundary-layer equations were used.

Coutelieris et al. (1993) used a sphere-in-cell procedure to find the velocity profile in an array of spheroidal particles. An analytic solution to the high-Peclet-number concentration field for adsorption at the particle surface showed that when the long axis of the spheroids are normal to the flow direction, the thinnest part of the concentration boundary layer is along the equator rather than at the front stagnation point. Mass transfer was found to be proportional to $Pe^{1/3}$ for all orientations. The

same authors later refined the boundary conditions used with the convection-diffusion equation and performed a numerical solution that was valid to Peclet numbers as low as 5 (Coutelieris et al., 1995).

The more difficult problem of mass transfer in disordered packings was first examined by Wang and Sangani (1997) for conditions of low *Re* and high *Pe*. Velocity fields for the two-dimensional problem were obtained using multipole expansions (Sangani and Yao, 1988). The heat-transfer problem was then solved by integrating the boundary-layer equation between stagnation points on the particle surfaces. This approach allowed differentiation between regions of the surface that are exposed to 'fresh' fluid versus regions of the surface next to recirculating fluid where the thermal boundary layer is thicker. For disordered arrays, the overall Nusselt number was found by averaging over all particles. Tables II and III from their paper show that the average rate of mass transfer is generally lower in random packings (except when flow is aligned with a regular array, in which case the recirculation patterns have a larger impact).

Bekri et al. (1995) studied dissolution phenomena in porous media based on a random walk model and on the finite difference formulation. The Stokes equation was solved quasi-statically by assuming the rate of the deformation of the solid surface to be very low. Then, the convection-diffusion equation was solved by a random walk model to determine the dissolution fluxes and the motion of the fluid-solid interfaces. By examining cubic sphere packings and the Menger sponge, three main regimes were identified. When the Pe Da < 1, dissolution is nearly uniform all over the solid surface. If Pe <1, diffusion is predominant, and dissolution occurs around the larger pores of the pore space. If Pe > 1, convection is predominant and the dissolution is mostly localized along the main flow path. Ponoth and McLaughlin (2000) simulated mass transfer from bubbles in water. A finite difference method and a stochastic Lagrangian method were used to compute the dissolution rate of the bubbles. The Sherwood number was found to be strongly affected by the stagnant surfactant cap angle, bubble size and

Reynolds number. The Lagrangian marker method used in their work is simply the random walk model in Lagrangian space.

Dillard and Blunt (2000) developed a pore network model to study nonaqueous phase liquid (NAPL) dissolution. The flow rates of both water and NAPL phase were solved from the multiphase Darcy equations and the aqueous-phase transport is solved by applying the solute flux equation at each network tube. The mass transfer from the NAPL blobs was represented using a corner diffusion model. The results of the simulated solute concentration vs. Peclet number, and simulations of Sherwood number vs. Peclet number matched well with the experimental data when the NAPL blob dissolution rate was neglected.

2.2.3 Random Walk Model and Convection-Diffusion Equation

Random walks (also known as particle-tracking) have been used since the 1950s (Scheidegger, 1958) to model flow of a tracer through a porous medium. The basic methodology is to approximate the transport quantity, such as heat or solute mass, by a set of moving particles. For the solution of the convection-dispersion equation, mass is divided into particles, each of which is subjected to convection by the velocity field as well as Brownian motion.

For the one-dimensional convection-dispersion problem, a constant time step equation is of the form

$$\mathbf{x}(t+\Delta t)-\mathbf{x}(t)=\mathbf{u}\cdot\Delta t+(2D\Delta t)^{1/2}\boldsymbol{\xi}, \tag{2.3}$$

where $\boldsymbol{x}(t)$ is the location at time t, $\mathbf{u}$ is the convective velocity, D is the diffusion coefficient, Δt is a constant time step, and each component of $\boldsymbol{\xi}$ is an independent normally distributed variable with zero mean and unit variance. The first term of the right hand side accounts for convection, and the second term accounts for diffusion.

The boundary conditions for the random walk model are classified into three types: the fully reflecting boundary, partially reflecting boundary, and the fully trapping boundary (Weiss, 1994). The particle movement equation imposed at each type of boundary is derived independently from the definition of the problem.

Random walk modeling is often used to simulate macroscopic transport phenomena such as hydrological pollutant transport (Scott, 1997), flow injection analysis (Wentzell et al., 1993), and Non-Gaussian dispersion in heterogeneous porous media (Scheibe and Cole, 1994; Sternberg et al., 1996).

At the pore-scale, dispersion of solute has been studied using a pore-level model and particle-tracking technique. Sahimi et al. (1983; 1984) used particle-tracking to trace solute through a network model of porous media. They calculated that the dispersion coefficient is proportional to the mean convective flow velocity. Sorbie and Clifford (1991) used particle-tracking to study dispersion over a wide range of Peclet numbers. Their calculated dispersion behavior is found to agree well with experimental results. The diffusion-dominated, mixed, and convection-dominated flow regimes are reproduced in this work.

The strength of the random walk model is its capability for solving the convection diffusion equation at high Peclet numbers. In contrast, the strong upwinding effects in this transport regime have limited the use of traditional methods such as the finite element method and the finite difference method.

CHAPTER 3. A DOMAIN DECOMPOSITION METHOD FOR MODELING STOKES FLOW IN POROUS MATERIALS

3.1 Introduction

The problem of two-dimensional Stokes flow through a random array of discs has been studied in relation to a number of phenomena. In our research, we are examining convective transport phenomena in heterogeneous porous media, and for certain applications, this 2D problem is used as an analog to 3D flows in sphere packings. Also, the problem is equivalent to three-dimensional flow transverse to parallel cylinders, which is important for modeling fluid flow in aligned fibrous materials (Spaid et al., 1997).

Analytic solutions to the Stokes equation exist only for simple geometries, so porous media problems generally require numerical approaches. If the structure is regular, one has more flexibility in choosing a numerical approach. However, for disordered media, the computational problems are much larger, and solution methods are more restricted. Typical limitations can include size, solid volume fraction, particle shape, and particle spacing, depending on the method.

The purpose of this work was to develop an efficient computational algorithm for relatively large domains that has few restrictions associated with pore structure or porosity. Although examples shown here are for two-dimensional arrays of discs, it has been tested using media composed of angular particles, and it could equally well be applied to unstructured domains with nearly arbitrary particle shapes. The solution method combines attributes of both boundary integral techniques and domain decomposition. Use of the boundary element method reduces the dimension of the numerical problem by one, therefore allowing for easy discretization of the flow domain and giving a smaller number of unknowns. Domain decomposition vastly improves the sparseness of the resulting matrix equation, thereby allowing one to solve much larger problems than standard boundary integral methods would allow.

3.2 Numerical Modeling of Stokes Flow in Two-Dimensional Porous Media

The problem of Stokes flow in periodic arrays of cylinders has been examined extensively. The general problem was first solved by Sangani and Acrivos (1982), who recast the Stokes equation in terms of the stream function and vorticity and employed a truncated series solution for these two variables that satisfied specific boundary conditions on the periodic unit cell. Coefficients in the series were found by approximately satisfying the remaining boundary conditions. Larson and Higdon (1987) studied flow in a similar periodic porous medium, but near the medium's interface with a bulk flowing fluid. The Stokes equation in each periodic cell was solved using a boundary element method. However, an iterative process was used to obtain boundary values as a function of distance from the plane-porous interface. The periodicity in structure allowed a highly efficient solution (comparable to a fully periodic solution) even though the flow was not periodic.

Solving for Stokes flow in random porous media is a more challenging problem. Sangani and Yao (1988) first addressed the 2D problem (i.e., transverse Stokes flow over random parallel cylinders) using the stream function formulation and a multipole expansion of the singularly forced Laplace equation. A numerical solution was used to determine coefficients in the resulting series expansion. Sangani and Mo (1994) were able to obtain solutions in somewhat larger random domains. They accounted for lubrication forces using multipole expansions along the centerline of near-particle gaps.

The lattice-Boltzmann method provides a flexible method for modeling flow in porous materials. In particular, it is readily applied to arbitrary domain shapes and can be applied to flows having finite Reynolds numbers. The problem of 2D flow through random discs has been modeled by Koch and Ladd (1997) for Reynolds numbers of order 100 and lower. Verberg and Ladd (1992) have recently developed a time-independent version for low-Reynolds number flow that converges much more quickly than the traditional method. Using the time-independent technique, flow in 2D random arrays of up to 790 particles was modeled. The disadvantages of the lattice-Boltzmann method is slow

convergence (using the traditional technique), especially at low porosities (Verberg and Ladd, 1992), and also the need for very fine discretization throughout a domain to accurately resolve velocity in small constrictions or very near particle surfaces.

All of the above methods, as well as finite difference methods, are powerful approaches, and the one best suited for a given problem depends on details of that problem and the specific information one requires from its solution. In this work, we sought to improve certain capabilities that were identified as part of a larger project to develop hybrid modeling techniques for very large heterogeneous porous media. First, we require that the high-resolution part of the modeling (e.g., where streamline resolution of flow is obtained) can be applied over relatively large characteristic lengths without assuming a smaller scale for periodicity. This attribute is crucial when modeling media where spatial correlation exists. Second, it was necessary that the algorithm be effective for arbitrary particle spacing, and porosity (and ideally, arbitrary pore structure). Finally, we required a method that allows for very accurate recovery of point velocities in the immediate region of specified solid-fluid interfaces. This last requirement is associated with studies of interfacial transport, where the hydrodynamics within thin concentration (or temperature) boundary layers around particle surfaces must be known accurately.

3.3 Problem Formulation

The method presented in this work is applicable to general 2D domains, and can likely be expanded to three dimensions. For simplicity, however, computations performed during this research were made using two-dimensional disordered arrays of discs as shown in Figure 3.1. The discs' radii are chosen randomly from a size distribution, and placed in the domain using a 2D analog to collective rearrangement algorithms for 3D (which remove overlaps) (Liu and Thompson, 2000). The collective rearrangement algorithms are powerful because of the control that one has over final porosity and spatial correlation. In two dimensions, a slight decrease in sphere radii was necessary

following the removal of overlaps to provide for flow paths. As an aside, the flow computations described below do not require an overlap-free domain; however, in our case it would require a slight modification to the boundary discretization subroutine that was used.

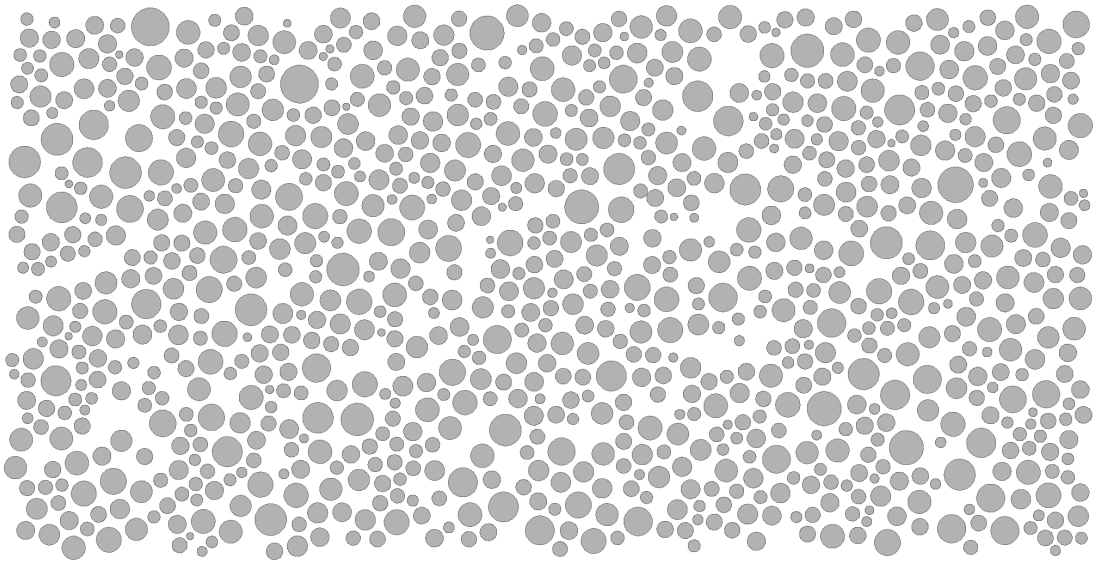

Figure 3.1. Example of a 1000-particle two-dimensional porous medium

Within the model porous medium, we wish to solve the Stokes equation for low-Reynolds-number flow. The Stokes equation and the continuity equation are

$$-\nabla p + \mu \nabla^2 \mathbf{u} = 0 \tag{3.1}$$

$$\nabla \cdot \mathbf{u} = 0 \,. \tag{3.2}$$

The Stokes equation is a time-independent boundary-value problem that can be solved using a variety of numerical techniques given an appropriate combination of boundary velocities and stresses.

Finite rather than periodic boundary conditions are used because the domain is viewed as modeling a piece of a larger heterogeneous medium; ultimately, the strategy would be to derive

appropriate boundary conditions for the Stokes-flow problem from a larger-scale simulation. However, in the problems shown here, we simply apply constant-pressure boundaries along two opposing sides of the domain, with no-flow boundaries parallel to this imposed pressure gradient. (The no-flow boundaries are shown in bold in subsequent figures). Mathematically, the constant-pressure conditions at the inlet and outlet are imposed by forcing the tangential velocity component equal to zero along these boundaries, which thereby allows one to equate the normal stress to the imposed pressure. These conditions provide a well-posed global problem.

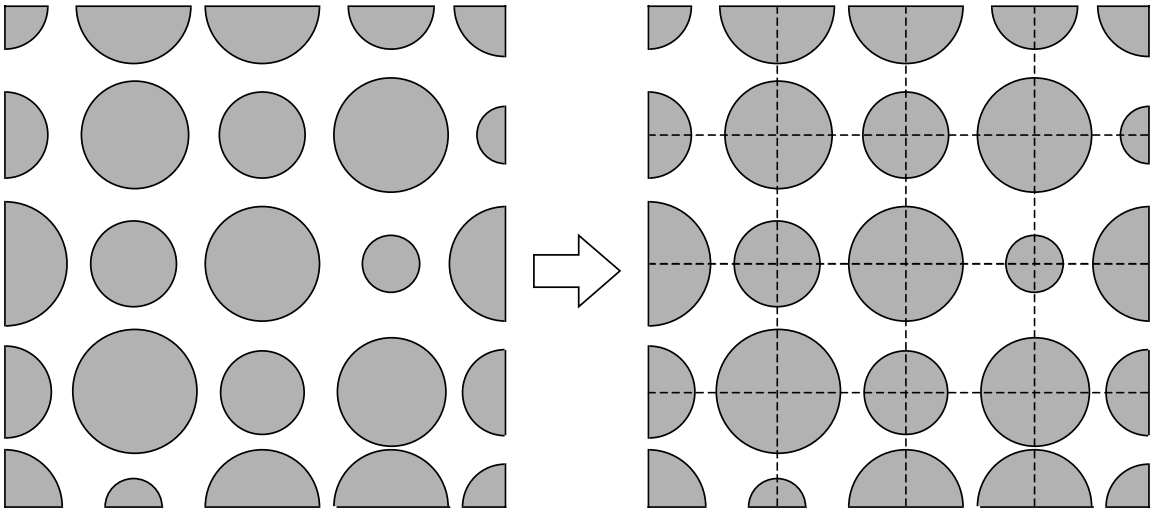

Figure 3.2. Schematic of domain decomposition on a regular grid, using particle centers as discretization points

3.4. Solution Method

3.4.1 Division of the Pore Space into Subdomains

Most techniques for the direct numerical solution of Equation (3.1) are impractical in a large domain such as the one shown previously. Domain decomposition, which helps address this problem, is shown schematically in Figure 3.2; each subdomain can be viewed as a smaller boundary-value

problem. In the following descriptions, subdomains are defined by the fluid phase only, rather than the whole region within a dashed box. Hence, each subdomain will typically include sections of zero-velocity boundary (i.e., any particle surfaces) as well as sections of boundary within the fluid phase. Boundary conditions along interior fluid-phase boundaries are not known initially (i.e., on those boundaries created by the subdivision process), which means the flow problem is not immediately solvable in any one subdomain by itself. As such, the objective of the method is to determine these interior boundary values; once they are known, velocity can be found at an arbitrary point by solving the Stokes equation in that point's subdomain.

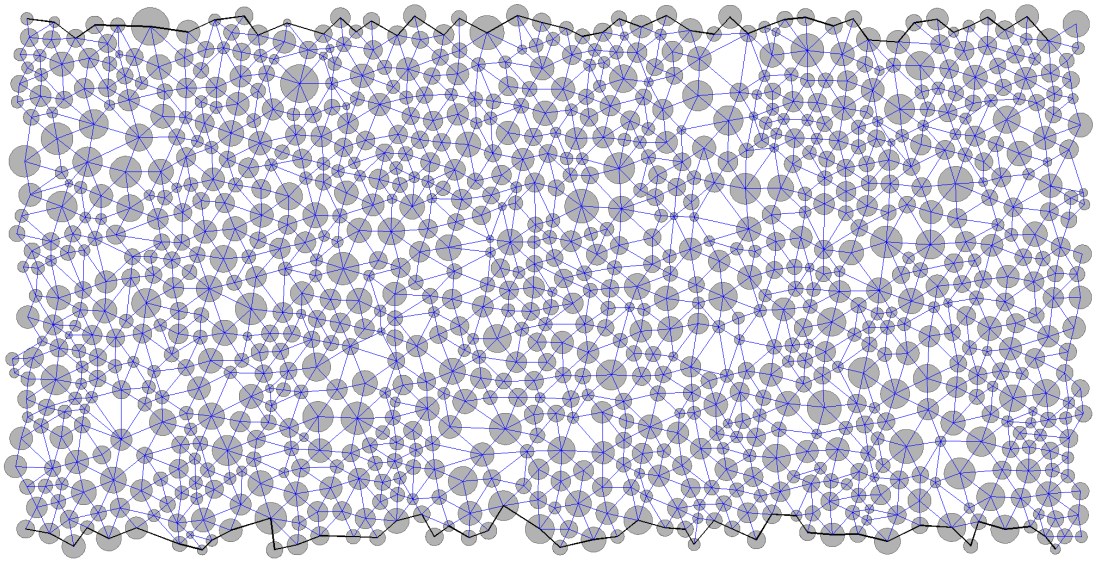

Figure 3.3. Delaunay tessellation of the random porous medium

For simplicity in the schematic, Figure 3.2 was drawn as a regular structure, which immediately suggests the square sudivisions that are shown. A random array does not provide such an obvious strategy, but the schematic still illustrates some important considerations. One question is whether an advantage is gained by pinning the subdomain lattice to the particle centers. As it turns out, this strategy is beneficial because it helps minimize the length of interior fluid-phase boundaries (as

discussed later). In principle, however, the subdivision process is arbitrary, which would be an important consideration if one were to work with media composed of arbitrarily shaped particles.

A Delaunay tessellation is a logical choice for initial discretization of a random domain. It is unique, it joins particle centers, and the structure can be stored and accessed very efficiently. Figure 3.3 is an illustration of the Delaunay tessellation applied to the Figure 3.1 domain. Further refinement of the subdomain can be made by removing internal boundaries from the Delaunay tessellation, and the strategy for this removal process is one of the major points discussed in this chapter. Figure 3.4 is a modified subdomain map that was created by removing the longest fluid-phase boundaries while constraining the maximum subdomain size to 25 particles.

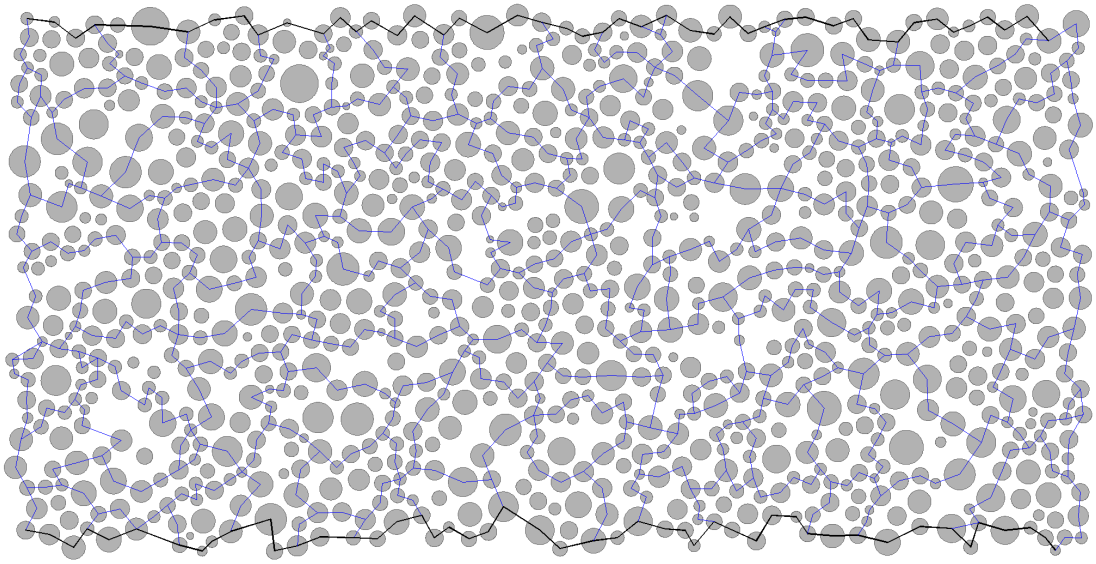

Figure 3.4. Final subdomain map, created by removing the largest internal fluid-phase boundaries from the Delaunay tessellation and limiting subdomain size to 25 particles

3.4.2 Solution of the Stokes Equations Within the Subdomains

A boundary integral method is used to solve Equations (3.1) and (3.2) within each subdomain. The numerical equations are derived from the following integral equation, written for a pole point $\mathbf{x}_0$

on a boundary of one of the subdomains, where *S* indicates the perimeter of the fluid phase in a subdomain (Pozrikidis, 1992):

$$u_j(\mathbf{x}_0) = -\frac{1}{2\pi\mu}\int_S f_i(\mathbf{x})G_{ij}(\mathbf{x},\mathbf{x}_0)dS + \frac{1}{2\pi}\int_S u_i(\mathbf{x})T_{ijk}(\mathbf{x},\mathbf{x}_0)n_k(\mathbf{x})dS\ . \tag{3.3}$$

The terms **f** and **u** are the stress and velocity along the boundary. The Stokeslet **G** and its associated stress tensor **T** depend on the boundary geometry (see Pozrikidis, 1992). For numerical solution, the boundary integral is approximated using a series of *N* finite boundary elements:

$$u_j(\mathbf{x}_0) = -\frac{1}{2\pi\mu}\sum_{n=1}^{N} f_i^n \int_{S_n} G_{ij}(\mathbf{x},\mathbf{x}_0)dS + \frac{1}{2\pi}\sum_{n=1}^{N} u_i^n \int_{S_n} T_{ijk}(\mathbf{x},\mathbf{x}_0)n_k(\mathbf{x})dS\ . \tag{3.4}$$

In this discrete form, the boundary values (stress and velocity) are assumed to be constant over each element and the integrals are evaluated analytically. In two dimensions, one typically must know two of the four boundary values on each element, and the boundary integral equations result in a set of linear equations for the remaining two unknowns. (The four boundary conditions referred to are two velocity plus two stress components.) If velocity is specified everywhere, the equation can be solved only to within an arbitrary pressure. We do not encounter this problem since pressure is specified over the inlet and outlet of the overall flow domain.

In a subdivided domain, (e.g., Figure 3.4), two boundary values (zero velocity) are known along any solid-fluid boundary because of the no-slip condition. Internal fluid-phase boundaries have no known boundary values, but are subject to four equations (i.e., the two vector components of Equation (3.4) written for the two neighboring subdomains). Hence, the subdivided problem, like the original, is well posed.

Since the boundary element method allows discritization on the boundary, the problem is smaller (in term of unknowns) compared with the finite element and finite difference methods, which require discretization of the whole fluid domain. Furthermore, because point velocities in the fluid phase are calculated from the boundary integral equation after the boundary force and velocity are solved, the

velocity field within the fluid domain is continuous even though the values on the boundary are discreet. This is an advantage in the applications in the chapter 4 and 5, where the velocity at arbitrary points in the fluid phase is required to model solute transport in the medium.

The global problem becomes one of solving for all unknown boundary values (two on some boundaries, four on others). Once these are determined, the velocity at an arbitrary point can be determined by computing a relatively small boundary integral defined by the point's associated subdomain. A slight variation of Equation (3.4) (i.e., with different constants) is used to calculate these internal velocities.

3.4.3 Structure and Solution of the Global Problem

The structure of the coefficient matrix in the global problem impacts the method and efficiency of solution. Combining all the unknowns in each block to form a global system, the matrix has a block-diagonal structure with sparse off-diagonal components. Terms in the blocks are integral coefficients for variables associated with the subdomain whose boundary is being integrated. Off-diagonal terms are integral coefficients for variables on that same boundary, but which have been assigned to neighboring subdomains. Non-zero terms in the right-hand-side vector are from boundary integral terms where the velocity or stress is known.

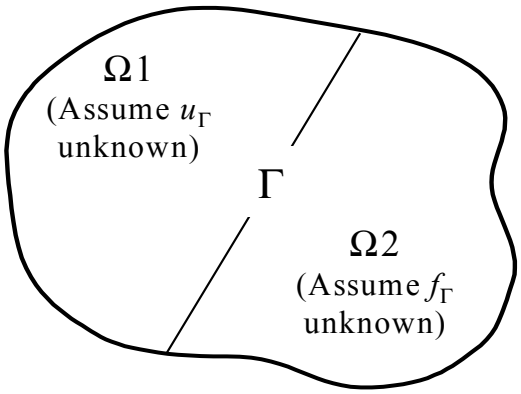

Figure 3.5. Hypothetical subdivided domain with split boundary conditions along the common boundary

The resulting matrix structure is shown schematically for the simple subdivided domain in Figure 3.5. Assume that stresses are known on the external boundaries of Ω1 and Ω2 (and that no-slip conditions exist somewhere in each subdomain). Assume also that unknown stresses on Γ are

assigned to the Ω1 subdomain while unknown velocities on Γ are assigned to the Ω2 subdomain. Then, the resulting block-diagonal matrix has the form

$$\begin{bmatrix} (1-\mathbf{T}_{11}) & \mathbf{G}_{1\Gamma} & -\mathbf{T}_{1\Gamma} & \\ -\mathbf{T}_{\Gamma 1} & \mathbf{G}_{\Gamma\Gamma} & (1-\mathbf{T}_{\Gamma\Gamma}) & \\ & -\mathbf{G}_{\Gamma\Gamma} & (1-\mathbf{T}_{\Gamma\Gamma}) & -\mathbf{T}_{\Gamma 2} \\ & -\mathbf{G}_{2\Gamma} & -\mathbf{T}_{2\Gamma} & (1-\mathbf{T}_{22}) \end{bmatrix} \begin{bmatrix} \mathbf{u}_{S1} \\ \mathbf{f}_{\Gamma} \\ \mathbf{u}_{\Gamma} \\ \mathbf{u}_{S2} \end{bmatrix} = \begin{bmatrix} -\mathbf{G}_{11}\mathbf{f}_{S1} \\ -\mathbf{G}_{\Gamma 1}\mathbf{f}_{S1} \\ -\mathbf{G}_{\Gamma 2}\mathbf{f}_{S2} \\ -\mathbf{G}_{22}\mathbf{f}_{S2} \end{bmatrix} \tag{3.5}$$

where S_1 and S_2 are the outer boundaries of the two subdomains, **G** and **T** are matrices containing the discretized boundary integrals, and **u** and **f** are vectors containing the discretized velocities and forces. The upper half of the matrix represents the boundary integral equations for Ω1, and the off-block terms (shown in the first two rows of column three) are from velocities along Γ, because $\mathbf{u}_\Gamma$ terms were assigned to Ω2.

For multi-domain problems, Equation (3.5) is solved by a block-by-block approach (Schwarz method), in which the block solutions are patched to form the solution of the global problem. In order to solve problem in each block, two of the four unknowns along shared boundaries must be treated as known values, in order to formulate a square matrix that can be solved. Additionally, one must incorporate known stresses into each subdomain to avoid creating singular blocks.

The logistics of these variable assignments are dealt with using a depth-first search (Chartrand and Oellermann, 1993). Each bond in the depth first graph search represents one boundary while each node represents one subdomain. The search starts with one subdomain with known stress (pressure) at the entrance of the packing, and the subdomain above each bond will take velocity as "known" while the subdomain below each bond takes the stress as "known". The starting subdomain has a known stress boundary while all other subdomains appear on the depth first search graph has at least one bond that is assigned as stress boundary. Accordingly, each subdomain is assigned both stress and velocity (non-slip boundary on the sphere surface) boundary conditions. Using this approach, Equation (3.5) can be divided into two systems as shown by Equations (3.6) and (3.7).

$$\begin{bmatrix} (1-\mathbf{T}_{11}) & \mathbf{G}_{1\Gamma} \\ -\mathbf{T}_{\Gamma 1} & \mathbf{G}_{\Gamma\Gamma} \end{bmatrix} \begin{bmatrix} \mathbf{u}_{S1} \\ \mathbf{f}_{\Gamma} \end{bmatrix} = \begin{bmatrix} -\mathbf{G}_{11}\mathbf{f}_{S1} + \mathbf{T}_{1\Gamma}\mathbf{u}_{\Gamma} \\ -\mathbf{G}_{\Gamma 1}\mathbf{f}_{S1} - (1-\mathbf{T}_{\Gamma\Gamma})\mathbf{u}_{\Gamma} \end{bmatrix} \tag{3.6}$$

$$\begin{bmatrix} (1-\mathbf{T}_{\Gamma\Gamma}) & -\mathbf{T}_{\Gamma 2} \\ -\mathbf{T}_{2\Gamma} & (1-\mathbf{T}_{22}) \end{bmatrix} \begin{bmatrix} \mathbf{u}_{\Gamma} \\ \mathbf{u}_{S2} \end{bmatrix} = \begin{bmatrix} -\mathbf{G}_{\Gamma 2}\mathbf{f}_{S2} + \mathbf{G}_{\Gamma\Gamma}\mathbf{f}_{\Gamma} \\ -\mathbf{G}_{22}\mathbf{f}_{S2} + \mathbf{G}_{2\Gamma}\mathbf{f}_{\Gamma} \end{bmatrix} \tag{3.7}$$

For small problems, the iterative Schwarz method can be used directly to solve this problem by a two-step process. First, Equation (3.6) is solved for $\mathbf{u}_{S1}$ and $\mathbf{f}_{\Gamma}$, and then Equation (3.7) is solved for $\mathbf{u}_{\Gamma}$ and $\mathbf{u}_{S2}$. This approach, which is equivalent to a block Gauss-Seidel technique, is nonconvergent for the larger problems that we tested.

Table 3.1: The Multidomain and Multiplicative Schwarz Algorithm

Solve $DU = f$ with a BiCGStab method using

$v =$ MatrixMultiply (U)

$v1 = D1 \cdot U1 + D12 \cdot U2$

$v2 = D2 \cdot U2 + D21 \cdot U1$

$v =$ Precondition (U)

$v1 = D1^{-1} \cdot U1$

$v2 = D2^{-1}(U2 - D21 \cdot v1)$

Where $\boldsymbol{U}$ is input vector and $\boldsymbol{v}$ is output

By using the information from more than one previous iterative step, a Krylov subspace method typically can improve the convergence. A stabilized biconjugate gradient method was used because it leads to smooth convergence and economic implementation (Van Der Vorst, 1992). A multidomain multiplicative Schwarz method (Smith et al., 1996) is used as a preconditioner. In order to illustrate this algorithm, we rewrite the Equation (3.5) as

$$\begin{pmatrix} D1 & D12 \\ D21 & D2 \end{pmatrix} \begin{pmatrix} U1 \\ U2 \end{pmatrix} = \begin{pmatrix} f1 \\ f2 \end{pmatrix}, \tag{3.8}$$

by letting $D1 = \begin{bmatrix} (1-\mathbf{T}_{11}) & \mathbf{G}_{1\Gamma} \\ -\mathbf{T}_{\Gamma 1} & \mathbf{G}_{\Gamma\Gamma} \end{bmatrix}$, $D12 = \begin{bmatrix} -\mathbf{T}_{1\Gamma} & \mathbf{0} \\ (1-\mathbf{T}_{\Gamma\Gamma} & \mathbf{0} \end{bmatrix}$, $D12 = \begin{bmatrix} 0 & -\mathbf{G}_{\Gamma\Gamma} \\ 0 & -\mathbf{G}_{2\Gamma} \end{bmatrix}$, $D1 = \begin{bmatrix} (1-\mathbf{T}_{\Gamma\Gamma}) & -\mathbf{T}_{\Gamma 2} \\ -\mathbf{T}_{2\Gamma} & (1-\mathbf{T}_{22}) \end{bmatrix}$

The multidomain multiplicative Schwarz algorithm can be stated in Table 3.1.

The two steps MatrixMultiply and Precondition in the algorithm above are used in the BiCGStab algorithm that is stated in Table 3.2 (Van Der Vorst, 1992).

Table 3.2 The BiCGStab Algorithm

Given the linear system **Du** = **f**, we can start with an initial guess $\mathbf{u}_0$ for **u**, we have:

1. $\mathbf{r}^0 = f - Du^0$, $\mathbf{p}^0 = \mathbf{q}^0 = \mathbf{0}$, $\alpha = \omega_0 = 1$
2. For m =1, 2, … until converge
   - 2.1 $\beta = \left[(\mathbf{r}^0, \mathbf{r}^{m-1})\alpha\right] / \left[(\mathbf{r}^0, \mathbf{r}^{m-2})\omega_{m-1}\right]$
   - 2.2 $\mathbf{p}^m = precondition(\mathbf{r}^{m-1} - \beta\omega_{m-1}\mathbf{q}^{m-1}) + \beta\mathbf{p}^{m-1}$
   - 2.3 $\mathbf{q}^m = MatrixMultiply(\mathbf{p}^m)$
   - 2.4 $\alpha = (\mathbf{r}^0, \mathbf{r}^{m-1}) / (\mathbf{r}^0, \mathbf{q}^m)$
   - 2.5 $\tilde{\mathbf{s}}^m = \mathbf{r}^{m-1} - \alpha\mathbf{q}^m$
   - 2.6 $\mathbf{s}^m = precondition(\tilde{\mathbf{s}}^m)$
   - 2.7 $\mathbf{t}^m = MatrixMultiply(\mathbf{s}^m)$
   - 2.8 $\omega_m = (\mathbf{t}^m, \tilde{\mathbf{s}}^m) / (\mathbf{t}^m, \mathbf{t}^m)$
   - 2.9 $\mathbf{u}^m = \mathbf{u}^{m-1} + \alpha\mathbf{p}^m + \omega_m\mathbf{s}^m$
   - 2.10 $\mathbf{r}^m = \tilde{\mathbf{s}}^m - \omega_m\mathbf{t}^m$

The stiff matrix and variables are all stored locally in the implementation. Index arrays are used to combine data in each subdomain together. This strategy also facilitates parallelization of the algorithm, which could be employed in the future.

3.5 Results and Analysis

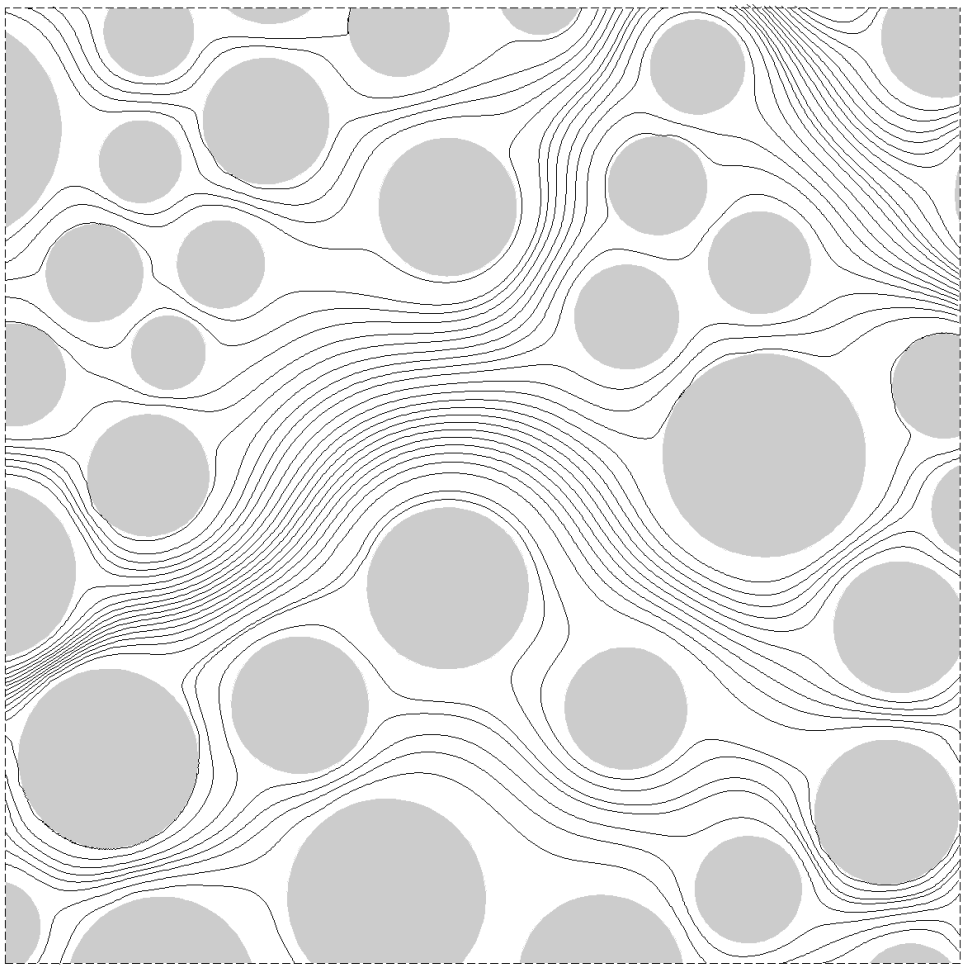

Figure 3.6 Streamlines in a small region of the 1000-particle domain

3.5.1 Format of the Solution

The solution consists of all boundary values that were originally not known: velocities over the inlet and outlet, stresses on all particle surfaces, stresses on no-flow boundaries, and both velocity and stress on the internal fluid-phase boundaries. One advantage of this approach is that the final data set, which might be stored for subsequent stochastic simulations, is very compact, requiring only the pore and subdomain structure, the boundary discretization, and the boundary values. The latter two

data sets are relatively small because of the reduction in dimension associated with the boundary integral method.

Once the global solution is found (or loaded from a previous run), the velocities at arbitrary points in the fluid phase can be recovered by calculating local boundary integrals. Because analytic expressions for the integrals in Equation (3.4) are available, this calculation is quite efficient and works well when coupled with stochastic algorithms for solute transport.

Figure 3.6 shows a streamline plot within a small area of the larger porous medium. This plot was generated by recovering velocities in the manner described above and integrating along a streamline using Euler's method.

3.5.2 Effect of Subdomain Structure

For a random packing there will exist a unique Delaunay tessellation (in the absence of degeneracies and/or numerical error). The final subdomain structure, on the other hand, is not unique since it is generated by removing internal boundaries from the original Delaunay tessellation. The strategy used to create this map is of critical importance for the convergence behavior.

Our results show that the most effective strategy is to remove internal boundaries that span the largest fluid-phase gaps (thus leaving internal boundaries across the smallest particle-particle gaps). At first, removal of large internal boundaries will create more ‘pore-like’ subdomains because many boundaries in the tessellation span large void spaces (see Figure 3.3). As removal continues, the subdomains tend to become large convoluted shapes that no longer resemble pores, and the remaining internal boundaries span only the smallest particle-particle gaps in the domain (see Figure 3.4).

The effect that this removal strategy has on convergence is related to the generation of off-block matrix coefficients. Specifically, all internal fluid-phase boundaries generate off-block coefficients because of the boundary-value assignments described above, and the preconditioner does not operate above the diagonal (or more precisely, above the blocks). In essence, removing an internal fluid-

phase boundary eliminates a set of unknowns that appear explicitly in the global problem. Their effect is still felt implicitly in the boundary integral equations and therefore in the structure of the blocks. This implicit presence seems to be preferable since blocks are inverted directly during preconditioning.

The suggestion made above that subdomains should be created by removing larger boundaries is illustrated quite dramatically by comparing the two subdomain maps shown in Figure 3.7. Both maps are generated on the identical 81-particle porous medium (very slightly disordered), and both maps contain 64 subdomains. The boundary-element discretization was performed so as to generate the same number of equations and the same number of off-block coefficients in both cases. However, convergence was achieved in 19 iterations for the case shown in Figure 3.7a, versus 73 iterations when the longer internal boundaries were chosen (Figure 3.7b).

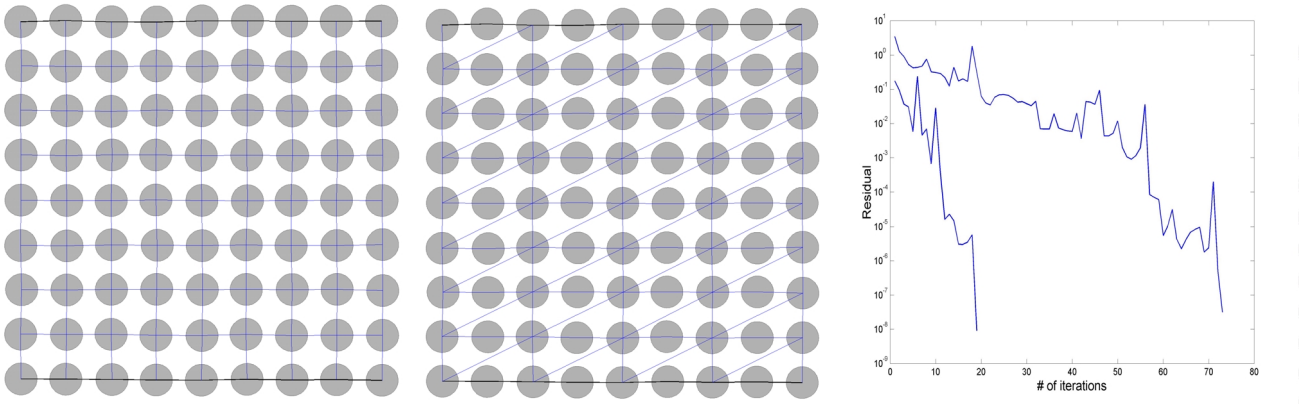

(a) (b) (c)

Figure 3.7.81-particle domain: (a) short interior subdomain boundaries; (b) long interior subdomain boundaries; (c) convergence of the (a) and (b) divisions

The equivalent structure of the matrices in the above example suggests that conditioning is the dominant factor in solution efficiency. This effect can be quantified using the six-particle flow cell shown in Figures 3.8a and 3.9a. Like the larger example, it can be subdivided in the two different

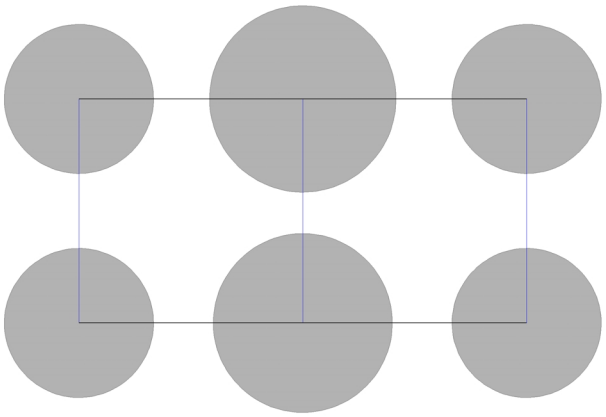

(a)

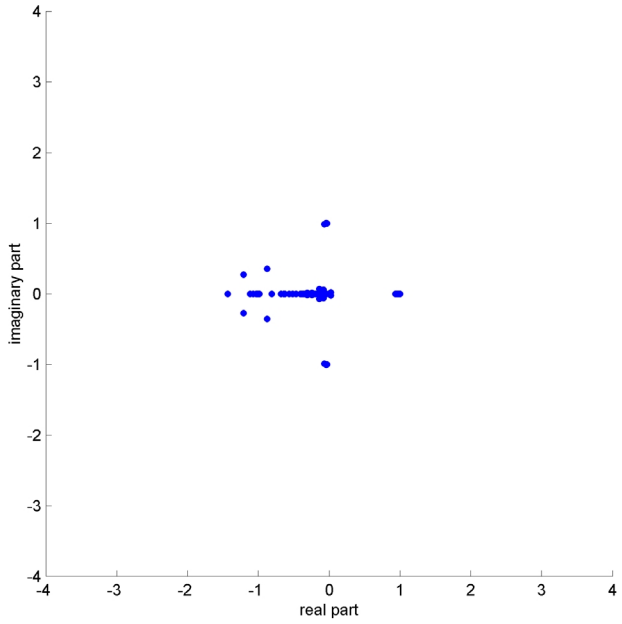

(b)

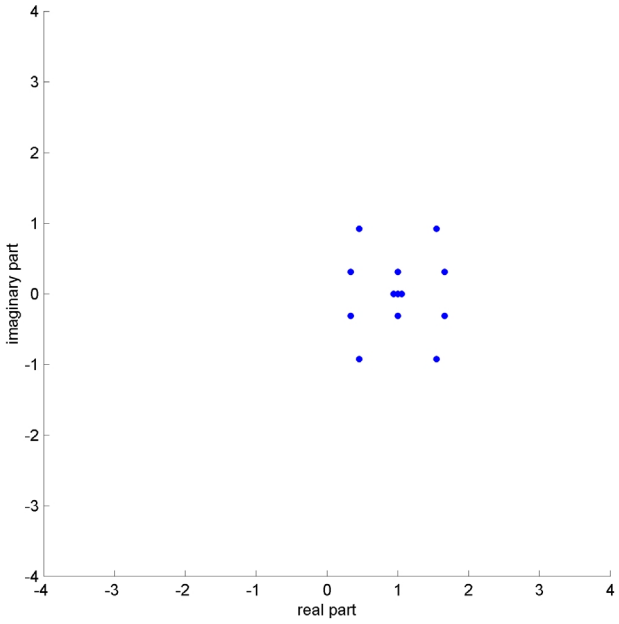

(c)

Figure 3.8. (a) six particle domain with short subdomain boundary; (b) eigenvalue distribution for block matrix before preconditioning; (c) eigenvalue distribution for block matrix after preconditioning

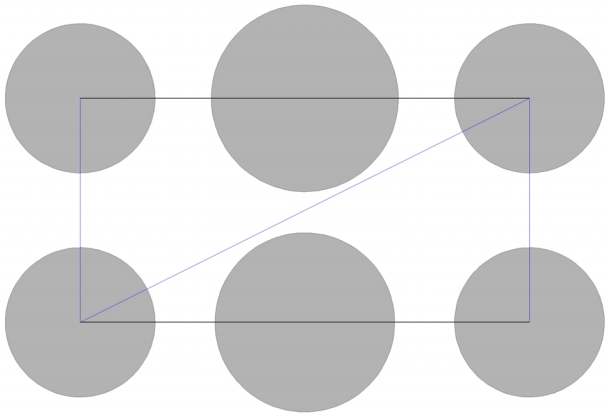

(a)

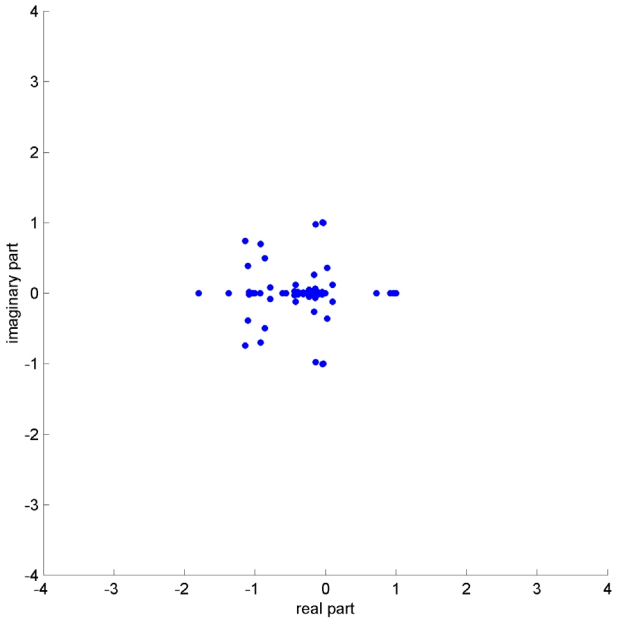

(b)

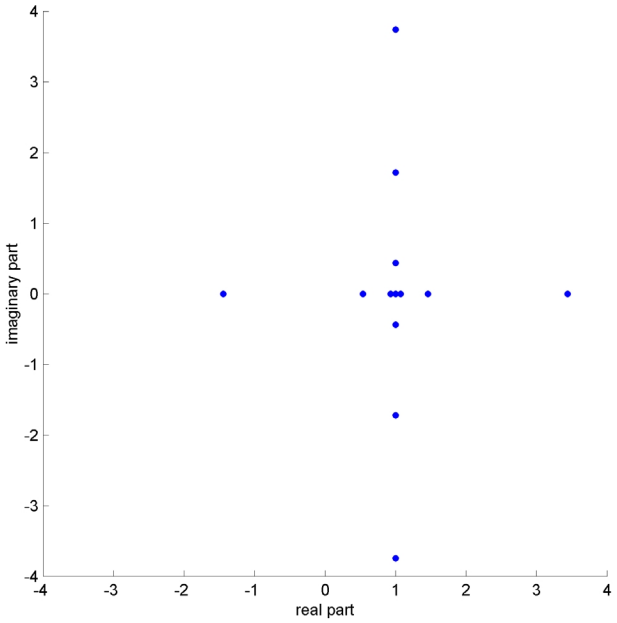

(c)

Figure 3.9. (a) six particle domain with long subdomain boundary; (b) eigenvalue distribution for block matrix before preconditioning; (c) eigenvalue distribution for block matrix after preconditioning

ways shown. The small size of this problem allows us to set up the two-block global matrix equation and examine the conditioning directly. Figures 3.8b and 3.8c show eigenvalues for the short-boundary case before and after preconditioning using the Schwarz method. Figures 3.9b and 3.9c show eigenvalues for the long-boundary case before and after preconditioning. The condition numbers remain large for both matrices after preconditioning. However, the eigenvalues are more closely clustered around $\lambda = 1$ for the short-boundary case, which improves the convergence of Krylov-subspace-based iterative techniques (Trefethen and Bau, 1997).

3.5.3 Effect of Subdomain Size on Convergence

The other aspect of boundary removal is the size of the resulting subdomains. Larger subdomains result in larger but fewer blocks in the coefficient matrix, which one would expect to affect solution times. We quantify the size of these blocks using the number of particles per subdomain (either on or inside the boundary) for a couple of reasons. First, this parameter is used to monitor and control subdomain size in the boundary removal subroutine. Second, since the boundary element method requires a boundary discretization, the number of particles per subdomain is more-or-less proportional to the number of equations per block that end up in the matrix.

Figure 3.10 shows number of iterations (for convergence) versus subdomain size for a 100-particle random medium. The sharp improvement in convergence for small subdomains (i.e., changes from three particles with the Delaunay tessellation to four or five particles per subdomain) is observed for two reasons. First, long fluid-phase boundaries are removed (which contributes to improved convergence and fewer equations). Second, there appears to be a beneficial effect that occurs because larger pieces of the flow problem are being solved directly during the preconditioning step. (Recall that blocks are inverted for preconditioning, which is equivalent to directly solving subdomain flow problems using current guesses for boundary values.)

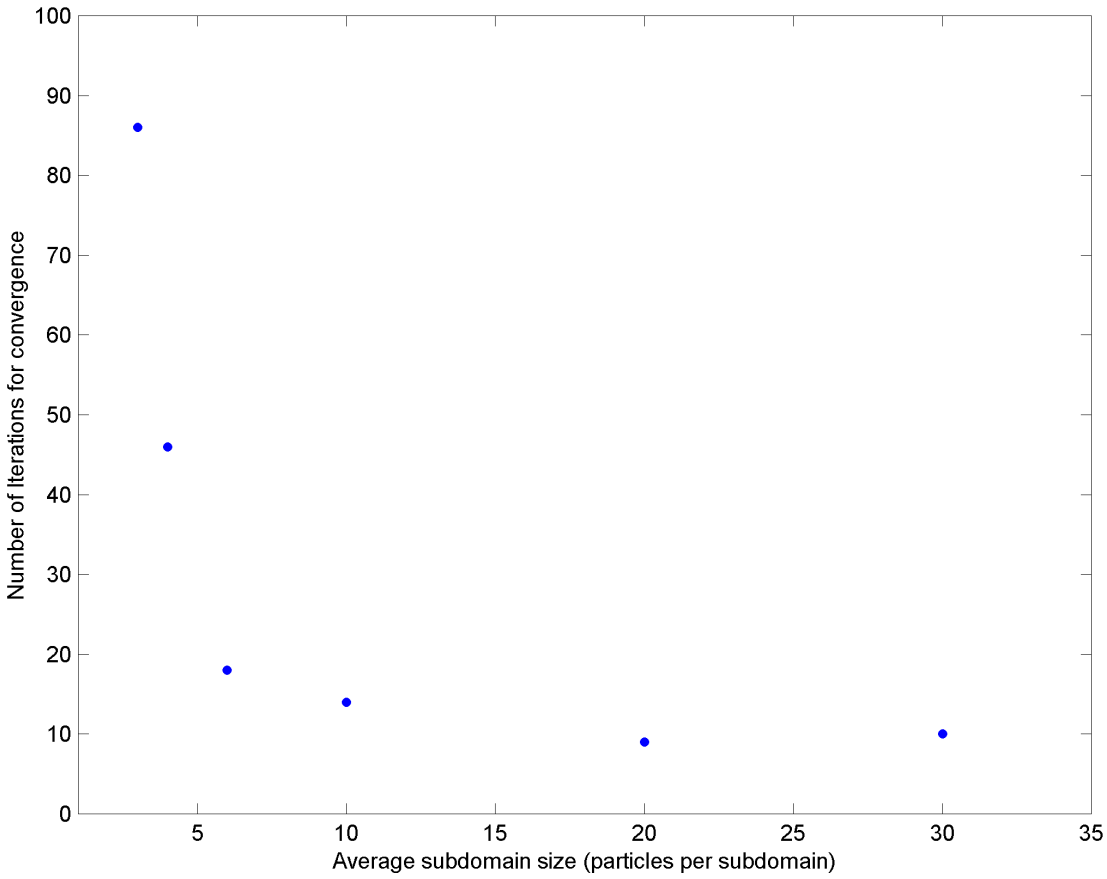

Figure 3.10. Number of iterations for convergence versus subdomain size for a 100-particle random domain

3.5.4 Overall Efficiency

The overall efficiency is more complicated to analyze because it is related not only to subdomain size and shape, but also to practical issues such as memory limits and whether parallel processing is used.

Consider first the overall efficiency in the absence of memory limits and assuming sequential rather than parallel processing (single-processor computations have been used in this work). The overall time for solution is consumed mostly by two operations: the inversion of all blocks (to be

used for subsequent preconditioning steps) and the iterative solution process. Inversion of the blocks in the matrix must be performed only once, and the time requirement is proportional to N^3, where N is the number of equations per block (which we assume for the moment to be constant). Once the inversions are complete, the iterative part of the solution requires an additional time

$$t_i = \textit{number of iterations} \times \textit{number of subdomains} \times \textit{calculation time per subdomain.}$$

The calculation time per subdomain scales as N^2 for the vector operations in the biconjugate gradient algorithm. However, this penalty is essentially offset by two competing factors: the improved efficiency (i.e., fewer iterations) as the blocks become larger and the decrease in the total number of subdomains on which to operate. There is a rather complicated relationship between subdomain size (in number of particles) and total number of subdomains in the system. Hence, the efficiency and number of subdomains were measured empirically from our calculations.

These empirical data were combined with the scaling arguments to produce the plot of approximate solution time versus subdomain size shown in Figure 3.11. The y-axis is nondimensionalized using the hypothetical time that would be required with only a single subdomain (i.e., inversion of the entire full matrix). For small subdomains, a rapid improvement with size occurs because of two effects: first, the removal of large internal boundaries (as discussed above), and second, changes in subdomain shape (e.g., from two triangles to a square), which often reduce the total perimeter and therefore the number of equations considerably. However, for larger subdomains, performance becomes slower with increasing size because as two large subdomains are combined, the improvement in efficiency and the very small reduction in the total number of equations cannot offset the cost of doubling the block size (which is a one-time N^3 penalty for preconditioning plus a repeated N^2 penalty during iteration). The net effect of these factors produces an optimum theoretical performance at around six particles per subdomain for the 100-particle domain used in this example.

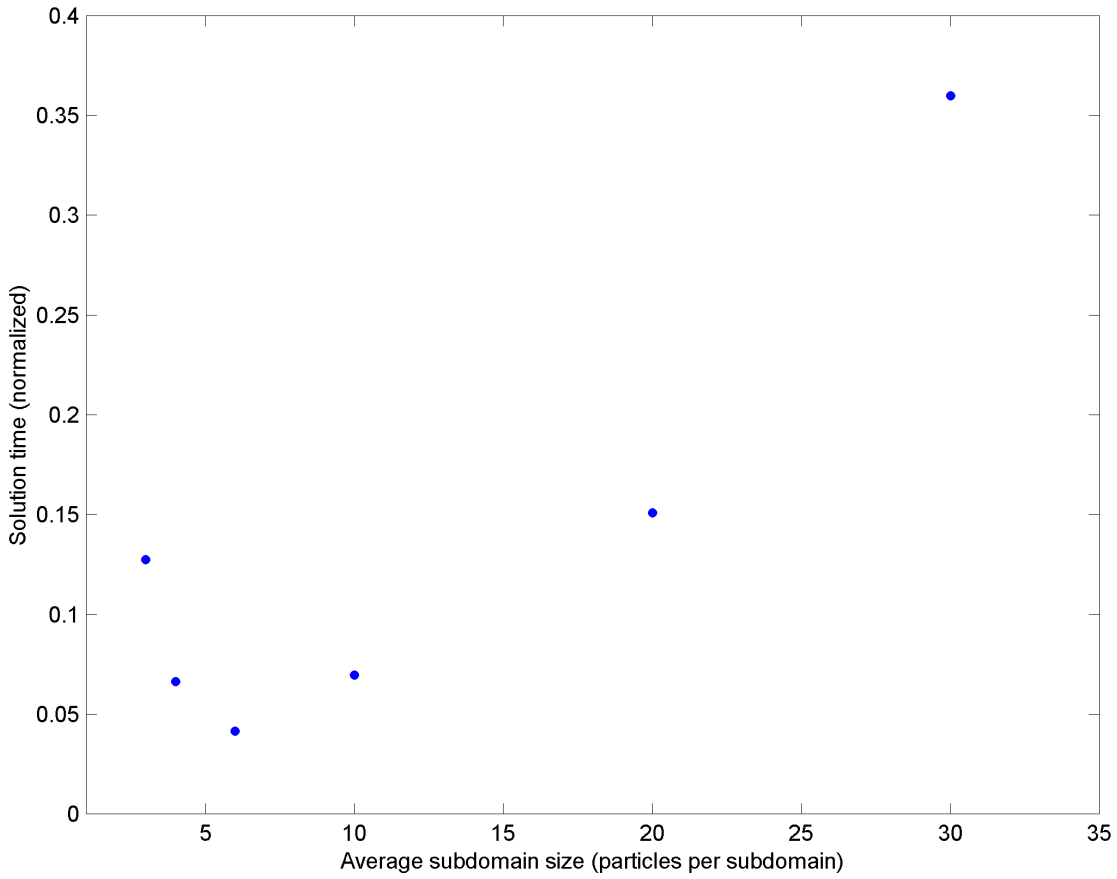

Figure 3.11. Theoretical solution time versus subdomain size for a 100-particle random domain

Recalling that the above arguments neglected memory limitations, they must be tempered with practical considerations. In the single-processor solutions performed in our work, the nonzero matrix coefficients as well as the inverted blocks are stored on disk because of their large size, and repeated retrieval of these data dominates the total solution time (90-95%). Consequently, we observe continued improvements in efficiency well past the subdomain size shown in Figure 3.11 because it is more efficient to read coefficients from a large block and its inverse at once, whereupon they are used for multiple vector operations in the biconjugate gradient method. An optimum still occurs in

these single-processor calculations at the point where data associated with a single block exceeds the random-access memory of the processor and begins using virtual memory.

For parallel processing (which is being used for future work), the considerations are slightly different. Uniformity of subdomain size and the number of subdomains should be considered. With sufficiently large distributed memory, optimum performance should occur nearer the theoretical minimum (calculated for a given problem) than it did in our computations.

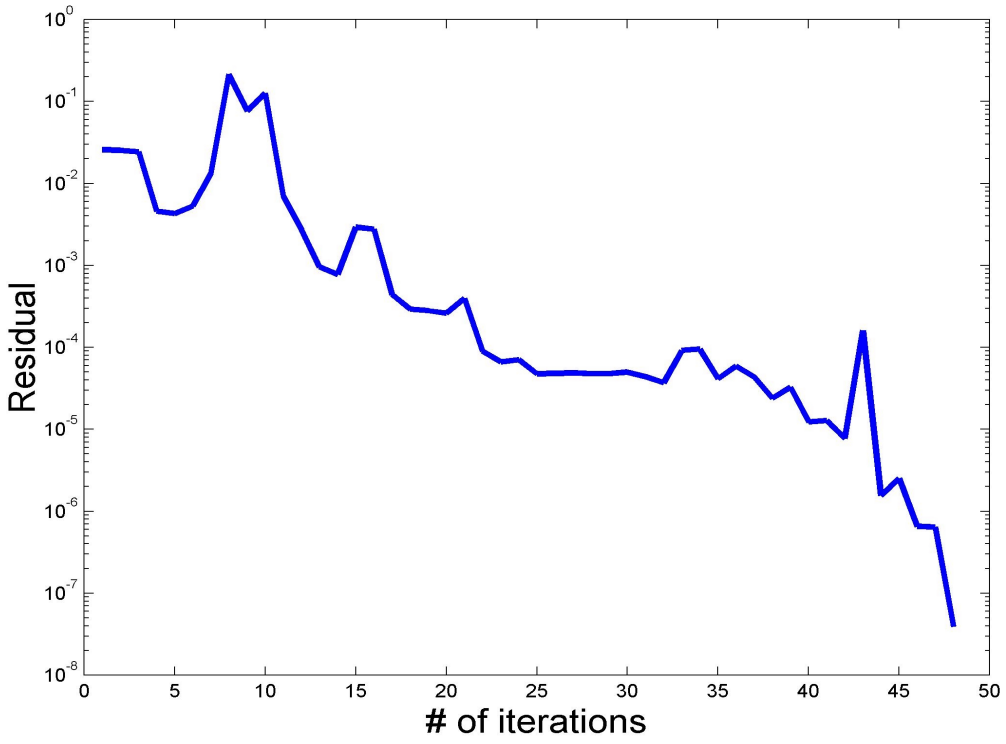

Figure 3.12 Convergence of domain with 1000 particles after optimized domain decomposition

Figure 3.12 shows convergence of one realization of the domain shown in Figure 3.1 after the optimized domain decomposition. The Fortran 77 program was run on a 500 MHz PC with 256M RAM. 48 iterations were needed for the converge and each iteration takes about 25 minutes of CPU time. However, 95% of the total solution time was spent on read/write operations to the disk due to memory limitations. This limitaiton is significant considering the problem size (about 5E5 variables).

One of the most important aspects of this type of problem is how the solution time scales with problem size, because poor scaling will prevent one from significantly increasing the problem size, even with more powerful computers.

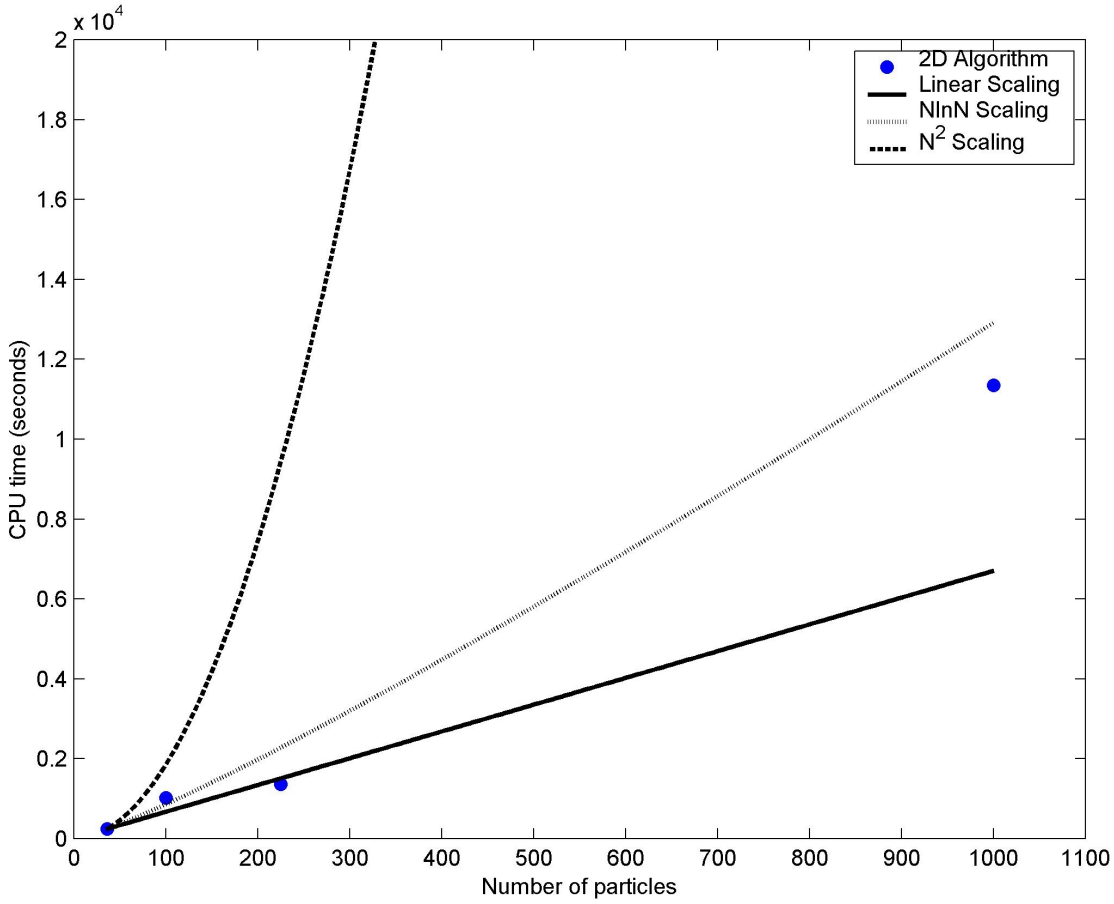

Figure 3.13 Scaling efficiency of the algorithm

To investigate the scaling efficiency of this algorithm, we compare the CPU time for solution in packings having 36, 100, 225 and 1000 particles under otherwise similar conditions (i.e., the same subdomain size and the same computer). Figure 3.13 shows the empirical results, which scale as $N \ln(N)$, or even slightly better. This is a very significant result, as most algorithms scale as N^2, although other recent advances have also produced $N \ln(N)$ algorithms (Higdon and Viera, 2000).

3.6 Summary and Conclusions

While lattice-Boltzmann methods have become the method of choice for solving low-Reynolds-number flow problems in unstructured porous materials, efficient algorithms for direct numerical solution may have advantages in certain situations. The technique discussed here combines important attributes of domain decomposition and boundary-integral methods. The approach is used on a comparatively large, very heterogeneous problem, which demonstrates its flexibility and efficiency.

Numerically, the method gives a strongly block-diagonal matrix that is solved using a biconjugate gradient method with block preconditioning. We show that the subdomain structure strongly affects the solution efficiency. In particular, minimizing the length of subdomain boundaries in the fluid phase is important. This effect is related to the generation of off-block terms in the coefficient matrix, some of which are not operated on by the block preconditioner. Subdomain size is the second important parameter. We show, using scaling arguments and empirical results that an optimum subdomain size exists (in the absence of memory limitations). Our runs were performed on a single processor; consequently data retrieval time dominated the solution time and the optimum subdomain size was much larger than the predicted optimum.

The large problems required relatively few iterations for convergence given the very large matrix sizes (e.g., 45 iterations for the 1000-particle problem shown above, which produced ~ 5×10^5 equations). We expect that in the parallel framework being used in future work, iterations for this size problem will require on the order 10-20 seconds. Hence, the overall time requirements for solution are very reasonable.

A couple of other issues are of interest in the context of stochastic modeling of transport processes (for which these simulations are being used). First, the complete solution set can be stored very compactly since it consists of only the boundary discretization and boundary values. Second, the recovery of point velocities is efficient since it requires only a local boundary integral calculation

once the global solution is known. Third, local grid refinement is trivial in this algorithm because of the one-dimensional discretization. This allows one to obtain very accurate velocities in critical regions of the domain such as tight particle-particle gaps or near solid-fluid interfaces undergoing heat or mass transfer.

CHAPTER 4. HIGH RESOLUTION AND NETWORK MODELS FOR SIMULATION OF DISPERSION IN POROUS MEDIA

4.1 Introduction

Modeling transport in porous media is most often performed at the continuum scale. However, the continuum approach requires the estimation of macroscopic parameters such as permeability, dispersion coefficients, etc. Typically, the prediction of these and other parameters is performed experimentally or using existing empirical correlations. However, experiments can be slow and costly, while generalized empiricism has not proved to be effective for many complex processes such as multiphase flow.

The obvious alternative is the modeling of these transport processes at the microscale, which allows more fundamental governing equations to be used than with continuum approaches. The obvious drawback is that because of the complex structure found in porous media, the solution of the fundamental equations rapidly becomes intractable as the domain size increases or the physics of the transport processes becomes complex. Network modeling strikes a compromise between fundamental and approximate approaches. It resolves a porous medium's structure at the pore scale, yet uses a number of simplifications to avoid direct solution of the equations of motion. Network modeling techniques have become increasingly quantitative in recent years, which improves the likelihood that they can be used as predictive tools. Still, the approximations inherent to this approach prevent a first-principles analysis of most processes, and it is important to quantify the effect of the various limitations on network modeling results.

The purpose of the research described in this chapter is to study two important assumptions inherent to network modeling: 1. the discretization of the pore space into pores and pore throats; 2. The complete mixing assumption in pore bodies. To quantify these effects, a direct comparison is

made between results from network modeling and results from high-resolution modeling (the latter of which is a new method to obtain streamline resolution of flow by direct solution of the equations of motion). The porous medium used to make these comparisons is a two-dimensional, heterogeneous packing of circular particles. While current network modeling techniques allow much larger and more complicated materials to be modeled, the use of this simpler structure enables high-resolution modeling to be performed on the same packing. Two macroscopic parameters were chosen for comparison: single-phase permeability and the solute dispersion tensor.

4.2 Hydrodynamic Modeling

4.2.1 Description of the Model Porous Medium.

The model porous material used in this work is a two-dimensional packing of discs. It contains a significant size distribution, which leads to a fairly heterogeneous packing as shown in Figure 3.1. This two-dimensional packing was used so as to allow for detailed solution of the hydrodynamics, while at the same time allowing for reasonably large length scales within the packing. Both the high-resolution modeling technique and the network approach for this packing are described below.

4.2.2 High-Resolution Modeling of Stokes Flow

Flow through porous media can oftentimes be represented by Stokes equations for low-Reynolds-number flow because of the low velocities and small characteristic lengths within the voids. In Chapter 3, we developed an efficient solution technique using domain decomposition combined with a boundary element method, which allows for the efficient modeling of Stokes flow in reasonably large, disordered porous media. Its advantages are its efficient scaling (of computation time) with domain size, and the ease with which local grid refinement can be implemented. This latter fact allows for very accurate resolution of flow, even within tight particle-particle gaps, which is necessary for modeling transport in thermal or concentration boundary layers, for instance.

Once the flow field is known, permeability is calculated from the total flux using the one-dimensional form of Darcy's law:

$$k = \frac{Q}{L_y} \cdot \frac{L_x}{\Delta P} \cdot \mu, \tag{4.1}$$

Here, k is the permeability of the simulated packing, Q is the total flux, L_x is the length of the packing at the mean flow direction, L_y is the width perpendicular to the flow, ΔP is the total pressure drop, and μ is the viscosity of the fluid.

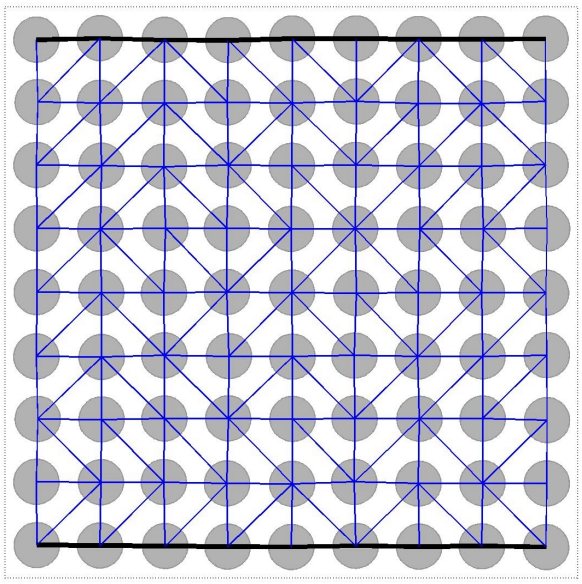

Figure 4.1 Delaunay tessellation of a square packing

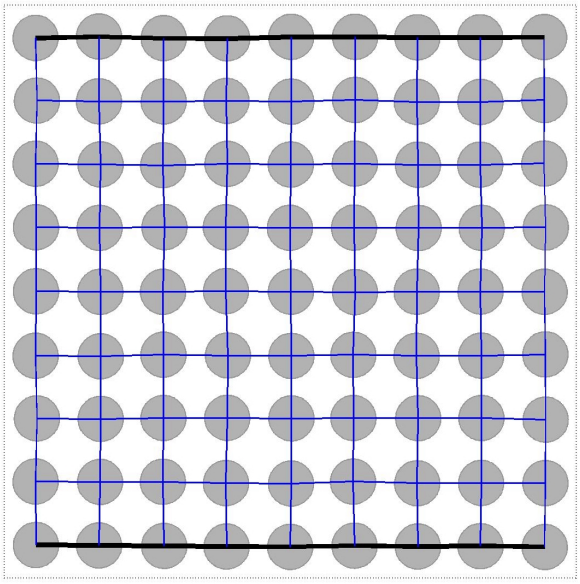

Figure 4.2 Square discretization of a square packing

4.2.3 Network Modeling of Fluid Flow

To create a pore and pore-throat network from the two-dimensional packing, a Delaunay tessellation was used, which is a common technique in three dimensions (e.g., Bryant et al., 1993). The technique was modified slightly to allow for different network structures, and is summarized as follows.

1. Perform a Delaunay tessellation (of the positions of the particle centers), which in two dimensions produces an array of triangles, each having the centers of three circles at its vertices.
2. Merge Delaunay cells by removing certain boundaries that may not be good representations of network throats.
3. Calculate the conductivity of each throat according the local geometry, where pore throats are defined by the common edges between any two polygons defined in step 2.
4. Determine the pore locations in the network, using the centers of mass of the polygons defined in step 2.
5. Determine the length and radii of each pore throat in the network. The length of each throat is determined by the positions of its two associated pores; the radius is back calculated from the length and conductivity obtained in step 3. The purpose of this step is to maintain proper pore-space dimensions. It is necessary for capturing correct displacements during dispersion modeling because the network approximation neglects flow in the network pores.

Steps 1 and 2 are illustrated in Figures 4.1 and 4.2 for a 9×9 particle medium on a square lattice, which contains slight disorder to allow for a non-degenerate Delaunay tessellation. Figure 4.1 is a schematic of the tessellation. Figure 4.2 is a schematic of the modified tessellation, in which the diagonal boundaries have been removed to generate square cells. Each square cell is defined to be a pore, while each boundary is defined to be a throat in the network model.

In the current work, a simplistic approach is used to calculate the throat hydraulic conductivities, based simply on the geometry of the gap between two spheres. The conductivity is given by the equation

$$g = \frac{1}{3}\left(\frac{d}{2}\right)^2 \cdot \frac{(L1 + L2)}{2\mu} \tag{4.2}$$

where the parameters in this equation are defined in Figure 4.3. The rationale for this simplistic approach is that the most important factor in this definition is to represent the *relative* conductivity of various sized throats; a single, scalar adjustment to all throats can be made at a later time based on an empirical match to a known permeability.

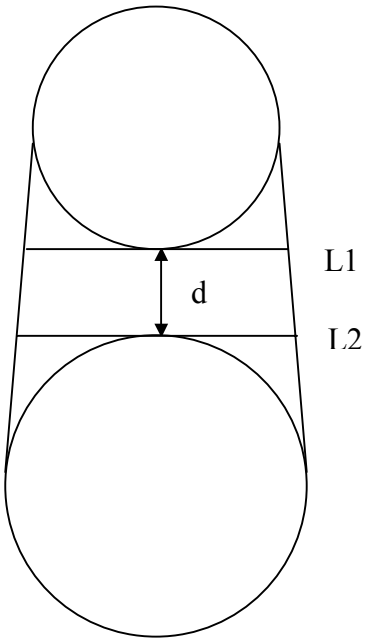

Figure 4.3 Schematic of the pore throat for the conductivity calculation

As described in Step 5 above, each bond is assigned a length (from the cell positions) and radii (from the conductivities). The network model constructed as such retains the basic structure of the two-dimensional porous medium, but allows for highly simplified hydrodynamic calculations. Specifically, the flow is calculated from the pressure distribution, which is obtained from a system of linear equations (as described elsewhere; see Thompson, 2002). Once the pressure field is known, the permeability of the network can be calculated directly from Darcy's law.

4.3 Dispersion Modeling

Solute transport processes in porous media are conveniently described at the continuum scale using the convection dispersion equation. For the particular case of unidirectional flow in two-dimensions the equation is

$$\frac{\partial C}{\partial t} + U_x \frac{\partial C}{\partial x} = D_{xx} \frac{\partial^2 C}{\partial x^2} + D_{yy} \frac{\partial^2 C}{\partial y^2}, \tag{4.3}$$

The velocity U_x in this macroscopic equation refers to superficial velocity over a sample volume along the x direction. Both pore-scale flow variations and molecular diffusion are included the dispersion terms D_{xx} and D_{yy}, where D_{xx} refers to longitudinal dispersion coefficient and D_{yy} refers to the transverse dispersion coefficient. The values of the dispersion coefficients are strongly dependent on the porous medium structure, average flow direction, and molecular diffusion. Understanding these dependencies is crucial for describing transport in porous media for applications such as reaction engineering and contaminant transportation in subsurface.

A great deal of fundamental research has been directed at dispersion processes in porous media. Koch and Brady (1985) gave a comprehensive analysis using an asymptotic approach. By ensemble-averaging the basic conservation laws in the porous medium, a macroscopic equation of mass conservation is obtained, from which the dispersion term is obtained for the long-time limit. Dispersion mechanisms were analyzed asymptotically over a range of Peclet numbers. Sahimi pioneered the use of network modeling for solute dispersion using a Monte Carlo method (Sahimi et al., 1984). In summary, the flows in each capillary tube of the network model can be solved using a general network-modeling approach in which zero pressure drop is assumed at each network junction, and the Hagen-Poiseuille equation is applied to each bond. Once known, bond flow rates are used in a Monte Carlo method to simulate the solute transport through the network. Specifically, a substantial number of tracer particles (representing the solute molecules or fluid packets of some concentration) are followed through the network by expanding their movements into two terms. One is the convective term, which is determined by the local flow field. The second is a random displacement, which is meant to capture molecular diffusion effects. The final position and travel time of the each tracer particle are recorded for the calculation of dispersion coefficients. While this model has been used successfully to relate the dispersion coefficients with flow rate and network percolation structure

(Sahimi et al., 1986), there are certain limitations of the process, which are especially apparent for quantitative modeling of dispersion.

The first problem is the network calibration. Network models with a random distribution of tube conductivities do not necessarily represent real porous materials since the pore sizes and conductivities in real materials tend to have strong spatial correlation (Bryant et al. 1993). Incorporating an invalid conductivity distribution leads to an incorrect flow pattern in the pore level, which of course can have an adverse affect on dispersion modeling because of the importance of mechanical dispersion in the averaged coefficient.

A second problem is the complete mixing assumption at network junctions, which is required because the streamlines from each tube are not continuous in the network pores. This situation limits the effectiveness of a network approach for modeling dispersion, because it imposes an artificial diffusivity at each node. (Outlet paths are typically selected based on the proportionality of fluxes, without regard for the continuity of streamlines.) Sahimi et al. (1986) investigated the effects of the nodal mixing assumption. By comparing the simulation results between streamline routing and nodal mixing algorithms, it was found that the dispersivity computed with nodal mixing is independent of the mean flow velocity, while a slight increase was observed wne streamline routing was used. This same effect is discussed by Dillard and Blunt (2000) in the context of contaminant transport in network geometry. They concluded that under the groundwater conditions being modeled, the artificial diffusion caused by mixing was not a significant factor. However, neither work included molecular diffusion in the simulation. This limitation, in essence, constrains the Peclet number to a fixed but unknown value. Sorbie and Clifford (1991) did account for molecular diffusion in a network model by simulating diffusion within pore throats (while allowing complete mixing to occur in

pores). This technique enabled the Peclet number to be varied, but nodal mixing effects were neglected.

Clearly the most rigorous approach for modeling dispersion is to make use of a detailed solution to the hydrodynamics. This method will be used here to examine dispersion over a large range of Peclet numbers, and the results will be compared to results obtained using various network modeling techniques.

4.3.1 High-Resolution Modeling of Dispersion

Dispersion is the statistical description of convective and diffusive solute transport in the pore space over a sample volume. In modeling this process from first principles, one must solve for the solute transport in the pore space, and then find the correct statistical description for the spreading of the solute. Assuming that the solute is dilute, so that the hydrodynamics are independent of the concentration, we need only to solve the convection-diffusion equation for solute transport, which in this case is decoupled from the hydrodynamics so that the velocity **u** appears only as a parameter in the governing equation:

$$\frac{\partial C}{\partial t} + \nabla \cdot (\mathbf{u} C) - \nabla \cdot (D \nabla C) = 0 , \tag{4.4}$$

Because of the strong convection effects, direct methods such as the finite difference or finite element methods are not generally effective at high Peclet numbers. An alternative approach is stochastic modeling, which is appropriate because dispersion modeling requires only a statistical description of the solute behavior rather than the detailed concentration profiles.

Stochastic methods use a random walk approach, which splits particle transport into two independent components: (1) a convective component related to the velocity field, and, (2) a diffusive component, representing transport by molecular diffusion. If the velocity field is known, a straightforward approach is to use the equation

$$\mathbf{x}(t+\Delta t) - \mathbf{x}(t) = \mathbf{u}(\mathbf{x}(t))\Delta t + [2D\Delta t]^{1/2}\boldsymbol{\xi}\,, \tag{4.5}$$

where $\boldsymbol{x}(t+\Delta t)$ denotes the new-time particle position, and $\boldsymbol{x}(t)$ the previous position. Δt is the time step, and $\boldsymbol{\xi}$ is a two-dimensional vector in which each element is a Gaussian random number of zero mean and unit variance.

The first term on the right-hand-side of Equation 4.5 is a deterministic step that moves a tracer particle's position along the tangent to a streamline. The second term on the right-hand-side is a random movement whose magnitude is determined by the solute diffusion coefficient D. In this work, the velocity term in equation 4.5 was obtained independently from the high-resolution flow solution described above.

Because no mass is able to pass through the solid surfaces of the porous medium, the solid-phase boundaries are treated as fully reflective boundaries (Weiss, 1994), which means that any stochastic movements attempting to cross the surface will be reflected back into the fluid.

To model dispersion in this work, a large number of solute particles were followed through the packing, and their final positions and travel times were recorded. The dispersion coefficients were calculated using the method described by Sahimi (1983). The squared deviations between 'real' and expected position are defined as

$$S_x = (x - x_0 - \bar{v}\cdot t)^2,\;\; S_y = (y - y_0)^2\,, \tag{4.6}$$

Where $\bar{v}$ is the average velocity in the x direction. The average velocity in the y direction is zero. The dispersion coefficients are the calculated as

$$D_{xx} = \left\langle S_x^2 / 2t \right\rangle; \qquad D_{yy} = \left\langle S_y^2 / 2t \right\rangle. \tag{4.7}$$

In this definition, the average can be either a spatial average at a fixed time or a temporal average for a fixed displacement; the same results are found if the dispersion is macroscopically diffusive

(Sahimi et al., 1986). In this work, the dispersion coefficients are calculated using the fixed displacement.

4.3.2 Network Modeling of Dispersion

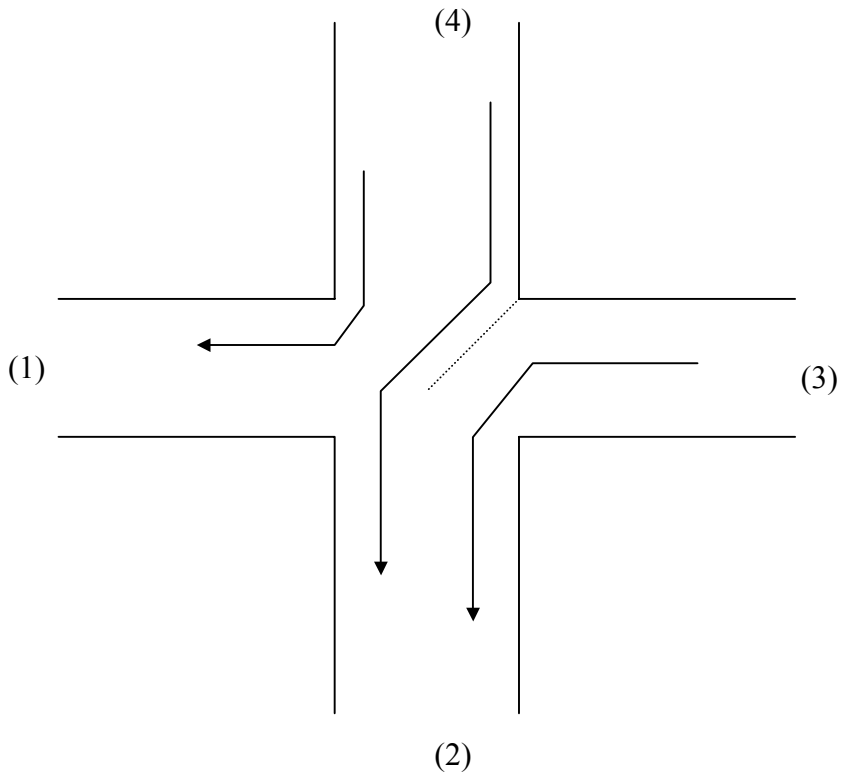

Figure 4.4 Schematic of streamline routing for the square network

For the network model, a similar random walk technique is used to simulate dispersion, except that the velocity field is obtained from the Hagen-Poiseuille equation applied to each network bond. Two problems are apparent with this approach. First, this velocity field is only an approximation to the true local velocity. More importantly, there is no easy way to approximate the velocity in network junctions. The most common approach for solving this latter problem is to assume that complete mixing of the solute particles occurs at the pore junctions, and to select outlets for the stochastic

particles based on a probabilistic argument weighted according to outlet fluxes. While this approach is simple, it causes a discontinuity in streamlines at each pore, therefore introducing an artificial diffusivity. The consequence is that dispersion modeling can be performed only up to some finite value of the Peclet number.

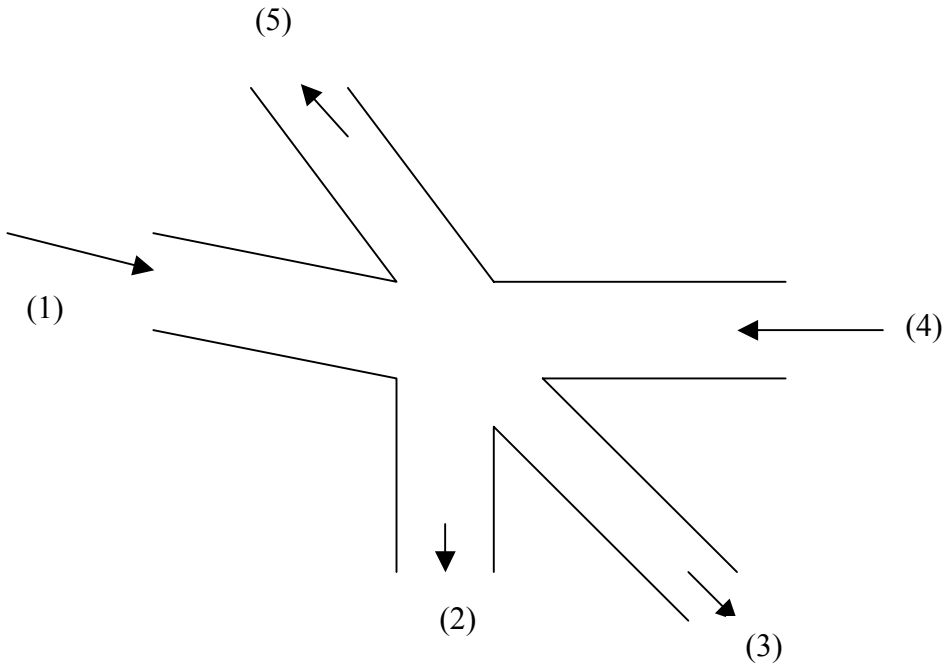

Figure 4.5 Schematic of flow-splitting algorithm. The priority outlet list for inlet (1) is ((2), (5), (3)) and for inlet (4) is ((5), (3), (2)).

In this work, we examine the use of a streamline routing algorithm to connect streamlines at each node. Previously, Hull and Koslow (1986) and Dillard and Blunt (2000) have used a similar approach to calculate outlet solute concentrations based on the proportional contribution of inlet solute fluxes. For dispersion modeling, the total flux in each bond is used to split the streamlines in the junction, which allows them to remain connected as they traverse a pore junction. The concept is illustrated in Figure 4.4. For a two-dimensional square lattice, the inlet and outlet configuration is labeled 14

according to the terminology of Dillard and Blunt (2000). Since the network model in this research is constructed from a two-dimensional random packing, the coordination number and the bond orientations are variable at each junction. This makes the assigning the flow configurations significantly more complicated. As a result, the following three-step algorithm was implemented.

Step1: Determine the Outlet Priority List

The flow into each inlet is assigned to a priority list, linking flow from that bond to an outlet bond. The priority list is determined by a "short" and "straight" rule. This means the outlet closest to the inlet with the largest angle will have the highest priority (as illustrated in Figure 4.5).

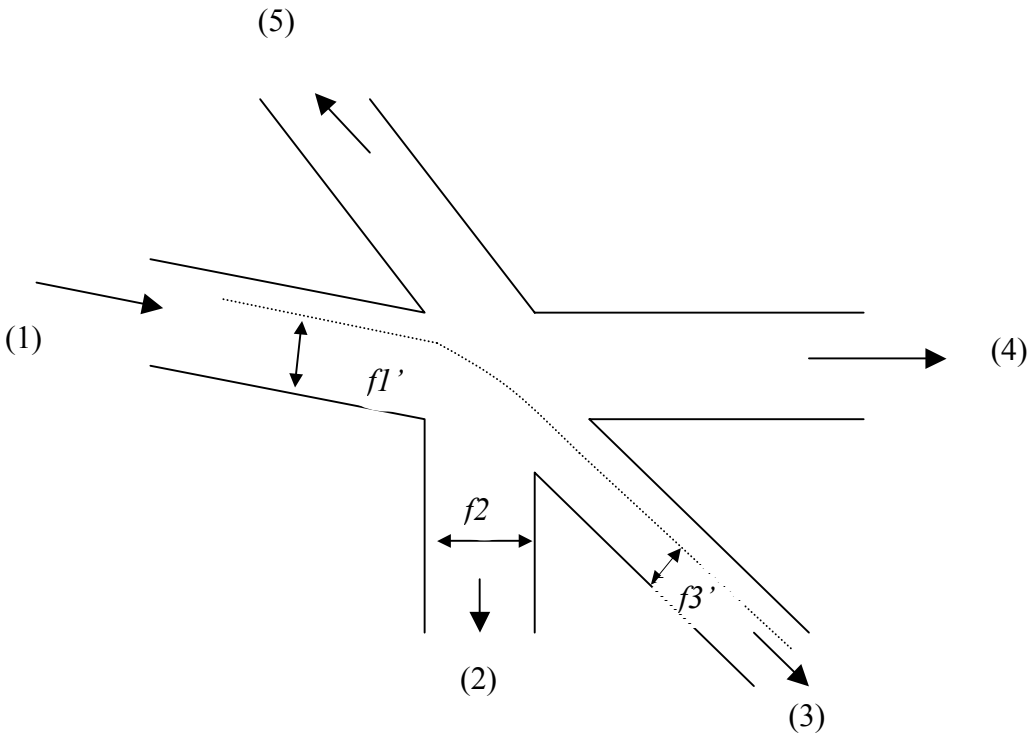

Figure 4.6 Schematic of streamlines connections between inlet and outlet.

Step2: Split the Flux

The flow is split according to the proportion of flux in each bond and the priority list determined above. The flow from any one inlet is sent to the outlet with the highest priority first. If one outlet is given highest priority for two different inlets, the inlet with a higher flux is used first. If the highest-priority outlet bond becomes 'full,' the remaining flux is sent to the outlet with next priority that is not yet full. In Figure 4.6, the fluid from inlet (1) will flow to outlet (2) first; if outlet (5) is fully taken by inlet (4), the remaining flux from inlet (1) goes to (3). If there is still remaining flux from inlet (4), it is also sent to (3).

Step3: Connect Streamlines

The inlet flow is split into several fractions in step 2, with the flow from each fraction going to one specific outlet. Hence, one streamline from one inlet will connect to one streamline in the corresponding outlet. The position of the streamline in the outlet is determined in proportion to the volume flux. For the example shown in Figure 4.6, the flux below the dashed inlet streamline $f1'$ is larger than $f2$, so that this streamline will connect to a streamline in outlet 3. The flux $f1' = f2 + f3'$. The location of the streamline in the outlet 3 is found by integrating the outlet velocities counter-clock-wise until the flux $f1'$ was reached.

This algorithm was implemented in the network model for tracking the transport of injected solute. At each pore, the path of the tracer particle is determined by the streamline routing algorithm, and in each bond the streamline simply follows the Poiseuille flow solution (i.e., unidirectional flow for the convective contribution). A diffusive component is introduced using a random walk equivalent to the one used with the high-resolution model.

4.4 Results

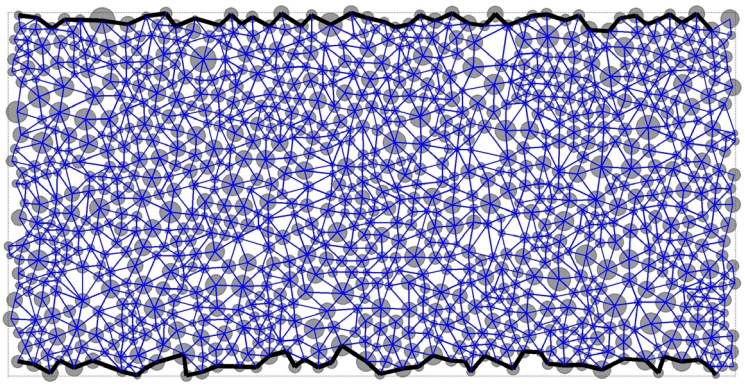

Figure 4.7 Network discretization for $z = 3$.

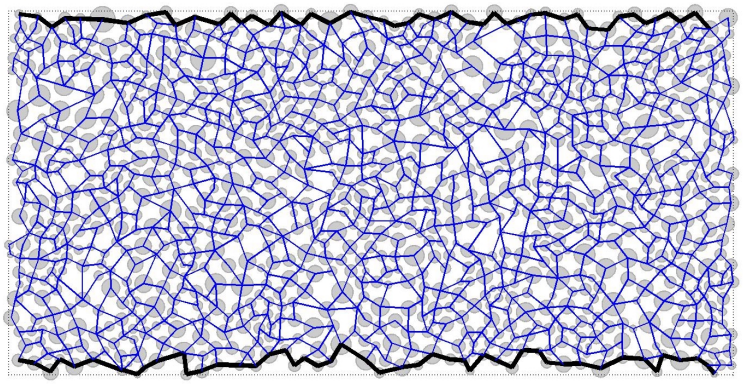

Figure 4.8 Network discretization for $z_{ave} = 4.51$.

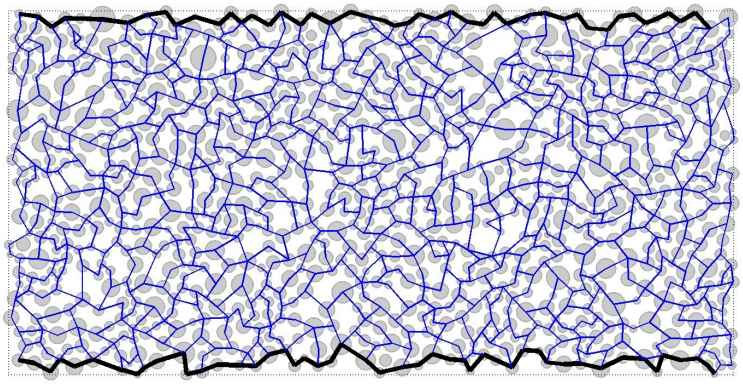

Figure 4.9 Network discretization for $z_{ave} = 6.57$.

4.4.1 Hydrodynamics

Physically representative network models have been shown to accurately predict single-phase permeability as well as other parameters (Bryant et al., 1993; Thompson and Fogler, 1997). Still, because of the significant assumptions inherent to the network approximation, and because of the

simplifications typically made for hydraulic conductivity calculations, it is of interest to assess the accuracy of the local hydrodynamics as predicted by the network model.

Permeability is the most obvious parameter with which to characterize single-phase conductivity. But, because it can be corrected by a single scaling factor, it is not as rigorous a test as the spatial distribution of velocities. If the velocity distribution is erroneous, even after the permeability is empirically scaled, this fact would be indicative of a more fundamental problem with the network approach. In this study, we examine both the permeability and the velocity distribution in three different networks. Each network is representative of the same porous medium, but reflects a different approach to discretization.

The first network model is constructed directly from the Delaunay tessellation, which discretizes the porous medium into triangles. As described previously, the region within each triangle is viewed as a pore, while the sides of each triangle (which necessarily fall along the smallest particle-particle gaps) are viewed as throats in the network model. One drawback to this technique is that it gives a fixed coordination number for all of the pores, whereas real porous materials have a distribution of coordination numbers. (Recall Figures 4.1 and 4.2.)

The other two networks are constructed by removing segments from the tessellation that are viewed as poor representations of pore throats, and by merging the Delaney cells together. The choice for which boundaries to remove is made by finding the longest gap between neighboring cells. (This same method was used in Chapter 3 to refine the subdomain size when performing domain decomposition. The rationale here is that having only small gaps between neighboring cells leads to better approximations for network throats.) If removal of this boundary does not cause the local coordination number to exceed some maximum value, then it is removed. Figures 4.7, 4.8, and 4.9 show the three different networks used here, which have average coordination numbers of 3, 4.51,

and 6.57. (Coordination numbers of the latter two networks were constrained to ≤ 5 and ≤ 8 respectively.) Figure 4.10 is the resulting network, which corresponds to the discretized structure shown in Figure 4.8.

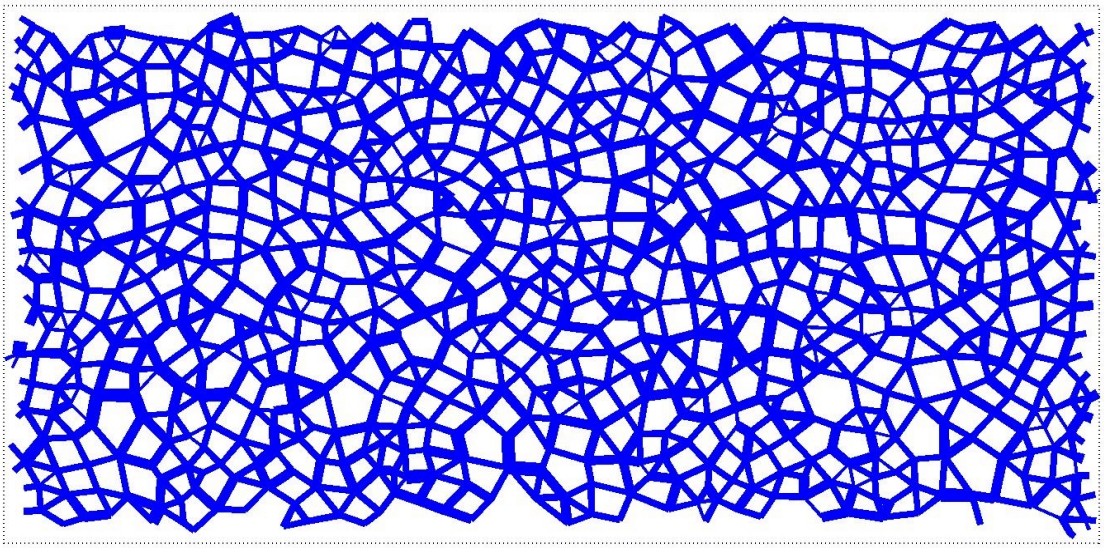

Figure 4.10 Network model constructed using the discretization shown in Figure 4.8. Each line represents one throat of the network. The line widths are drawn in proportion to the real throat widths.

Table I shows the permeabilities calculated for the three networks, as compared to the result from the high-resolution model. It should be noted that the simplistic approach described by Equation 4.2 is expected to underestimate the throat hydraulic conductivity, because the converging-diverging nature of the throat is not accounted for. Consequently, permeability is underestimated for the $z_{avg} = 3$ network. However, by increasing the coordination number, throats are lost from the network, and the permeability increases significantly with increasing coordination number for the two-dimensional network model. While these results indicate that the $z_{avg} = 4.51$ network provides the best

discretization for reproducing permeability, this conclusion is not of special significance because of the simplistic conductivity calculations, and because an empirical correction can be easily added to the model.

Table 4.1 Permeability Predictions from the High-Resolution Model and Three Network Models.

	High-resolution	$z = 3$	$z = 4.51$	$z = 6.57$
Permeability	9.5510×10^{-3}	6.10126×10^{-3}	9.83689×10^{-3}	12.865×10^{-3}

In the following analysis, we scale the permeability of the three networks to match the value from the high-resolution model (by adjusting all throat conductivities by a scalar value, which is unique for each network geometry but constant for all throats in any one network). This correction will compensate for errors caused by the simple conductivity calculation and, more importantly, allow quantitative comparison of the velocity distributions within the porous medium. Figures 4.11-13 are parity plots of average pore throat velocities, comparing the true value from the high-resolution model versus the three network models respectively. Figures 4.14-16 are histograms quantifying the error made by the network model for this distribution of fluxes. The sign of the velocity is used to denote flow out of a node (negative) and into a node (positive).

A number of observations can be made by comparing the velocity distributions. First, after scaling the permeability, the $z = 3$ discretization appears to provide the best network structure as evidenced as the much denser distribution of points along the 45° line in Figure 4.11. This result is somewhat surprising for a couple of reasons. First, from examination of Figure 4.7, intuitive arguments would suggest that many of the cell boundaries in this Delaunay tessellation are poor representations of pore throats. Second, when comparison of high-resolution versus network fluxes are made for a nearly square network, results are significantly better when diagonal throat boundaries

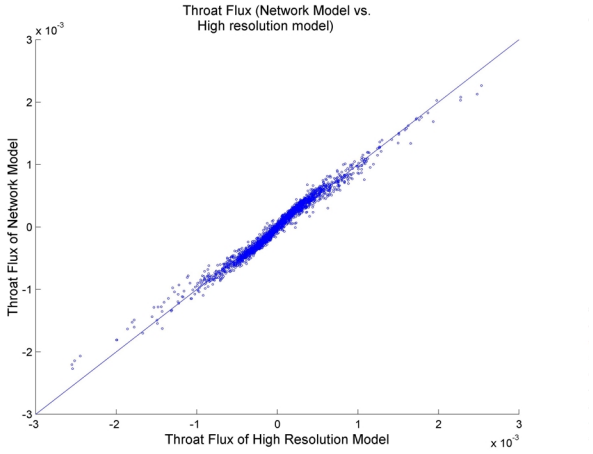

Figure 4.10 The parity plot of throat flux and network model (z_{avg}= 3)

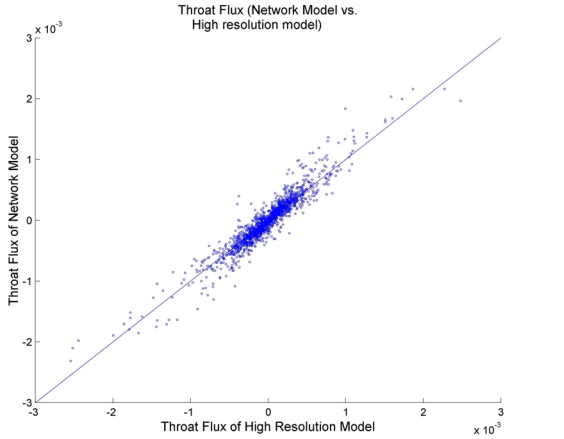

Figure 4.11 The parity plot of throat flux and network model (z_{avg}= 4.51)

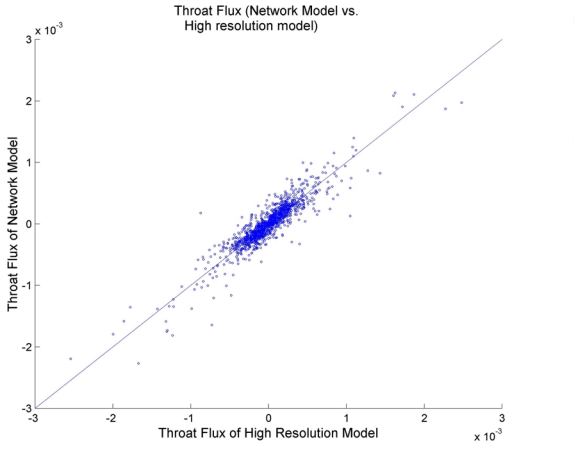

Figure 4.12 The parity plot of throat flux and network model (z_{avg}= 6.57)

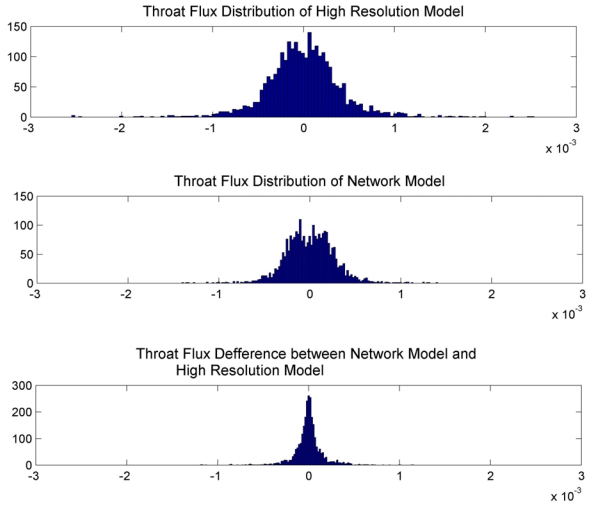

Figure 4.13 Distribution of throat velocities in the $z = 3$ disordered network

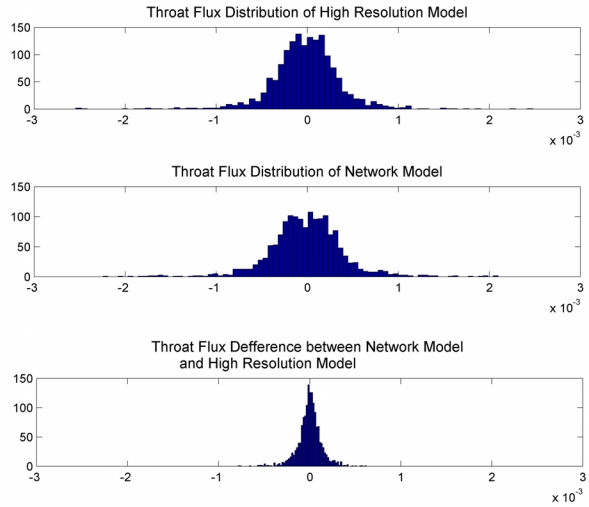

Figure 4.14 Distribution of throat velocities in the $z = 4.51$ disordered network

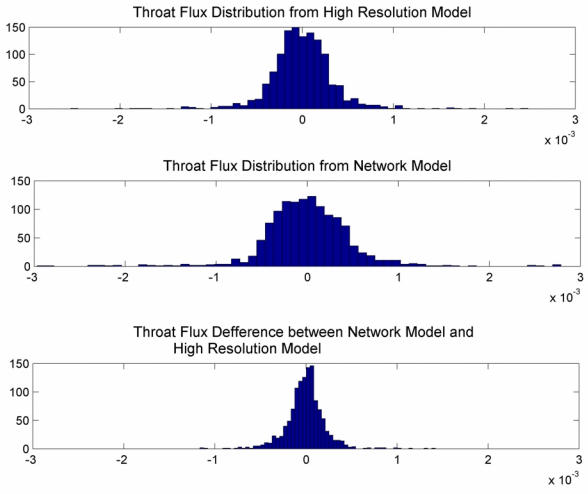

Figure 4.15 Distribution of throat velocities in the $z = 6.57$ disordered network

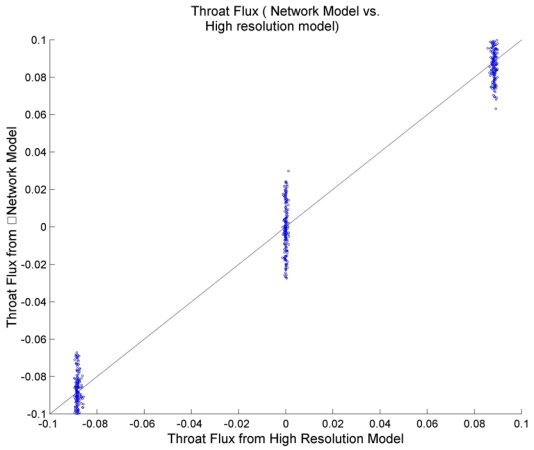

Figure 4.16 The parity plot of throat flux and network model (z_{avg}= 3) for the square packing

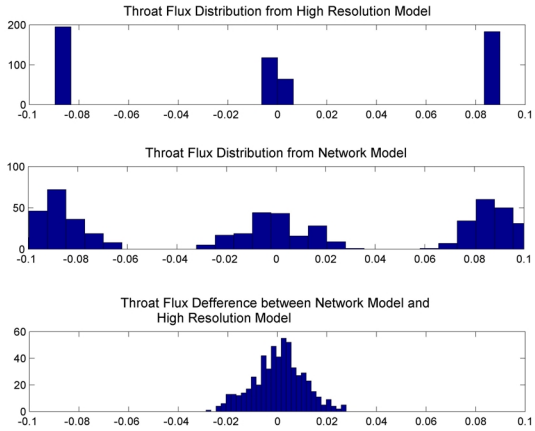

Figure 4.17 Distribution of throat fluxes in the z_{avg}= 3 network from the square packing

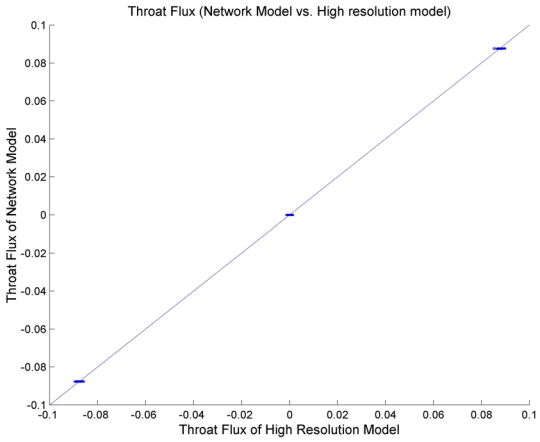

Figure 4.18 The parity plot of throat flux and network model (z_{avg}= 4) for the square packing

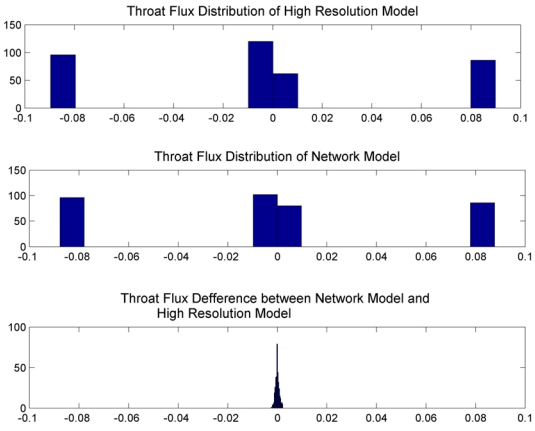

Figure 4.19 Distribution of throat fluxes in the z_{avg}= 4 network from the square packing

are removed. Specifically, Figures 4.17-20 contain comparisons of the velocity distributions for larger versions (15×15) of the networks shown in Figures 4.1 and 4.2. Clearly, the square network is significantly better than the triangular network for this specific case, although the symmetry of the flow pattern (when the pressure gradient is aligned with the lattice) perhaps makes this an overly simplistic comparison.

The reason for the behavior seen in Figures 4.11-16 appears to stem from the traditional network assumption that no pressure drop occurs in the pores themselves. Because removal of the questionable pore throats from the network also creates larger and more convoluted pores, it becomes increasingly difficult to represent the local hydrodynamics using single-valued pressure for each pore.

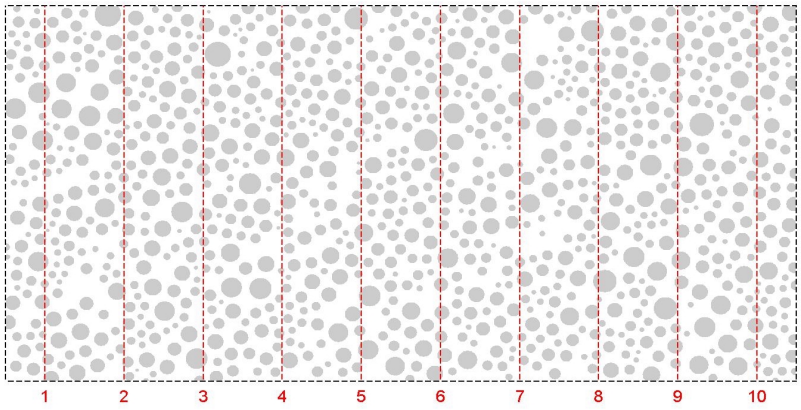

Figure 4.21 Cross sections for calculations of the dispersion coefficients

4.4.2 Dispersion in the High-Resolution Model

For dispersive transport, if the sample volume is much larger than the characteristic length for pore-scale heterogeneity, dispersion coefficients are independent of the time and the size of the material. In this case, dispersion is referred as "normal" or "Gaussian," which means that the spread of a solute can be described by a Gaussian distribution. Simulating dispersion in the high-resolution

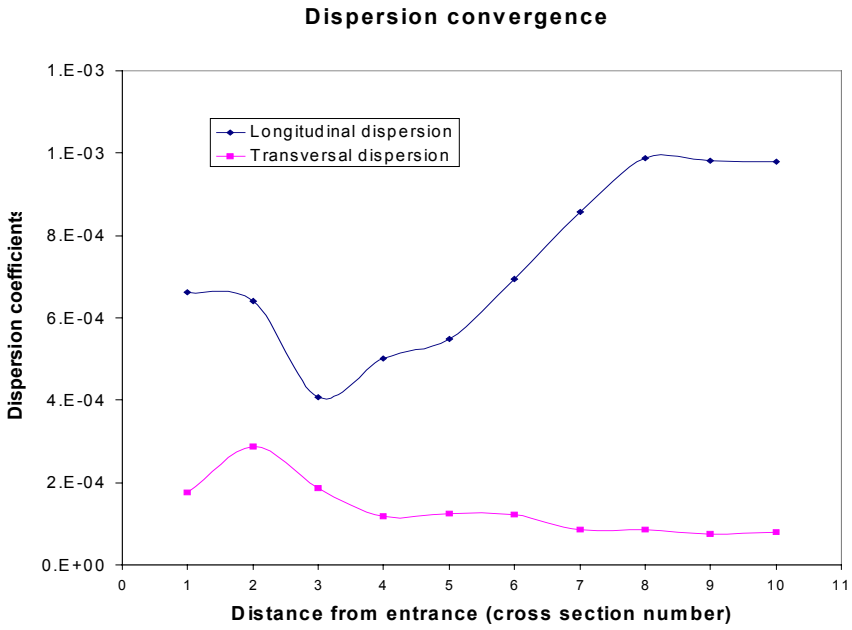

Figure 4.22 Convergence of dispersion coefficients for high-resolution model at Pe = 59.8

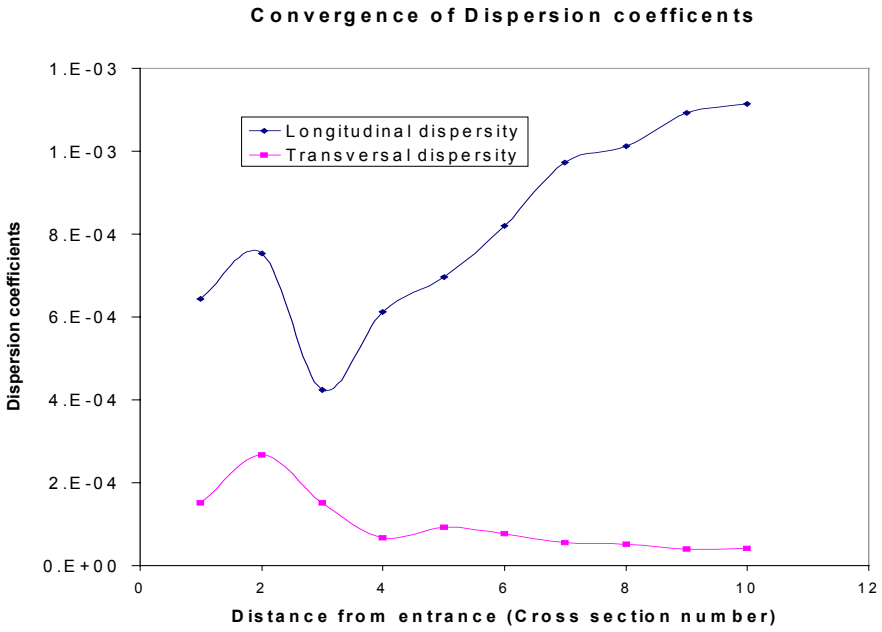

Figure 4.23 Convergence of dispersion coefficients for high-resolution model at Pe = ∞

model was performed using the Monte Carlo method described above. The starting positions of each tracer particle were selected within a finite vertical segment centered along the inlet of the porous medium so as to reduce the edge effects. The particle density within this beginning segment is proportional to the flux at this position, which is necessary for the Monte Carlo model to capture the correct dispersion coefficient.

A significant amount of research has been performed in recent years to better understand conditions under which Gaussian versus non-Gaussian dispersion occurs. This first goal of this study was to characterize the sample size over which Gaussian dispersion can be observed. For the two-dimensional porous medium used here, ten cross sections were selected along the x direction (Figure 4.21). As each tracer particle passed through one section, the residence time was recorded and the dispersion coefficient was calculated using equations 4.6 and 4.7.

This comparison of dispersion coefficient versus sample length was made at two Peclet numbers: $Pe = 59.8$ and $Pe = \infty$ (which represents purely mechanical dispersion). Figures 4.22 and 4.23 show the dispersion coefficients at various positions in the x direction. Figure 4.22 suggests that for $Pe = 59.8$, convergence of the dispersion coefficient occurs before the end of the porous medium. For the $Pe = \infty$ case, convergence is not observed over the same characteristic length. This difference is seen because, without molecular diffusion, a longer characteristic length is required before the tracer particles are able to sample a representative distribution of velocities. Although convergence for $Pe = \infty$ is not apparent from the data alone, we believe that it has nearly occurred by the end of the porous medium because of the quantitative comparisons made next. For subsequent sections, dispersion coefficients are obtained by tracing particles through the entire length of the porous medium.

One of the important attributes of high-resolution modeling is the ability to perform rigorous analysis of both longitudinal and transverse dispersion for specific pore structures. This type of

deterministic modeling cannot be performed using traditional network modeling because of the nodal mixing problems discussed above. Using the Monte-Carlo approach, dispersion coefficients were calculated over the entire Peclet number range by following 1000 particles through the packing at each Peclet number selected.

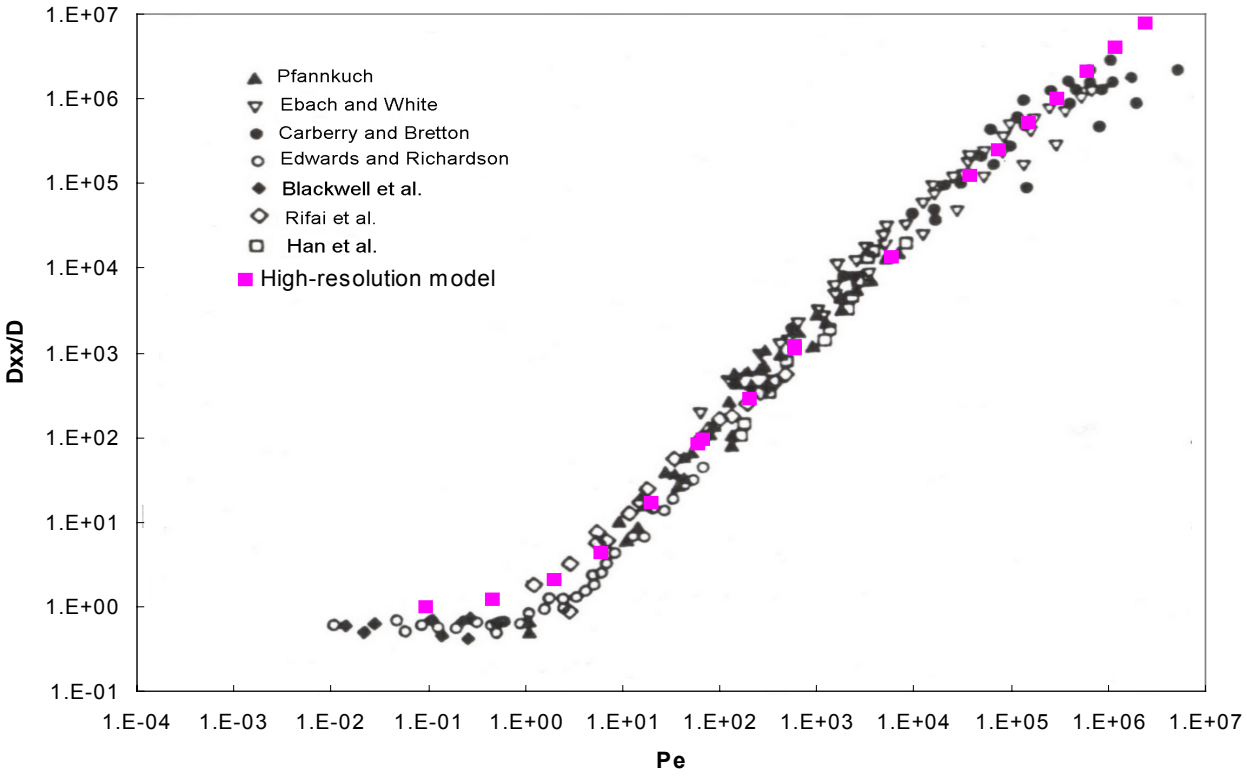

Figure 4.24 Longitudinal dispersion coefficients from the high-resolution model compared to experimental data from the literature (literature data comes from Han et al., 1985)

Figures 4.24 and 25 show the simulated dispersion coefficients superimposed upon data from literature: the data were collected by Han et al. (1985); they obtained data from Harleman and Rumer (1963), Edwards and Richardson (1968), Rifai et al. (1956), Carberry and Bretton (1958), Ebatch and

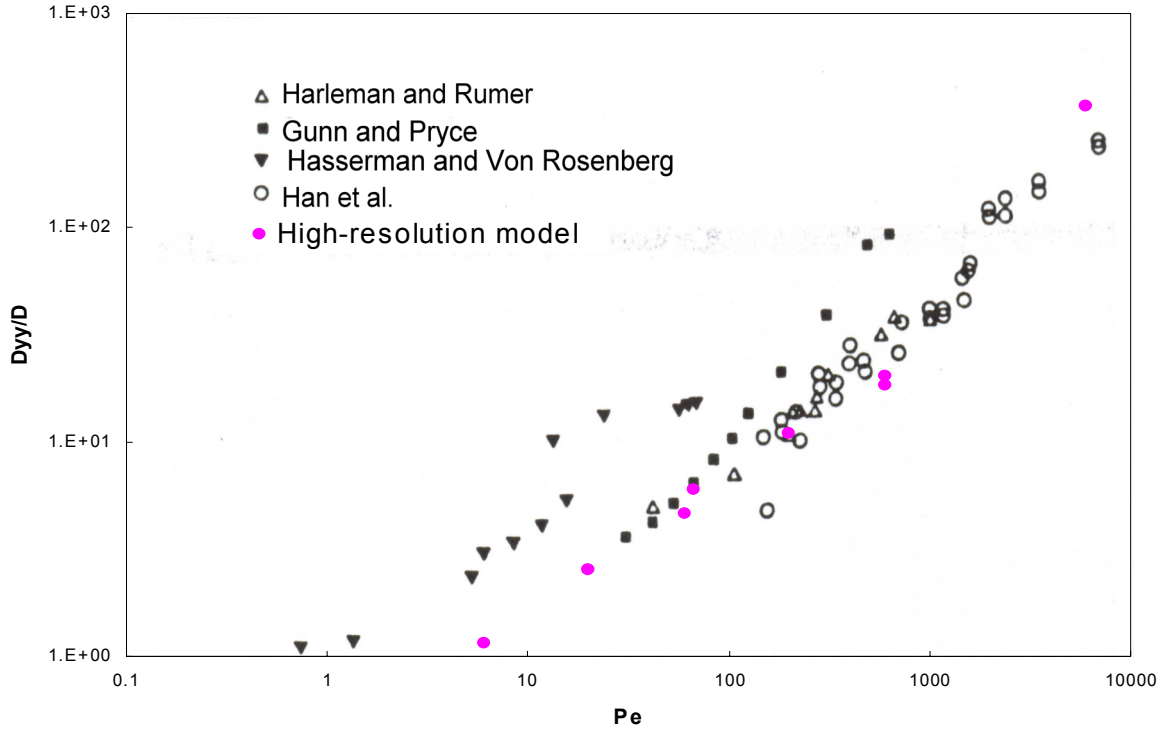

Figure 4.25 Transverse dispersion coefficients from the high-resolution model compared to experimental data from the literature (literature data comes from Han et al., 1985).

White (1958), Pfannkuch (1963), Blackwell et al. (1959), Gunn and Pryce (1969). For the longitudinal case, there is excellent agreement over most of the range, which was not necessarily expected because the current model is for a two-dimensional material. (While is it straightforward to show that the results are equivalent if the model is viewed as a three-dimensional model for flow over an array of parallel cylinders, the cylinder problem is fundamentally different than the problem of flow through packed beds, which were used in the experimental studies.) The only range with significant differences is the very-high-*Pe* range. One possible explanation is that, even in the $\mathrm{Pe} \to \infty$ limit, the hydrodynamics in the model are for $Re = 0$. While this assumption can easily be justified for the case of solutes with very low diffusion coefficients, it is more likely in experiments

that high-*Pe* results also correspond to higher Reynolds numbers, which would cause the hydrodynamics to be influenced by inertial effects, or possibly even turbulence.

Data for transverse dispersion coefficients are significantly more scattered, but the trend (Figure 25) is again captured well. Even without fully understanding the relationship between dispersion in the current two-dimensional problem and dispersion in a packed bed, these results can nonetheless be used to compare with equivalent network modeling simulations.

4.4.3 Modeling Dispersion Using the Network Model

Obviously, there are computational advantages to modeling dispersion using a network model, namely the much larger network sizes that can be accommodated and the increased speed of stochastic simulations. A primary point of concern, however, is whether the network model can effectively capture the Peclet-number functionality.

Assuming that the network model adequately predicts the velocity distribution, then its main limitation for dispersion modeling is the problem of maintaining streamline continuity at nodal points (where pore throats join). The standard assumption is that complete mixing occurs at each node. However, this assumption is equivalent to imposing an artificial diffusivity, and hence an upper limit on the Peclet number. In previous work, Sahimi et al. (1986) compares the nodal mixing effects with a proportional routing algorithm. No explicit molecular diffusion term was introduced in his work, but both nodal mixing and proportional routing algorithms introduce an unknown term that acts as molecular diffusion. Sorbie and Clifford (1991) varied the Peclet number in network modeling simulations by allowing diffusion between streamlines within the network bonds.

For comparison, we plot the dispersivity at different Peclet numbers for the streamline routing, the nodal mixing, and the high-resolution model in Figures 4.26-27. For *Pe* greater than 100, all three models reproduce the longitudinal dispersion coefficient well. This fact can be explained by noting

that mechanical dispersion dominates over this *Pe* range, so the dispersion simply reflects the fluctuations of the velocity fields. And, in the last section it was shown that the network model represents well the true velocity distribution from the high-resolution flow field. However, both the nodal mixing and streamline routing algorithm significantly overestimate the transverse dispersion coefficients. This result is expected because the network model assumes axial flow in each tube so the streamlines in the network necessarily follow the zig-zag path of the tubes.

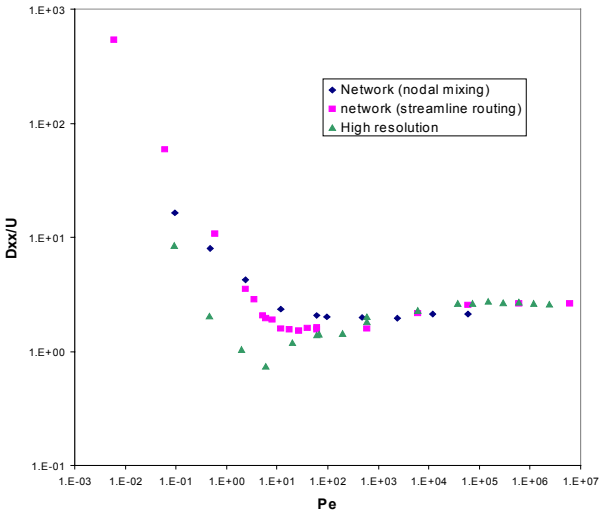

Figure 4.26 Longitudinal dispersion from the network model (streamline routing and nodal mixing) and high-resolution model

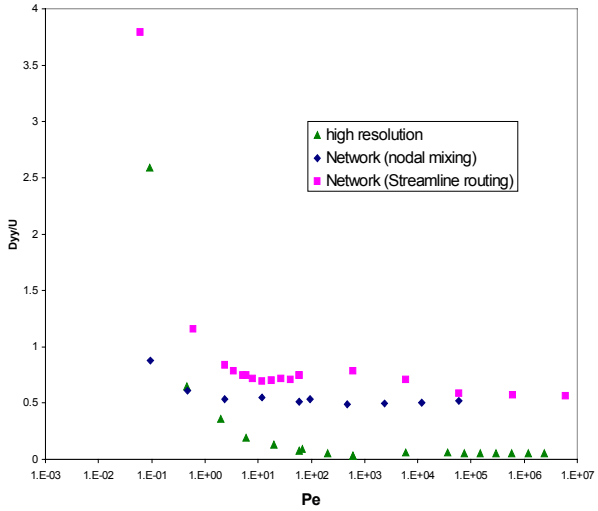

Figure 4.27 Transversal dispersion from the network model (streamline routing and nodal mixing) and high-resolution model

In the very low *Pe* range, *Dxx* as predicted by the network model is overestimated. One possible cause may be the porosity change during the network discretization, since the volumes of the pores are neglected. In this small *Pe* range, the dispersion is dominated by molecular diffusion, and smaller pore spaces will lead to high dispersion (Koch and Brady, 1985).

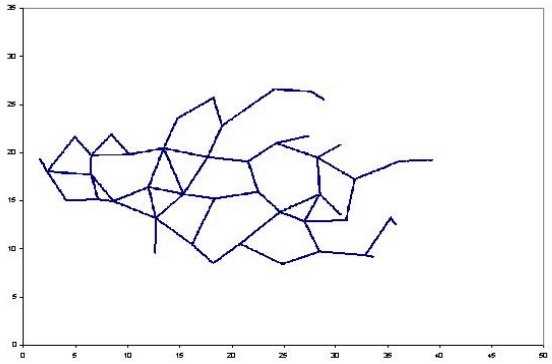

Figure 4.28 The tracer particle trajectories from one starting point (nodal mixing) at Pe = ∞

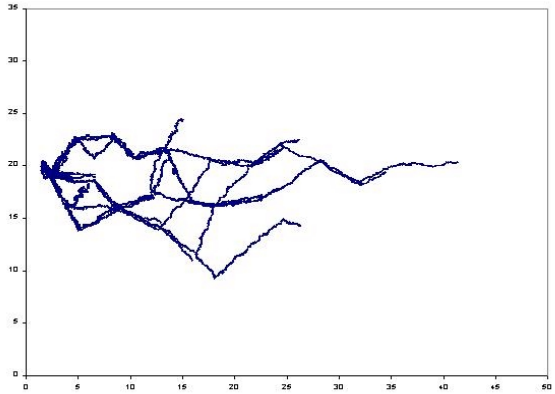

Figure 4.29 The tracer particle trajectories from one starting point (nodal mixing) at Pe = 59.8

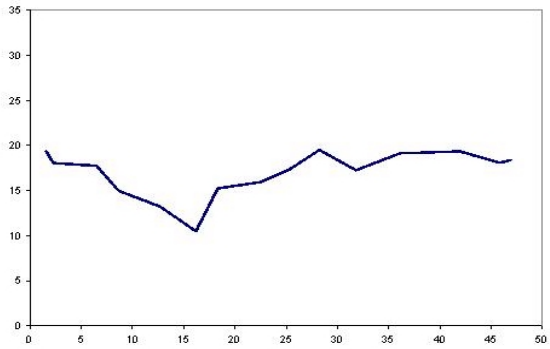

Figure 4.30 The tracer particle trajectories from one starting point (streamline routing) at Pe = ∞

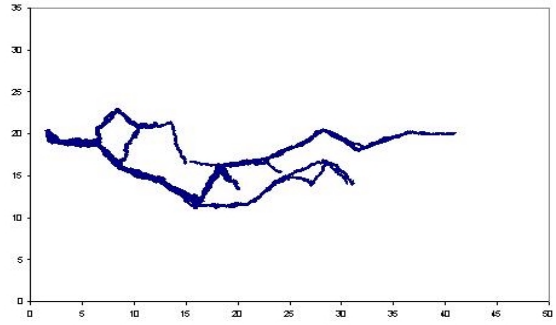

Figure 4.31 The tracer particle trajectories from one starting point (streamline routing) at Pe = 59.8

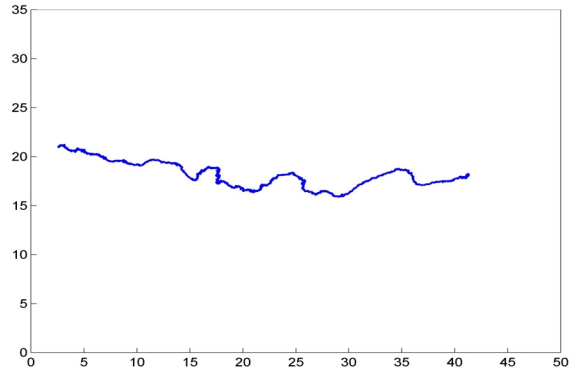

Figure 4.32 The tracer particle trajectories from one starting point (high-resolution model) at Pe = ∞

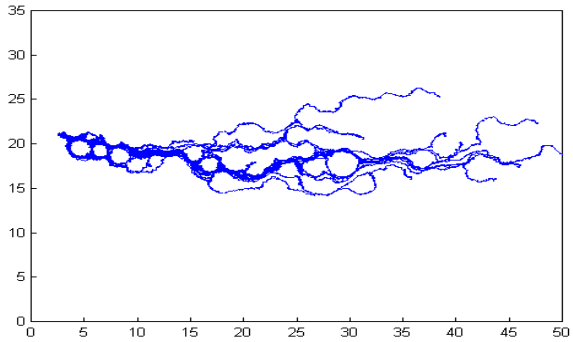

Figure 4.33 The tracer particle trajectories from one starting point (high-resolution model) at Pe = 59.8

One subtle difference for the nodal mixing algorithm is that the dispersivity is almost independent of the *Pe* number, whereas it slightly increases with *Pe* in both the high-resolution and streamline-routing models. The reason is that nodal mixing introduces an arbitrary diffusion term, so that molecular diffusion effects cannot be correctly represented in high *Pe* range. In order to illustrate this point, we compare the tracer dispersion from the same starting point for the three different models. At an infinite Peclet number, the high-resolution model and streamline routing model both give deterministic paths for all tracer particles, while nodal mixing spreads the particles through the medium. This spreading effect is significant at both high and low Peclet number (see Figure 4.28-29), which implies that the nodal mixing algorithm cannot reproduce solute transport at high *Pe* even if the average dispersion coefficient is correctly reproduced (because of sampling of the complete velocity profile).

4.5 Conclusions

In this part of the research, a high-resolution model was developed to simulate dispersion in porous medium. The Stokes flow in two-dimensional disordered packing was solved and the flow field was used in a random walk model to simulate the solution transport through the packing. In the algorithm, the final position and travel time of each particle are recorded and the dispersion coefficients are calculated from the deviation between the particle position and macroscopically predicted position. The simulated results agree well with literature data, which indicates that the high-resolution model successfully reproduces the dispersion phenomena. The high-resolution results were used to validate the network model constructed from the same two-dimensional sphere packing. A random walk model was also used in the network model simulation of dispersion, which employed both a nodal-mixing algorithm and a streamline-routing algorithm (which connects streamlines at each network junction). The nodal mixing assumption for particle transport was investigated. The results shows that over a wide *Pe* range ($Pe > 10$), the dispersivity from the nodal mixing is independent of the *Pe* number. The reason is that nodal mixing does not reflect the molecular diffusion correctly at this *Pe* range. The simulation of solute transport at infinite *Pe* from one point proves that the nodal mixing assumption significantly spreads the tracer particles, while the high-resolution model and streamline routing give a deterministic path.

A full range of Peclet number simulations were run using the network model with the streamline routing algorithm developed in this research. The comparison between the results from both the high-resolution model and the network model show that our network model can reproduce longitudinal dispersion coefficients in the range ($10 < Pe < 100000$). However, the network model typically overestimates the transverse dispersion coefficients, partly due to the geometric simplification in the network, and partly due to the overestimation of streamline hopping by solute particles.

CHAPTER 5. A STOCHASTIC MODEL FOR SOLVING INTERFACIAL MASS TRANSFER OF SINGLE SOURCE PARTICLES IN HETEROGENEOUS POROUS MEDIA

5.1 Introduction

The rate of mass transfer in packed beds and porous media can usually be quantified using one of many empirical relationships between the Sherwood number and the Peclet number. If inertial forces are significant, the Reynolds number also affects mass transfer independently of the Peclet number. And, for special cases such as multiphase flow, other parameters are often introduced into the equations. These additional terms usually account for factors such as phase saturation or interface area.

Mass transfer coefficients represent spatially averaged quantities, and can thus be used for continuum-level modeling of transport. At the pore scale, however, spatial variations in the mass-transfer rate will occur because of the disorder and heterogeneity found in most porous media, which in turn affects local hydrodynamics. In many applications, knowledge of these local values and their variation is of little use or interest. However, in cases where mass transfer occurs from discrete sites distributed within the porous medium, the local variations are important because the average rate of mass transfer may be significantly different than what is predicted from empirical correlations. This discrepancy would be particularly evident if a spatial correlation existed between the location of the discrete sites for mass transfer and other morphologic parameters that influence flow. For real processes, this type of correlation is probably more the norm than the exception because of the high degree of coupling found in most porous-media transport processes.

Numerous engineering examples can be found where mass transfer does not occur uniformly within a material. The case that best illustrates the problems discussed above is probably the dissolution of organic contaminants in the subsurface. Organic contaminants become trapped as

discrete ganglia at the pore scale, and then dissolve slowly into the groundwater. At the continuum level, this dissolution is modeled using lumped mass-transfer coefficients, which in turn are quantified using empirical equations generated specifically for groundwater applications. A large number of these equations have been proposed (see Jia et al. (1999) for a representative table), and the wide variation in parameter values and functionality from one equation to another is indicative of the complexity of the mass-transfer processes. However, because equations for these complex situations are generated entirely by empiricism, they are not effective tools for studying the underlying fundamentals of mass transfer in heterogeneous porous media.

Guo and Thompson (2001) examined the effects of natural disorder on local mass transfer in packed beds experimentally (local meaning single-particle averaged). The mass-transfer rates were measured as a function of random location in packed beds in an effort to quantify the effects of local geometry and hydrodynamics on mass transfer. Experiments were performed by repeatedly placing single benzoic-acid spheres in packed beds, and measuring mass transfer rates for $0.2 < Re < 1$ and $200 < Pe < 1000$. Packings of uniform as well as distributed sphere sizes were used. Both types showed significant local variations in mass transfer in the form of distributed values of A and m when single-particle data were fit to the relationship

$$Sh = A \cdot Pe^{m}, \tag{5.1}$$

Pore-level modeling the mass transfer in the disordered porous media is typically a difficult problem because the geometry complexity impose tremendous computation hurdles for solving the governing equations. Wang and Sangani (1997) first examined the problem of mass transfer in disordered packings for conditions of low *Re* and high *Pe*. Velocity fields for the two-dimensional problem were obtained using multipole expansions (Sangani and Yao, 1988). The heat-transfer problem was then solved by integrating the boundary-layer equation between stagnation points on the

particle surfaces. This approach allowed differentiation between regions of the surface that are exposed to 'fresh' fluid versus regions of the surface next to recirculating fluid where the thermal boundary layer is thicker. For disordered arrays, the overall Nusselt number was found by averaging over all particles. Tables II and III from their paper show that the average rate of mass transfer is generally lower in random packings (except when flow is aligned with a regular array, in which case the recirculation patterns have a larger impact). Dillard and Blunt (2000) developed a pore network model to study nonaqueous phase liquid (NAPL) dissolution. The flow rates of the both water and NAPL phase were solved from the multiphase Darcy equations and the aqueous-phase transport was solved by applying the solute flux equation at each network tube. The mass transfer from the NAPL blobs was represented using a corner diffusion model. The results of the simulated solute concentration vs. Peclet number and Sherwood number vs. Peclet number match well with experimental data if the NAPL blob dissolution rate is neglected. Only averaged mass transfer rates were investigated in both Sangani and Dillard's works.

The major challenges in the numerical modeling of heat or mass transfer at moderate to high values of Pe are twofold. First, a very detailed solution for the velocity field is required in order to resolve effects within thermal or concentration boundary layers. Second, the strong convection effects at high-Peclet number can cause numerical errors during many types of direct solutions of the convection-diffusion equation (e.g., FEM or FDM methods).

The model presented in Chapter 3 is ideal for generating a detailed velocity field for low-Reynolds number flow, especially due to the ease of implementing local grid refinement. In this chapter, a stochastic model is developed for solving the steady convection diffusion equation for interfacial heat or mass transfer in the material. (The discussion is given in terms or mass transfer because of the environmental application discussed above). The model is capable of simulating mass

transfer over a wide Peclet-number range from source particles in a heterogeneous porous medium. This allows one to study mass transfer variations caused by the local hydrodynamics. The model is verified by comparing with asymptotic solution for a square packing (Sangani and Yao, 1988).

5.2 Description of the Numerical Techniques

In the model, we assume that the solute concentration is dilute everywhere and thus has no effect on fluid properties. Similarly, we assume that concentration profiles from upstream particles have no effect on downstream mass transfer. These assumptions allow the flow problem to be decoupled from the mass transfer problem, and the numerical modeling is performed in two steps: calculation of the velocity profile followed by calculation of the rate of interfacial mass transfer.

5.2.1 Velocity Calculations

Since we assume low-Reynolds number flow, the velocity is governed by the Stokes equation in two dimensions. The high-resolution flow field was obtained by following the numerical procedure given in chapter 3. Once the above solution is obtained, point velocities can be obtained quite rapidly by performing a local boundary integral calculation over a single subdomain. The efficiency with which these velocities can be recovered is crucial when using a stochastic algorithm.

5.2.2 Mass Transfer Calculations

In the steady-state, decoupled mass-transfer calculation, velocity appears only as a parameter in the convection-diffusion equation,

$$\mathbf{u} \cdot \nabla C = D \nabla^2 C \,. \tag{5.2}$$

Equation 5.2 can be directly solved using the finite element method with boundary conditions $C = C^*$ at the particle surface and $\mathbf{u} \cdot \nabla C = 0$ far from the particle. However this approach is typically effective at low to moderate Peclet numbers only, because the strong convection effects at high Peclet number cause numerical errors. A stochastic algorithm can be used to model the mass transfer process in the

large Peclet-number range. Stochastic methods have been used in similar studies, for instance the dissolution of porous media (Bekri et al., 1995), the dissolution of bubbles into water (Ponoth and McLaughlin (2000)), and the dissolution of fractured rock by acid (Verberg and Ladd, submitted).

Here, the stochastic algorithm is run by tracking a large number of tracer particles as they are displaced through the pore space by convective-diffusive motion. Each numerical displacement is made according to

$$\Delta \mathbf{r} = \mathbf{u}\Delta t + \sqrt{2D}\mathbf{W} , \tag{5.3}$$

where **W** is a random Gaussian variable with variance equal to Δt (18). To maintain computational efficiency as well as accuracy, a uniform characteristic displacement length δ_M is imposed regardless of whether a tracer particle is in a region of low or high velocity. Hence, the time step Δt associated with a displacement varies with position, and is calculated from the equation

$$\delta_M = \left|\mathbf{v}(\mathbf{r})\right|\Delta t + \sqrt{4D\Delta t} \tag{5.4}$$

for the two-dimensional case.

In this problem, our concern is determining the rate of mass transfer from a single circular interface in the bed, which can be thought of as a dissolving particle. The approach does not require the concentration profile itself to be determined, which simplifies the stochastic problem to some extent.

Consider a number of free solute molecules within a small distance from the source particle surface. Each molecular can be transported by diffusion or local convection. Whenever a molecule is released from the surface, another molecule from the source particle takes its position immediately. If a molecule in the fluid phase travels back to the surface, it will also replace a molecule in the same position so that the number of free molecule remains constant. This scenario corresponds to the boundary condition $C = C^*$ at the dissolving-particle surface. In the random walk model, the source

sphere surface can be modeled as a both a source and sink boundary (Weiss, 1994) for the stochastic molecular transport described above. Since we assume that the solute concentration is dilute, the interactions between solute molecules can be neglected. Hence, the stochastic algorithm can be run by sequentially releasing a large number of tracer particles from the interface and following their motion as governed by Equation 5.3. For each tracer particle released, the particle is followed until it either returns to the interface or it travels far enough away that it will not return within any reasonable probability. This escape criteria represents the boundary condition $\mathbf{u}\cdot\nabla C = 0$ which means the diffusion can be neglected and solute molecules follow convection streamlines. The number of escaped tracer particles is considered to represent the dissolution flux at steady state.

For calculating the mass transfer coefficient, we consider a thin layer of fluid adjacent to the dissolving interface. The thickness of this surface layer L is large compared to δ_M but small compared to the concentration boundary layer, and convective transport is negligible in the surface layer. In the surface layer, motion is primarily by diffusion. Hence, each displacement step represents a constant time interval

$$\Delta t = \delta_M^2 / 4D . \tag{5.5}$$

Furthermore, since a steady-state process is being modeled, the appearance of a tracer particle in the surface layer means that a tracer particle could be found at that same position during any snapshot of length Δt. This observation allows the number of tracer-particle observations in the surface layer (N_{sl}) to be related to the equilibrium solute concentration C^*. The number of tracer particles that ultimately escape the surface (N_{esc}) is equivalent to the number that escape during any time interval Δt. Viewing each tracer particle as a packet of solute, N_{sl} and N_{esc} can be related to the molar flux from the surface: where $C_0 \equiv 0$. Equation 5.6 allows the mass transfer coefficient to be calculated by counting N_{sl} and N_{esc} in an ensemble of tracer-particle trajectories.

$$\mathbf{q}\cdot\mathbf{n} = k(C^* - C_0) = \frac{N_{esc}}{\Delta t} C^* \frac{L}{N_{sl}}, \tag{5.6}$$

The critical parameters in the simulation are δ_M, L, and N_{rel}. The characteristic displacement distance δ_M is determined on a case-by-case basis by ensuring that the results are nearly invariant when it is decreased. Typically, choosing δ_M to be on the order of 1/100 of the expected boundary layer thickness has given satisfactory results. L must be sufficiently large to allow a true random walk within the surface layer, while at the same time being sufficiently small so that significant concentration gradients are not present in the surface layer. We have used $L = 10\delta_M$ for most results, again, ensuring that results are essentially invariant with respect to this parameter. Finally, N_{rel} is determined on a case-by-case basis by ensuring that convergence has occurred.

5.3 Results and Discussions

5.3.1 Mass transfer in a square cylinder packing

To validate the stochastic algorithm, mass-transfer coefficients for a regular two-dimensional packing were calculated and compared to asymptotic results of Wang and Sangani (1997) (which are valid for $\mathrm{Pe} \to \infty$). The two-dimensional packing is a 15×15 square packing with porosity of 0.9. The flow field was solved using the high-resolution model described in Section 3.1. Since our solution is not periodic, a particle in the middle of the packing was selected, for which the flow field was considered to be essentially

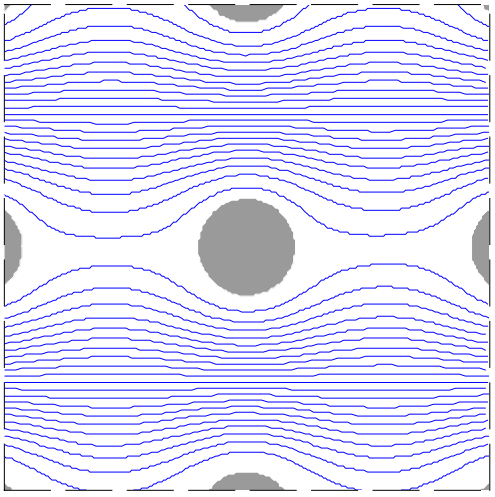

Figure 5.1. Streamline plot around a particle of two-dimensional square packing.

the same as for the periodic solution (Figure 5.1). The images in Figure 5.2 were created from the stochastic algorithm by plotting a point at each location that a tracer particle was detected (for a limited number of trajectories for clarity). The simulations represent Peclet numbers equal to 15.8, 158 and 3160. These images do not give a quantitative indication of solute concentration, but they clearly show the influence of the Peclet number on transport.

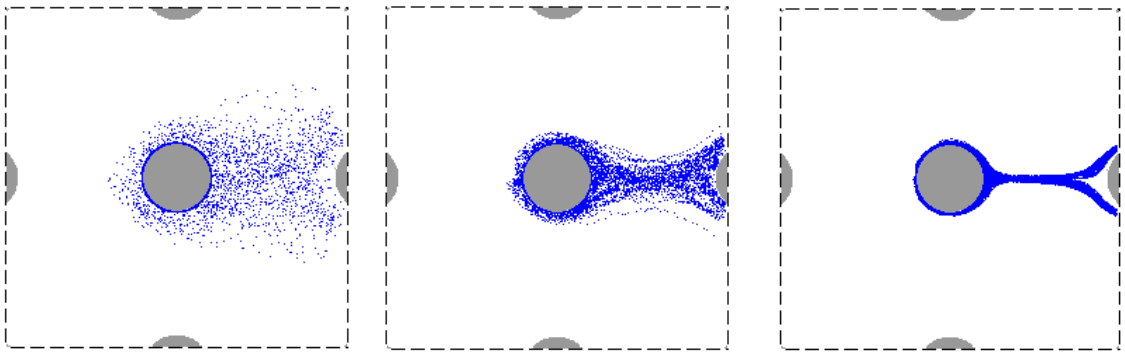

a) Pe = 15.8 b) Pe =158 c) Pe = 3160

Figure 5.2. Tracer particle locations of stochastic simulations of mass transfer: (a) *Pe* = 15.8; (b) *Pe* = 158; (c) *Pe* = 3160

Sangani and Yao's asymptotic analysis gives the relation of $Sh=A\cdot Pe^{1/3}$ where $A = 0.68$ for the square cylinder packing with porosity 0.9 and orientation angle 0 (Sangani and Yao, 1988). Our results gives $Sh=0.628\cdot Pe^{1/3}$ (see Figure 5.3). The discrepancy between the asymptotic and stochastic results may due to the difference in the numerical flow field and the analytical solution in Sangani and Yao's analysis.

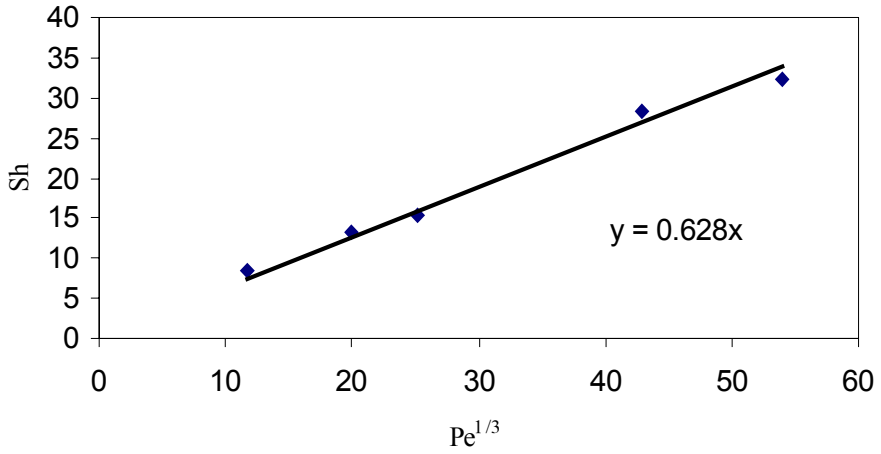

Figure 5.3. Sh versus $Pe^{1/3}$ relationship for mass transfer of the source particle in the square packing

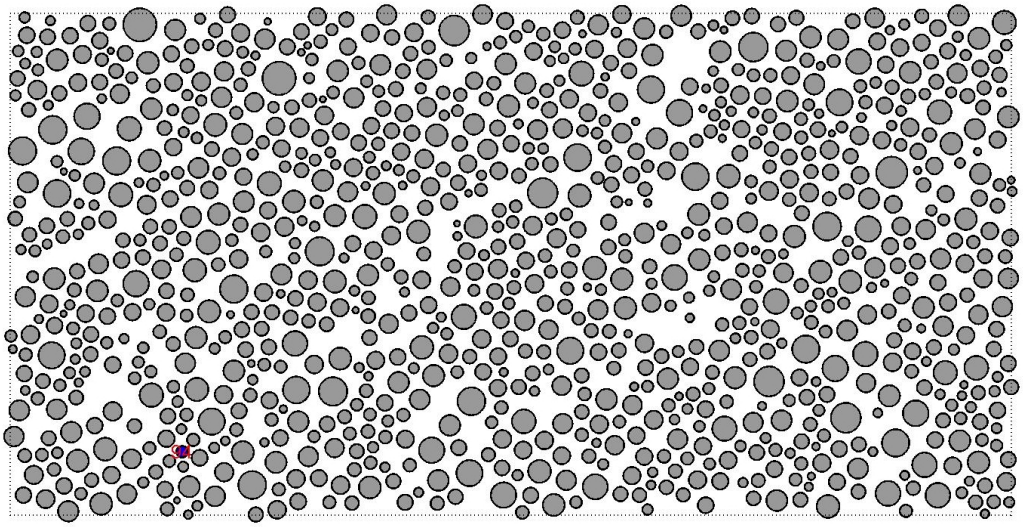

Figure 5.4. Two-dimensional, heterogeneous porous medium used for the mass transfer study. Shaded particle (#94) was selected for analysis.

5.3.2 Mass Transfer in Heterogeneous Media

The model porous medium shown in Figure 5.4 is the same medium used in chapter 3 (see Figure 3.1). The shaded particle (#94) is selected for analysis in this work.

Figure 5.5a shows local streamlines around particle #94. Figures 5.5b – 5e show the trajectories of a limited number of tracer particles (to maintain clarity in the figures). While this type of plot does not provide a quantitative picture of the concentration field, it clearly shows the qualitative boundary-layer behavior as the Peclet number is changed. This indicates that only at the high limit can the dissolution be approximated using the boundary layer approach. Figure 5.5f shows the Pe versus Sh plot for sphere 94. The relation does not follow the $Pe^{1/3}$ scaling that is predicted by boundary layer theory.

The technique described here is a powerful way of studying the effects of local hydrodynamics on interfacial heat and mass transfer, especially at high (but finite) Peclet numbers, which is a regime in which other numerical techniques are less successful. It is straightforward to add an interfacial reaction/adsorption term to the stochastic model. For example the equilibrium Langmuir adsorption can be represented by a partial reflective boundary condition on the adsorbing sphere surface. For tracer molecules that move on to the surface, the probability to stay can be calculated as

$$P = \frac{K(N_s - N_p)}{K(N_s - N_p) + N_p}, \tag{5.7}$$

where N_s is the total number of active sites and N_p is the tracer particles absorbed on the sphere surface and K is a equilibrium constant. For each particle on the surface, the desorbing probability is 1-P. Combined with the equation 5.3, the behavior of adsorption/desorption processes can be investigated.

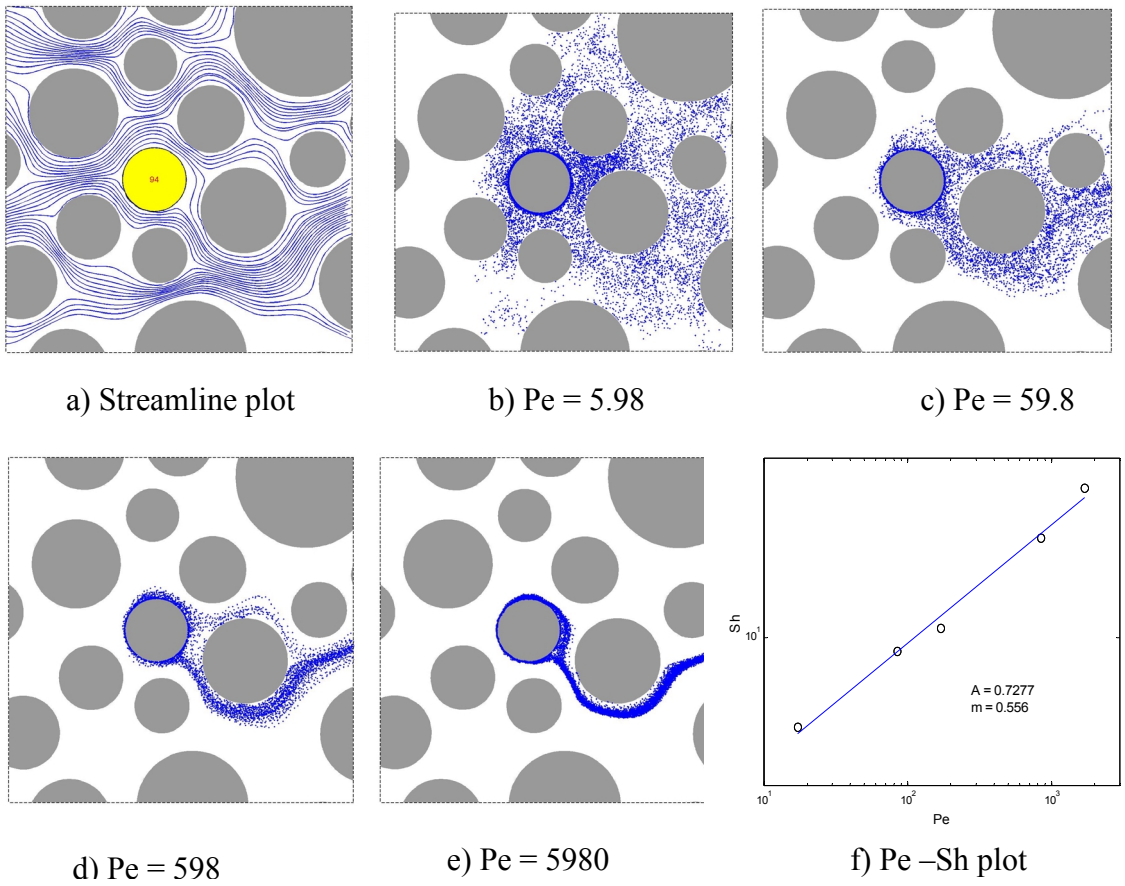

a) Streamline plot b) Pe = 5.98 c) Pe = 59.8

d) Pe = 598 e) Pe = 5980 f) Pe –Sh plot

Figure 5.5. Simulation of the mass transfer of source sphere (#94 shown in figure1). a) The streamline plot of the flow field around the source sphere. b) – e) The tracer trajectories at different Peclet number. f) The Pe – Sh plot shows a power law relation $Sh = A \cdot Pe^{m}$ with A = 0.7277 and m = 0.566

5.4 Conclusions

A stochastic model was developed to simulate the interfacial mass transfer in a disordered porous material. The flow field in the media was solved using the high-resolution model, and a random walk method was used to trace a large number of tracer particles which simulated dissolution from the source sphere. The dissolution rate was calculated from the number of particles that escape from the surface; the explicit concentration profile does not need to be solved. The model was verified by

comparing with Sangani's results in a two-dimensional square packing. Significant differences between this model and previous models include the following: 1. The heterogeneity of the porous media is fully represented by a high-resolution model and the interfacial mass transfer simulation can be performed on each single sphere in the disordered packing. 2. The influence of neighboring spheres is accounted for implicitly. 3. The concentration profile was not needed for the mass transfer rate calculation, which improves the efficiency of this algorithm

CHAPTER 6. CONCLUSIONS AND FUTURE RESEARCH DIRECTIONS

6.1 Summary of the Conclusions

This dissertation presents research on the pore-level modeling of transport in porous media. The focus of this work is on high-resolution modeling, a rigorous approach that represents detailed geometry and first-principle physics at the streamline scale. Three major topics are presented this dissertation: an efficient approach for solving Stokes flow in essentially arbitrary disordered porous media, high-resolution versus network simulations of dispersion phenomena, and a stochastic model for solving the interfacial mass transfer from source spheres in porous media.

First an approach was presented for solving the Stokes flow in a comparatively large, very heterogeneous 2D porous media. The technique developed in this research combines important attributes of domain decomposition and boundary-integral methods. The pore space of the two-dimwnsional disordered medium is initially divided into subdomains (Delaunay cells) using Delauney tessellation. Further refinement of the subdomains can be made by removing internal boundaries from the Delaunay tessellation. The flow field is solved independently in each subdomain by assuming proper boundary conditions, and at the same time the subdomains are related together by the common boundary values. The global problem is solved iteratively using a stabilized biconjugate gradient method while the local solutions for each subdomain are used as a preconditioner. The global coefficient matrix is a strong block diagonal matrix if it is formed explicitly, where the common boundary values generate the off-block elements. We show that the subdomain structure strongly affects the solution efficiency. In particular, minimizing the length of subdomain boundaries in the fluid phase is important. This effect is related to the generation of off-block terms in the global coefficient matrix, some of which are not operated on by the block preconditioner. Subdomain size is the second important parameter. We show, using scaling arguments and empirical results that an

optimum subdomain size exists (in the absence of memory limitations). Our runs were performed on a single processor; consequently, data retrieval time dominated the solution time and the optimum subdomain size was much larger than the predicted optimum. During the solution process, all the data were stored locally, and an index was used to correlate the solutions between subdomains.

One significant achievement of this approach is its efficiency, which relates to the selection of appropriate subdomain structures. The large problems required relatively few iterations for convergence given the very large matrix sizes (e.g., 45 iterations for the 1000-particle problem shown above, which produced ~ 5×10^5 equations). We expect that in the parallel framework being used in future work, iterations for this size problem will require on the order 10-20 seconds. Hence, the overall time requirements for solution are very reasonable. The scaling analysis of this algorithm gives the empirical scaling of solution time with size between N and $N\ln N$, which is a significant improvement compared with direct solution methods. The solution of the algorithm gives the boundary values (stress and velocity) for each subdomain. Point velocities can then be recovered by applying a local boundary integral calculation. Although the boundary values are discrete, the boundary integral formulation provides a smooth, continuum velocity field, which is important for solute transport modeling.

The second topic discussed in this dissertation is high-resolution versus network simulation of dispersion in porous media. Since network modeling techniques have become an important pore-level analysis tool for transport in porous media, it is of interest to evaluate the viability of this model under various conditions. The two important assumptions of the network model were investigated by comparing simulation results with the high-resolution model. The first assumption is the discretization of the pore space into pores and pore throats. By modifying the approach of Bryant et al. (1993), three networks with different coordination numbers were constructed from the same

packing used in the high-resolution model. The discretization process consists of first dividing the domain into triangles using a Delaunay tessellation, and then identifying long boundaries on Delaunay cells, which are considered poor representations of pore throats in the network because of the assumption of axial flow in the network throats. Surprisingly, the results show that the network with the smallest coordination number (3) gives the best flow representation. This fact is caused by the zero pressure drop assumption, which dictates the necessity of having small pore sizes in the discretization. However the axial flow assumption does play an important role during network discretization of a regular square packing, as we showed that by removing the long boundary of each Delaunay cell, the square network gives much better flow representation than a triangle network.

Dispersion was also investigated in order to study how well the network model is able to simulate solute transport. By assuming that the solute is dilute, the convection-diffusion equation for solute transport is decoupled from the hydrodynamics. In the high-resolution model, a random walk algorithm was used to trace the tracer particles through the pore space of the packing. In this algorithm the final position and travel time of each particle are recorded and the dispersion coefficients are calculated from the deviation between the particle position and macroscopically predicted position. Dispersion for the full Peclet number range was simulated and results were found to match well with the literature data, which indicates the valibility of this model. To study the network approach, two algorithms were developed: one employing a nodal mixing assumption (which is typically used in network modeling), the other employing a streamline routing algorithm, which connects streamlines through each network node. In both cases, the flow field was solved by assuming Hagen-Poiseuille flow in each bond, and a random walk method was used to reproduce the dispersion processes. By comparing the various simulation results, we found that the all three models (high resolution and both network models) give values for longitudinal dispersivity within a factor of

2 when $Pe > 100$. This agreement is because mechanical dispersion is the dominant factor within the high-Pe range, and the effects of mechanical dispersion are reproduced when the random walk process samples the entire velocity field. However, the dispersivity from the nodal mixing was found to be independent of Pe in the range $Pe > 10$, which indicates the inability of the nodal mixing technique to represent the molecular diffusion component of solute transport. This problem occurs because nodal mixing introduces an arbitrary diffusion term at each node.

Simulation of solute transport from a single point revealed that nodal mixing spread the tracer particles, even at a simulated value of $Pe = \infty$, while streamline routing and the high-resolution model (which both produce deterministic pathlines) do not. At low Pe number, both network model algorithms (nodal mixing and streamline routing) overestimate the longitudinal dispersion coefficient, which is due to pore-space simplification during constructing of the network from the 2D packing. Also, the network models significantly overestimate the transverse dispersion coefficient over the entire Peclet number range. This is because the axial flow assumption in the network model forces the flow to follow a zig-zag path, which dramatically increases the transverse spreading of the solute compared with the high-resolution flow field.

The third research topic presented was the development of a stochastic model for simulating the interfacial mass transfer at the surface of a single source sphere in a heterogeneous porous medium. A large number of tracer particles are released from the surface of the source sphere and are displaced by convective and random (diffusive) terms until they either return to the surface again or escape to a point far from the source sphere. The number of particles that escape is affected by the concentration boundary layer, which is related to the local Peclet number.

This model was validated by comparing results with the asymptotic analysis of Sangani and Yao (1988). There are three major advantages to this model. First, the approach is valid in the finite Peclet

number range, while boundary layer analysis is valid only at the high Peclet number limit. (At low Peclet numbers, the neighboring spheres have a strong effect on the concentration boundary layer.) Second the flow domain does not need to be discretized except to specify a surface bin layer that is used to count the surface concentration. Consequently, no concentration profiles are needed for calculating the mass transfer rate. Third, this model can be used to study multiple source spheres in the same heterogeneous medium. This allows the possibility for analyzing the relationship between the mass transfer rate distribution and the variation in local hydrodynamics, among other phenomena.

6.2 Future Research Directions

6.2.1 Develop More Efficient Algorithms for Three-Dimensional Random Sphere Packings

To quantitively represent transport in real porous media, three-dimensional high-resolution modeling is desirable. Using the algorithm developed here, there are no restrictions that prevent three-dimensional modeling, except for the straightforward computational issues that accompany any increase in dimensionality for numerical simulation. While the Delaney tessellation can still be used to divide the domain into subdomains (Thompson and Folger, 1996), the schemes for discretizing boundary elements on the surface of spheres will be significantly more involved. Also, higher-order boundary elements will probably be required because of the much larger computational demands in three-dimensional. (Brebbia et al., 1984).

To represent the heterogeneity in 3D, the packing size will be much larger than in two-dimension, which will in turn require a reduction in computation time. However, this can easily be accommodated by eliminating the need to access disk memory. Further increases in efficiency can be realized by using parallel computing. The domain decomposition approach in our algorithm is used primarily as a preconditioning method. However it also can be used to facilitate parallel computing (Smith et al., 1996). Since all the data are stored in local subdomains and the computations for the

matrix inversion and multiplication are also performed locally, it is straightforward to assign the computational load to multiple processors. However, the data communication structure becomes essential for parallel computing, which suggests that the load balance or the domain size may have important effects on the efficency.

6.2.2 Investigate other transport phenomena using the high-resolution model

Since both pore-level structure and first principle physics can be represented using the high-resolution model, fundamental studies of numerous porous media transport processes can be undertaken. Examples include microbial transport and immobilization (Camper et al., 1993; Harvey et al., 1993), reactive solute transport (Hu et al., 1995; Song et. al., 1994), polymer molecular diffusion and stretching (MacDonald, 1992; Shaqfeh and Koch, 1992), etc.

One important example is bacterial transport in the subsurface. Within a certain cell-size range, larger bacteria cells tend to travel along the high-velocity streamlines at the center of the pores, which causes faster overall transport. This phenomenon is called size exclusion chromatography (Lecourtier and Chauveteau, 1984; Brown and Sorbie, 1989). At the same time, filtration and clogging effects may dominate when bacterial cell sizes become larger and/or pore sizes smaller (Salles et al., 1993; Harvey et al., 1993). Pore-level heterogeneity also affects bacterial adhesion and growth (Murphy et al., 1997). This process can be modeled by modifying the convection-diffusion equations at the continuum level (Corapcioglu and Haridas, 1985). However, in most cases, the pore-level heterogeneity becomes so crucial that the volume-averaging approach fails. For example, the deposition and growth of the microbial colonies may take place in different regions of the pore space, which in turn changes the structure of the porous material. With detailed geometry and hydrodynamic information, high-resolution modeling is a powerful tool for investigations of the different phenomena, separately or as a whole.

REFERENCES

Sangani, A.S., C. Yao, "Transport processes in random arrays of cylinders. I. Thermal conduction," *Phys. Fluids,* **31**(9) 2426 (1988).

Acrivos, A., J.D. Goddard, "Asymptotic expansions for laminar forced-convection heat and mass transfer," *J. Fluid Mech.* **23**(2) 273-291 (1965).

Bacri, J.-C., Rakotomalala, N., Salin, D., "Anomalous dispersion and finite-size effects in the hydrodynamic dispersion," *Phys. Fluids A,* **2** (5) 674-680 (1990)

Bakke, S., and P.E. Oren, "3-D Pore-Scale Modelling of Sandstones and Flow Simulations in the Pore Networks, *SPEJ*, **2**(2), 136 (1997).

Bekri, S., Thovert, J.F., Adler, P.M., "Dissolution of porous media," *Chem. Eng. Sci*., **50** 2765-2791 (1995)

Blacwell, R.J., J.R. Rayne, and W.M. Terry, "Factors Influencing the efficency of miscible displacement", *AIME Petroleum Trans*., 217, (1972)

Brebbia, C.A., J.C.F. Telles, and L.C. Wrobel, *Boundary Element Techniques: Theory and Applications in Engineering*, Springer-Verlag, Berlin (1984).

Brown, W.D., and Sorbie, K.S., "Dispersion and Polydispersity Effects in the Transport of Xanthan in Porous Media", *Macromolecules*, **22** 2835-2845 (1989)

Bryant, S. L., Mellor, D.W., Cade, C. A., "Physically representative network models of transport in the porous media," *AICHE Journal*, **39** (3) 387-396 (1993)

Bryant, S.L., and M. Blunt, "Prediction of Relative Permeability in Simple Porous Media," *Phys. Rev. A*, **46**(4), 2004 (1992).

Bryant, S.L., P.R. King, and D.W. Mellor, "Network Model Evaluation of Permeability and Spatial Correlation in a Real Random Sphere Packing," *Transport in Porous Media*, **11,** 53 (1993).

Bryant, Steven L., David W. Mellor, and Christopher A. Cade, "Physically representative network models of transport in porous media", *AIChE Journal*, **39** (3) 387-396 (1993 A)

Bryant, Steven L., Peter R. King, and David W. Mellor, "Network model evaluation of permeability and spatial crrelation in a real random sphere packing", *Transport in Porous Media*, **11** 53-70 (1993 B)

Camper, A.K., Hayes, J.T., Sturman, P. J., Jones, W.L., and Cunningham, A.B., "Effects of Mobility and Adsorption Rate Coefficients on Transport of Bacteria through Saturated Porous Media," *Applied and Environmental Microbiology*, **59** (10) 3455-3462 (1993)

Carberry, J.J. and R.H. Bretton, "Axial Dispersion of Mass in Flow through Fixed Beds", *AICHE J.,* **4** 367 (1958)

Chartrand, G, Oellermann, OR. *Applied and Algorithmic Graph Theory,* McGraw Hill: New York, 1993; pp. 68-85.

Corapcioglu, M.Y. and Haridas, A., "Microbial transport in soil and groundwater: a numerical model," Adv. Water Resour., **8** 188-200 (1985)

Cruse, T. A., and F. J. A. Rizzo, "A direct formulation and numerical solution of the general transient elasto-dynamic problem", *J. Math. Anal. Appl*. **22** 244-259 (1968)

Dillard, L.A., Blunt, M.J., "Development of a pore network simulation model to study nonaqueous phase liquid dissolution," *Water Resources Research*, **36** 439-454 (2000)

Dullen, F.A.L., *Porous Media – Fluid Transport and Pore Structure*, Academic Press, New York (1979).

Ebach, E.A., and R.R. White, "Mixing of Fluid Flowing through Beds of Packed Solids", *AICHE J.* 161 (1958)

Edward, M.F. and J. F. Richardson, "Gas Dispersion in Packed Beds", *Chem Engr. Sci.,* **23** 109 (1968)

Coutelieris, F.A., V.N. Burganos, A.C. Payatakes, "Convective diffusion and adsorption in a swarm of spheroidal particles," *AIChE J.,* **41**(5) 1122-1134 (1995)

F.A. Coutelieris, V.N. Burganos, A.C. Payatakes, "On mass transfer from a Newtonian fluid to a swarm of adsorbing spheroidal particles for high Peclet numbers," *J. Colloid Interface Sci.,* **161** 43-52 (1993)

Fatt, I., "The network model of porous media: I. Capillary pressure characteristics," *Pet. Trans. AIME*, **207**144-159 (1956).

Finney, J.L., "Fine Structure in Randomly Packed, Dense Clusters of Hard Spheres," *Mater. Sci. Eng.*, **23** 199 (1976).

Fredd, C.N., and H.S. Fogler, "Influence of transport and reaction on wormhole formation in porous media," *AIChE J.*, **44**(9)1933-1949 (1998).

G. Baier, T.M. Grateful, M.D. Graham, E.N. Lightfoot, "Prediction of mass transfer rates in spatially periodic flows," *Chem. Eng. Sci*. **54** 343-355 (1999)

Guo, G., K.E. Thompson, 'Experimental analysis of local mass transfer in packed beds,' *Chem. Eng. Sci.,* **56** 121-132 (2001)

Ghassemzadeh, J., M. Hashemi, L. Sartor, and M. Sahimi, "Pore Network Simulation of Imbibition into Paper during Coating: 1. Model Development," *AIChE J.*, **47**(3) 519 (2001).

Gunn, D.J., and C. Pryce, "Dispersion in packed beds", *Trans. Inst. Chem. Eng.,* **47** T341 (1969)

Harlemen,D.R.F., and R. R. Rummer, "Longitudinal and Lateral Dispersion in an Isotropic Porous Medium", *J.Fluid Mech.,* **16** 385 (1963)

Harvey, R.W., Kinner, N.E., MacDonald, D., Metge, D.W., and Bunn, A., "Role of Physical heterogeneity in the Interpreataion of Small-Scale Laboratory and Field Observations of Bacteria, Microbial-Sized Microsphere, and Bromide Transport Through Aquifer Sediments," Water Resources Research, **29** (8) 2713-2721 (1993)

Hasimoto, H., "On the periodic fundamental solution of the Stokes equations and their application to viscous flow past a cubic array of spheres," *J. Fluid Mech*., **5** 317-328 (1959)
Higdon, J.J.L., Viera, M.N., "Colloidal Simulations with O(N ln N) Stokesian Dynamics," *Annual AIChE meeting, Los Angeles*, Nov. 12-17 (2000).

Hoefner, M.L., and H.S. Fogler, "Pore Evolution and Channel Formation During Flow and Reaction in Porous Media," *AIChE J.,* **34**(1), 45 (1988).

Hu, B.X., Deng, F., and Cushman, J.H., "Nonlocal reactive transport with physical and chemical heterogeneity: Linear nonequilibrium sorption with random K_d," Water Resources Research, **31**(9) 2239-2252 (1995)

Hull, L.C., Koslow, K.N., "Streamline routing through fracture junctions," *Water Resources Research*, **22** (12) 1731-1734 (1986)

Sørensen, J.P., W.E. Stewart, "Computation of forced convection in slow flow through ducts and packed beds – IV. Convective boundary layers in cubic arrays of spheres," *Chem. Eng. Sci.,* **29** 833-837 (1974)

Jia, C., K. Shing, Y.C. Yortsos, "Visualization and simulation of non-aqueous phase liquids solubilization in pore networks," *J. Contam. Hydrol*. **35** 363-387 (1999).

Thompson, K.E., H.S. Fogler, "Modeling flow in disordered packed beds from pore-scale fluid mechanics," *AIChE J.,* **43**(6) 1377-1389 (1997)

Karabelas, A.J., T.H. Wegner, T.J. Hanratty, "Use of asymptotic relations to correlate mass transfer data in packed beds," *Chem. Eng. Sci.,* **26** 1581-1589 (1971).

Kitanidis, Peter K., "Particle-tracking equations for the solution of the advection-dispersion equation with variable coefficients", *Water Resources Research*, **30** (11), 3225-3227 (1994)

Koch DL, Ladd AJC. "Moderate Reynolds number flows through periodic and random arrays of aligned cylinders," *J. Fluid Mech.,* **349** 31-66 (1997)

Koch, D. L., Brady, J. F., "Nonlocal dispersion in the porous media: nonmechanical effects," *Chem. Eng. Sci.*, **42** (6) 1377-1392 (1987)

Koch, D.L., Brady, J.F. , "Dispersion in fixed beds," *J. Fluid Mech.* **154** 399-427 (1985)

Koplik, J., "Creeping flow in two-dimensional networks", *J. Fluid Mech*. **119** 219-247 (1982)

Dillard, L.A., M.J. Blunt, "Development of a pore network simulation model to study nonaqueous phase liquid dissolution," *Water Resour. Res.* ***36***(2) 439-454 (2000)

Larson, R.E., and J.J.L. Higdon, "Microscopic flow near the surface of two-dimensional porous media. Part 1. Axial flow", *J. Fluid Mech*. **166** 449-472 (1986)

Larson, R. E., and J. J. L. Higdon, "Microscopic flow near the surface of two-dimensional porous media. Part 2. Transverse flow", *J. Fluid Mech*. **178** 119-136 (1987)

Lecourtier, J., and Chauveteau, G., "Xanthan Fractionation by Surface Exclusion Chromatography", *Macromolecules*, **17** 1340-1343 (1984)

Lee, Cheo K., Chin-Cheng Sun and Chiang C. Mei, "Computation of permeability and dispersivities of solute or heat in periodic porous media", *Int. J. Heat Mass Transfer*. **39** (40) 661-676 (1996)

Lemaitre, R.; Adler, P.M., "Fractal Porous Media IV: Three-Dimensional Stokes Flow Through Random Media and Regular Fractals," *Transport in porous media*, **5** (4) 325 (1990)

Liang, Z., M.A. Ioannidis, and I. Chatzis, "Permeability and electrical conductivity of porous media from 3D stochastic replicas of the microstructure," *Chem. Eng. Sci.*, **55**, 5247-5262 (2000).

Liu, G., and K.E. Thompson, "Influence of Computational Domain Boundaries on Internal Structure in Low-Porosity Sphere Packings," *Powder Tech.*, **113**, 185-196 (2000).

MacDonald, R.A., "Modeling macromolecular diffusion through a porous medium," *J. Membrane Sci*., **68** 93-106 (1992)

Maier, R.S., Kroll, D.M., Kutsovsky, Y.E., Davis, H.T., Bernard, R.S., "Simulation of flow through bead packs using the lattices Boltzmann method", *Phys. Fluids*, **10**(1), 60 (1998)

Murphy, E.M., Ginn, T.R., Chilakapati, A., Resch, T., Philips, J.L., Wietsma, T.W., and Spadoni, C.M., "The influence of physical heterogeneity on microbial degradation and distribution in porous media," *Water Resources Research,* **33**(5) 1087-1103 (1997)

Neung-won Han et al, "Longitudinal and Lateral Dispersion in packed Beds: Effect of Column Length and particle size distribution", *AICHE J.* **31** (2) P 277 (1985)

Öttinger, H.C., *Stochastic Processes in Polymeric Fluids*, Springer, Berlin (1996).

Pfannkuch, H.-O., "Contribution a l'Etude des Deplacements des Fluids Miscibles dans un Milieu Poreux", *Revue de l'Institut du Petrole*, **18** 215 (1963)

Pfeffer, R., J. Happel, "An analytical study of heat and mass transfer in multiparticle systems at low Reynolds numbers," *AIChE J.* **10**(5) 605-611 (1964).

Pozrikidis, C., *Boundary integral and singularity methods for linearized viscous flow*, Cambridge University Press, 1992

Rajaram, Harihar, lin A. Ferrand, and Michael A. Celia, "Prediction of relative permeabilities for unconsolidated soils using pore-scale network models", *Water Resources Research*, **33** (1) 43-52 (1997)

Reeves, Paul C., and Michael A. Celia, "A functional relationship between capillary pressure, saturation, and interfacial area as revealed by a pore-scale network model", *Water Resources Research*, **32** (8), 2345-2358 (1996)

Rege, S. D., and H. S. Fogler, "A network model for deep bed filtration of solid particles and emulsion drops", *AIChE Journal*, **34** (11) 1761-1771 (1988)

Rifai, M.N.E., W.J. Kaufman, and D.K. Todd, "Dispersion in Laminar Flow through Porous Media", Sanitary Eng. Res. Lab. Rpt. No.3. IER Series 90, Berkeley, CA (1956)

Ponoth, S.S., J.B. McLaughlin, "Numerical simulation of mass transfer for bubbles in water," *Chem. Eng. Sci.,* **55** 1237-1255 (2000)

Saeger, R. B., L. E. Scriven and H. T. Davis, "Transport processes in periodic media", *J. Fluid Mech*. **299** 1-15 (1995)

Sahimi, M., Davis, H.T., Scriven, L.E., "Dispersion in disordered porous media," *Chem. Eng. Commun*., **23** 329-341(1983)

Sahimi, M., Hughes, B.D., Scriven, L.E., Davis, H.T., "Dispersion in flow through porous media—I. One-phase flow," *Chem. Eng. Sci*., **41** 2103-2122 (1986)
Sangani AS, Acrivos A. "Slow flow past periodic arrays of cylinders with applications to heat transfer." *Int. J. Multiphase Flow*, **8** 193-206 (1982)

Sangani AS, Mo G. "Inclusion of lubrication forces in dynamic simulations," *Phys. Fluids,* **6** 1653-1662 (1994)

Sangani AS, Yao C. "Transport processes in random arrays of cylinders. II. Viscous flow." *Phys. Fluids,* **31** 2435-2444 (1988)

Sangani, A. S., and A. Acrivos, "Slow flow through a periodic array of spheres", *Int. J. Multiphase Flow*, **8** (4) 343-360 (1982)

Scheibe, T. D., and C. R. Cole, "Non-Gaussian particle tracking: application to scaling of transport processes in heterogeneous porous media", *Water Resources Research*, **30** (7), 2027-2039 (1994)

Scheidegger, A. E., "The Random walk model with autocorrelation of flow through porous media", *Can. J. of Phys*., **36** 649 (1958)

Shah, C.B., and Y.C. Yortsos, "Aspects of flow of power-law fluids in porous media," *AIChE J.*, **41**(5), 1099-1112 (1995).

Shaqfeh, E. S., and Koch, D.L., "Polymer stretch in dilute fixed beds of fibres or spheres," *J. Fluid Mech*. **244** 17-54 (1992)

Smith, B, Bj⊙rstad, P, and Gropp, W., *Domain Decomposition: Parallel Multilevel Methods for Elliptic Partial Differential Equations*, Cambridge: New York, 1996

Song, L., Johnson, P.R., and Ellimelech, M., "Kinetics of Colloid Deposition onto Heterogeneously Charged Surfaces in Porous Media," Environ. Sci. Technol., **28** 1164-1171 (1994)

Sorbie, K. S., Clifford, P. J., "The inclusion of molecular diffusion effects in the network modeling of hydrodynamic dispersion in porous media," *Chem. Eng. Sci*., **46** (10) 2525-2543 (1991)

Sorbie, K.S., Clifford, P.J., and E.R.W. Jones, "The Rheology of Pseudoplastic Fluids in Porous Media Using Network Modeling, *J. Colloid Interface Sci.*, **130**(2), 508 (1989).

Sørensen, J.P., W.E. Stewart, "Computation of forced convection in slow flow through ducts and packed beds – II. Velocity profile in a simple cubic array of spheres," *Chem. Eng. Sci.,* **29** 819-825 (1974).

Spaid MAA, Phelan FR Jr. “Lattice Boltzmann methods for modeling microscale flow in fibrous porous media.” *Phys. Fluids,* **9** 2468-2474 (1997).

Sternberg, Steven P. K., John H. Cushman, Robert A. Greenkorn, “Random walk in prefractal porous media”, *AIChE Journal*, **42** (4) 921-926 (1996)

Thauvin, F., and K.K. Mohanty, “Network Modeling of Non-Darcy Flow Through Porous Media,” *Transport in Porous Media*, **31**, 19 (1998).

Thompson, K. E., Fogler, H. S., “Modeling flow in disordered packed beds from pore-scale fluid mechanics,” *AICHE Journal*, **43** (6) 1377-1389 (1997)

Thompson, K.E., “Pore-Scale Modeling of Fluid Transport in Disordered Fibrous Materials,” *AIChE J.* (in press).

Trefethen, LN, Bau, D III., *Numerical Linear Algebra,* SIAM: Philadelphia, 1997; pp. 266-275.

Van Der Vorst HA, “BI-CGSTAB: A fast and smoothly converging variant of BI-CG for the solution of nonsymmetric linear systems,” *SIAM J. Stat. Comput.* **13** 631-644 (1992)

Verberg R, Ladd AJC. “Simulation of low-Reynolds-number flow via a time-independent lattice-Boltzmann method,” *Phys. Rev. E* , **60** 3366-3373 (1999)

W. Wang, A.S. Sangani, Nusselt number for flow perpendicular to arrays of cylinders in the limit of small Reynolds and large Peclet numbers, Phys. Fluids, 9(6) (1997) 1529-1539.

Weiss, G.H., *Aspects and Applications of the random work*, North-Holland press, New York (1994)

Wentzell, Peter D., Michael R. Bowdridge, Elizabeth L. Taylor and Craig MacDonald, “Random walk simulation of flow injection analysis. Evaluation of dispersion profiles”, *Analytica Chimica Acta*, **278** 293-306 (1993)

Whitaker, S., “Flow in Porous Media I: A Theoretical Derivation of Darcy’s Law,” *Transport in Porous Media*, **1** 3-25 (1986)

Yeh, T.-C. Jim, Rajesh Srivastava, Amado Guzman, and Thomas Harter, “A Numberical Model for Water Flow and Chemical Transport in Variably Saturated Porous Media”, *Ground Water*, **31**(4) 634-644 (1993)

Youngren, G. K., and A. Acrivos, “Stokes flow past a particle of arbitrary shape: a numerical method of solution”, *J. Fluid Mech*., **69**(2), 377-403 (1975)

Zick, A. A., and G. M. Homsy, “Stokes flow through periodic arrays of spheres”, *J. Fluid Mech*., **115** 13-26 (1982)

VITA

Guangli Liu was born on the Shandong, China, on January 18, 1968. He enrolled in the Yantai University in 1985 and obtained his Bachelor of Science degree in Chemical Engineering in 1989. He joined the graduate program of chemical engineering of Beijing University of Chemical Technology for pursuing a Master of Science degree in same year. At 1992, he started to work as R&D engineer in biochemical industry. In 1996, he enrolled in the doctoral program in the Department of Chemical Engineering of Louisiana State University and Agriculture and Mechanical College.